OPTIMIZATION OF VIBRATION TESTING TIME

Prepared for
George C. Marshall Space Flight Center
Huntsville, Alabama

AUTHOR I. F. Gerks

ACTIVITY Environmental Analysis Group
Spacecraft Systems Division
Collins Radio Company
5200 C Avenue N.E.
Cedar Rapids, Iowa

TYPE Technical Summary Report of Research Performed under Contract NAS8-11278, During The Period of 29 June 1964 to 10 October 1965

DATE 15 June 1966

APPROVED W. F. Gerks

ABSTRACT

A System of equations was developed to scale the vibration levels occurring in a structure subjected to field vibration so that a laboratory test consisting of sine dwell, sine sweep, random vibration, or any sequential combination of these, will cause equivalent fatigue damage in a similar structure. A Miles type analysis was made using the Palmgren-Miner and Corten-Dolan fatigue damage hypotheses. The resulting equivalence equations are based on the specimen's dynamic characteristics, natural frequency and transmissibility with the negative reciprocal of the slope of the damage accumulation curve appearing as the only fatigue characteristic in the equations. A linear single degree freedom system is the idealized dynamic model but the analysis will apply to higher mode responses.

A computer program using the Palmgren-Miner version of the equivalence equations was developed which generates families of curves of equivalent test levels for varying values of specimen natural frequency and transmissibility, once the field vibration and the desired type of equivalent test is known.

The equations were indirectly validated by vibrating sets of test specimens to the different types of input and comparing the predicted damage to the actual damage. The test specimens were 6061T-6 aluminum alloy cantilever beams with an end mass which gave the specimens an average resonance of 340 cps when damped to a transmissibility of 20. Four basic investigations were made, one of which was invalidated due to faulty instrumentation.

The Palmgren-Miner fatigue hypothesis was found more accurate than the Corten-Dolan hypothesis in the prediction of damage for the three valid tests.

ACKNOWLEDGMENTS

The author thanks Mr. R. Schock, MSFC Huntsville, for his assistance and guidance. Special acknowledgments are also made to Collins Radio Company personnel, L. W. Root and L. G. Poulos. Also, the author is further grateful to the Environmental Test Facility Personnel at Collins Radio Company.

TABLE OF CONTENTS

I. INTRODUCTION

Laboratory vibration testing to reproduce or simulate field problems has had the attention of mechanical engineers for many years. Increased interest in random processes, stimulated by more stringent design requirements in the area of spacecraft vibration environments, has shown a need for further analytical work in the definition of equivalent test programs.

Considerable effort is being expended in an attempt to transform field vibration histories into meaningful laboratory vibration tests which produce equivalent fatigue damage[4][5][10]. The object of this research effort was to develop and experimentally verify transformations between field experiences and laboratory tests. The analysis performed was directed toward the prediction of equivalent fatigue damage.

A system of equivalence equations was developed and used as a basis for a computer program which calculated equivalent test levels.

The "Summary and Conclusions" section of this report covers the findings of the study effort, and supporting data and derivations are included in the various appendices.

II. DISCUSSION

The analytical derivation was based on two fatigue damage hypothesis; Palmgren-Miner (P-M)[1][2] and Corten-Dolan (C-D)[3].

The P-M hypothesis was selected because of it's widespread use and simplicity.

The C-D hypothesis was chosen because it is able to account for damage phenomena in areas of known inadequacy in the P-M hypothesis[3]. Further, the C-D approach may be expressed in a form similar to the fundamental P-M equation. The C-D hypothesis was interpreted to mean that the characteristics which apply to repeated applications of 2 level sinusoidal stress will also apply to nonrepeating, multi-level, applications of random stresses.

Several assumptions were made to reduce the complexity of the theoretical development of equivalence equations:

1) The S-N curve is a straight line on a log log plot.
2) The various types of field vibration occur sequentially.
3) More than one vibration component could exist at one time; however, these components would have sufficient frequency separation so as to avoid simultaneous excitation of any one resonance.
4) The change in level of field vibration is very small in the neighborhood of the specimen resonances.
5) Field vibration is steady state.
6) Multiple degree of freedom systems are representable by groupings of noninteracting linear single degree of freedom systems.

The development of the equivalence equations is given in Appendix B. See equations 5,53,55, 57, 59, and 61. These six equations were used as the basis for the computer program used in transforming field vibration to equivalent laboratory vibration tests.

After determining the type of equivalent test desired, frequency range to be covered, length of test, and expected range of transmissibilities in the test item, the computer program may be used. Based on the P-M hypothesis, three steps are involved in transforming field vibration to equivalent levels:

1) The first step involves combining all similar types of field vibration inputs into one intermediate equivalent test. For example, all the field vibration random levels are combined into one equivalent random vibration level. The new level would produce the same equivalent damage within t_e seconds as all the field vibration random inputs. The defining equations for this phase are (symbols and terms in appendix A).

   (a) Several sine dwells to one sine dwell

$$A_{sd,e}=\left[\sum_{i=1}^{m}\left[\frac{f_{ii}}{f_n}\right]\left[\frac{t_i}{te}\right]\frac{A_{sd,ij}^{b}}{\left[Q^2\left[1+\left[\frac{f_{ii}}{f_n}\right]^4\right]-\left[\frac{f_{ii}}{f_n}\right]^2\left[2Q^2-1\right]\right]^{b/2}}\right]^{1/b}$$

   (b) Several sine sweeps to one sine sweep

$$A_{ss,e}=\left[\sum_{i=1}^{m}\left[\frac{\ln\left(f_{2e}/f_{1e}\right)}{\ln\left(f_{2i}/f_{1i}\right)}\right]\left[\frac{t_i}{te}\right]A_{ss,i}^{b}\right]^{1/b}$$

   (c) Several random levels to one random level

$$W_e=\left[\sum_{i=1}^{m}\left[\frac{t_i}{te}\right]W_i^{b/2}\right]^{2/b}$$

2) In the second step, the type of test is changed to the final desired type of equivalent test. For example, the first step random equivalent is scaled to a log sine sweep equivalent or vice versa. The ϕ term appears in this step and it is a term which appears in the sine sweep damage. It is defined for all materials as being:

$$\phi = 1.89/b^{.645}$$

The equations for this step are:

(a) Log sine sweep to sine dwell

$$A_{sd,ss,e} = A_{ss,e}\left[\frac{\phi}{Q \cdot \ln(f_{2e}/f_{1e})}\right]^{1/b}$$

(b) Sine dwell to log sine sweep

$$A_{ss,sd,e} = A_{sd,e}\left[\frac{Q \cdot \ln(f_{2e}/f_{1e})}{\phi}\right]^{1/b}$$

(c) Random to log sine sweep

$$A_{ss,r,e} = \left[\frac{W_e \pi f_n}{Q}\right]^{1/2}\left[\frac{Q \cdot \ln(f_{2e}/f_{1e})\,\Gamma(1+b/2)}{\phi}\right]^{1/b}$$

(d) Log sine sweep to random

$$W_{ss,e} = \frac{A_{ss,e}^2\, Q}{\pi f_n}\left[\frac{\phi}{Q \ln(f_{2e}/f_{1e})\,\Gamma(1+b/2)}\right]^{2/b}$$

(e) Random to sine dwell

$$A_{sd,r,e} = \left[\frac{\pi f_n W_e}{Q}\right]^{1/2}\left[\Gamma(1+b/2)\right]^{1/b}$$

(f) Sine dwell to random

$$W_{sd,e} = \frac{Q\, A_{sd,e}^2}{\pi f_n}\left[\frac{1}{\Gamma(1+b/2)}\right]^{2/b}$$

3) In the third step the final equivalent level is derived by combining all the similar types of vibration resulting from steps 1 and 2. For example, the final equivalent random damage is equivalent to the damage of the random equivalent (W_e) due to the summation of all the field random inputs (step one), plus the random equivalent of the field sine dwells, plus the random equivalent of the field sine sweeps (both from step two). The equations for this step are:

(a) Final random equivalent

$$W_{ee} = \left[W_e^{b/2} + W_{sd,e}^{b/2} + W_{ss,e}^{b/2} \right]^{2/b}$$

(b) Final sine sweep equivalent

$$A_{ss,ee} = \left[A_{ss,e}^{b} + A_{ss,r,e}^{b} + A_{ss,sd,e}^{b} \right]^{1/b}$$

(c) Final sine dwell equivalent

$$A_{sd,ee} = \left[A_{sd,e}^{b} + A_{sd,r,e}^{b} + A_{sd,ss,e}^{b} \right]^{1/b}$$

All of the above equations are based on the P-M hypothesis but equivalent levels based on the C-D hypothesis appear in Appendix B.

The test specimens were externally damped cantilever beams machined from 6061-T6 aluminum. They had a first mode resonance around 330 cps with an associated transmissibility of about 20. The specimen response to dynamic excitation is almost identical to a single degree of freedom system when the specimen is excited in the 100 cps to 800 cps range. The amplitude linearity is good, with the peaks in random vibration

satisfying a Rayleigh distribution. The stress-deflection ratio is nearly constant in the resonant frequency range for a wide range of amplitudes.

The fatigue properties of the specimens were determined by vibrating undamped specimens to failure to obtain S-N curves for both sine and random vibration. The C-D damage exponent was also obtained using undamped specimens. Several sets of specimens were made and because of variations which existed from set to set, it was necessary to determine the fatigue properties for each set.

The vibration tests performed to verify the analysis were conducted using damped specimens. The specimens were intended to represent a typical natural frequency and transmissibility more characteristic of actual structure. Four different correlation tests were adequate to determine the accuracy of the analysis. They were: Field vibration, random vibration, sine sweep vibration, and sine dwell vibration. Repetition of these tests were performed to get additional statistical data. The field vibration test was composed of varying levels of different types of vibration. (Fig.J1&2)

The actual test procedure was complicated because the external dampers changed stiffness and damping under high level vibration. Also, the failure detection technique used requires that the specimen be undamped. These damper variations were determined by taking repeated measurements during the test to determine transmissibility and natural frequency. These measurements were complicated by the

fact that six specimen were vibrated at once to conserve setup time and actual vibration testing time. The failure criteria was a 1/2% shift in the original beam resonance rather than complete fracture,[5] and this shift was measured by removing the damper to perform a resonant search at a low input. The correlation test was stopped just short of failure and the resonances of the six specimens were checked. All specimens which did not fail were individually subjected to a resonant sine dwell. This sine dwell produced higher stresses than occurred during the preceding correlation test. The final run-out-to-failure vibration produced a predictable damage level allowing computation of the damage accumulated by each specimen during the correlation test.

The experimentally measured damage was compared to the damage predicted by the analysis to determine correlation. The reduction of data, which was performed so that an analytical prediction of damage could be made, was complicated by several factors. Since the specimen's properties change during a test, it was necessary to divide test time into one or more increments and use average values of transmissibility and natural frequency over each increment. Another correction was applied to compensate for the specimen's deviation from a single degree of freedom response at higher inputs. Finally, it was necessary to reduce the data for each specimen separately since each had a slightly different dynamic response.

The results of the correlation tests are plotted on Weibull distribution paper, (fig. G-8). The horizontal scale is not cycles-to-failure but damage in terms of $\Sigma\ n/N$. The reason for this change is presented in Appendix G.

The four correlation tests are listed with the Weibull mean predicted damage at failure, in brackets, and the significant result of that test:

1) Resonant sine dwell of 6 specimens; (1.03), the use of a two part test (correlation and run-out-to-failure portions) is practical.

2) Log sine sweep of 10 specimens; (.98), the P-M hypothesis predicts this damage level better than does C-D hypothesis.

3) Flat random of 10 specimens; (1.01), the P-M hypothesis predicts this damage level better than does C-D hypothesis.

4) Field vibration of 6 specimens - 2 levels of random followed by sine sweep; (.52). This test is considered invalid with an instrumentation discrepancy as the source of error.

The results of the fatigue tests are applicable to judge suitability of the fatigue hypothesis to the following extent:

1) The slope and position of random fatigue curve is more compatible with P-M than with C-D. Each of the three sets of specimens gave similar results.

2) The C-D damage exponent d for this project is 72% of b rather than the average of 85%.[3]

The final computer program was checked at several points to determine the accuracy of scaling and whether the resulting predicted equivalent test level would produce the same damage. This was accomplished for a case where the field or use vibration parameters are: fn = 325 cps and Q = 20. The results were:

	Use Vibration	Sine Sweep Equivalent	Random Equivalent	Sine Dwell Equivalent
Damage	3.087×10^{-3}	2.645×10^{-3}	3.080×10^{-3}	2.05×10^{-3} 2.56×10^{-3}
Computer Level	---	24.67 g's	1.439 g^2/cps	12.64 g
Slide Rule Level	---	24.57 g's	1.425 g^2/cps	12.59 g

The damage resulting from the use vibration was mostly due to the random vibration portion. The random equivalent test produces the most nearly equal damage. The sine sweep test produces 16.5% less damage because the transformation from random damage to sine damage assumes a theoretical separation of the random and sine fatigue curve which is 2.4% different than the actual measured case. This 2.4% variation in stress can result in an error of about 20% in life and is in close agreement with the computed damage. The damage predicted by the sine dwell equivalent test deviates 50% from the field vibration damage. The reason for this is that the resulting stress is lower for this test than for any of the other tests. In using the actual S-N fatigue curves, a difference will result from computer derived damage. This difference is accountable because the slope of the curves used in the computer program is 7.8, the mean of the random slope (7.66) and the sine slope (7.94). The

extrapolation of these curves results in a large error. If the equivalent test time and equivalent test level are scaled by the following equation:

$$t_1\sigma_1^{\,b} = t_2\sigma_2^{\,b}$$

where b is 7.8 and σ_2 is a stress which is in the range for which the curves were measured, then a test time t_2 will result which will produce a damage which is not distorted by the variation slope of the actual fatigue curve with respect to that used for the computer equations. Using σ_1 = 31,600 psi and $N_1 = 10^6$ cycles, a damage of 2.56×10^{-3} was computed. This is 20% off the field vibration damage and 3% off the sine sweep equivalent vibration damage. These results are considered to be proof that the scaling equations are accurate.

III. CONCLUSIONS

The correlation was excellent for all tests except the field vibration test, which was considered invalid due to instrumentation error. Therefore it is assumed that the equivalence equations are valid. From the tests it is felt that the P-M equations are more accurate for the specimen used than the C-D equations. These reasons are itemized:

1) The P-M hypothesis more accurately predicted the spacing and slope of the random fatigue curve with respect to the sine fatigue curve than did the C-D hypothesis. Three sets of fatigue property tests support this conclusions.

2) The P-M hypothesis gave better correlation for two of the equivalent tests and identical for the third equivalent test.

3) The P-M hypothesis simplifies the computation of equivalent test levels because:

   (a) sequence of stress application does not affect fatigue damage. (C-D hypothesis assumes that the amount of damage is dependent on when the highest stress occurs)

   (b) C-D damage exponent values are not readily available.

There are many effects which change equivalent test levels as much as the noted difference between the P-M and C-D hypotheses. These are itemized as to importance:

1) Errors in measurement of field vibration and statistical variation from measurement to measurement will give larger changes in equivalent test levels then would be expected in substituting P-M hypothesis for C-D hypothesis or vice-versa.

2) Errors in measurement or estimation of specimen characteristics could change equivalent test levels as much as the choice of fatigue hypothesis.

3) The available value of 'b' or 'd' probably would originate from fatigue tests on polished specimens, whereas actual structure surface conditions would require a 'b' or 'd' based on notched specimens. This variation in fatugue slope due to surface conditions could exceed the variation in predicted damage due to the choice of fatigue hypothesis.

4) Variations in the actual distribution of peak stresses under random loading may cause the random fatigue curve to vary its position relative to the sine fatigue curve. In this test, the assumption of a Rayleigh distribution was valid but it is likely that there will be cases where:

   (a) Specimen characteristics will limit the extreme deflections.
   (b) The field vibration is severely clipped so that the specimen response will be clipped.

5) Variations occuring in:

   (a) vibration characteristics of different field vibration tests.
   (b) response characteristics of a given specimen as the impedance of the mounting changes.
   (c) response characteristics of several outwardly similar specimens.
   (d) values of transmissibility and natural frequency due to non-linearities with respect to input amplitude.
   (e) The field vibration will in general be a three dimensional input while the equivalent test will be one dimensional.

It is concluded that any rational fatigue damage hypothesis could be used in the development of the equivalence equations since the above items could cause larger variations in the equivalent test levels than the choice of the fatigue hypothesis.

Appendix J illustrates how an equivalent random vibration test would be derived.

IV. RECOMMENDATIONS

It is recommended that restrictions be placed on the application of the set of equivalence equations. The P-M hypothesis is not accurate in predicting sine-random fatigue relations in some materials and loading conditions[7]. If a large mean stress is applied so that the resulting applied random stresses are all tensile or all compressive, the effect of residual stresses caused by 3σ peaks may significantly change the effect of the damage caused by lower random stresses. It is expected that materials which show significant deviation from the linear damage accumulation rule when subjected to fluctuating loading will probably be the same materials which would show the most significant deviation from the random S-N fatigue curve predicted by the P-M hypothesis. Some materials which strain harden such as 24 S-T Alclad aluminum, electrically pure copper, 24 S-T aluminum, and 75 S-T aluminum[7] would probably fit into this class. Investigation of such materials could influence the applicability of the equivalent equations which scale damage between random loading and sine loading.

BIBLIOGRAPHY

(1) A. Palmgren, "Endurance of Ball Bearings" Z. Ver. Dtsch. Ing. 68 (1924) pg. 339.

(2) M. A. Miner, "Cumulative Damage in Fatigue" J. of Appl. Mech. 12 (1945) A-159.

(3) H. J. Corten and J. J. Dolan, "Cumulative Fatigue Damage" Proc. Int. Conf. on Fat. of Met. (1956) pg. 235.

(4) J. W. Miles, "On Structural Fatigue Under Random Loading" J. Aero. Sci. 21, (1945) pg. 753.

(5) M. Vet, "Study Program to Modify the Vibration Requirements of MIL-T-5422E and MIL-E-5272C" NADC Contract N62269-1452, Collins Radio CER1582.

(6) L. Root, "Random-Sine Fatigue Data Correlation" 33rd Symp. on Sh. and Vibr. (1963).

(7) Forrest, "Fatigue of Metals" Addison-Wesley (1962) pg. 117-118.

(8) F. Bollenrath and H. Cornelius, "Effect of Rest Periods on Endurance and Fatigue Strength of Metals" Bull. British Non-Ferrous Met. Res. Assoc. (1940) pg. 264.

(9) Anon, "Recovery and Permanent Damage to Metals Under Fatigue Conditions" Flumer Res. Inst. Rpt. R94/8 (1957).

(10) H. R. Spence and H. N. Luhrs, "Structural Fatigue Under Combined Sinusoidal and Random Vibration" J. of Acoust. Soc. of Amer. (33-8) (1961) pg. 1098.

APPENDIX

CONTENTS

APPENDIX A

SYMBOLS AND TERMS

a	Peak stress. Dimensions consistant with σ
A	Amplitude of sinusoidal vibration input level. In units of peak g's of vibration.
A_{fi}	Amplitude of sine vibration at frequency f_i.
A_{sd}	Vibration amplitude of sine dwell vibration
A_{ss}	Vibration amplitude of sine sweep vibration
$A_{sd,e}$	Vibration amplitude of sine dwell vibration which has been scaled in level from the original sine dwell level to produce the equivalent damage in the time duration of the final equivalent test, and with the equivalent vibration component applied at the specimen resonance.
$A_{ss,e}$	Similar to the above definition except that it applies to sine sweep vibration and, in addition to scaling to the equivalent test time, the extreme frequencies of the equivalent sine sweep test are the same as the frequency limits of the final equivalent test.
$A_{sd,ss,e}$	Vibration amplitude of sine dwell vibration which has been scaled from a sine sweep vibration test.
$A_{ss,sd,e}$	Similar to above but that scaling is from sine dwell to sine sweep.
$A_{sd,r,e}$	Similar to above but that scaling is from random to sine dwell.
$A_{ss,r,e}$	Similar to above but that scaling is from random to sine sweep.
$A_{sd,ee}$	Final equivalent sine dwell test which is a summation of all the original field vibration tests.
$A_{ss,ee}$	Similar to the above definition except that the final equivalent test is sine sweep.
b	The negative reciprocal of the S-N curve on log-log plot.
c	The linear damping coefficient used in the equations of motion.
c_c	Critical damping; $2\sqrt{km}$
C_s	The value of N which would result from the hypothetical extrapolation of the S-N fatigue equation to σ = 1psi
C-D	Abbreviation for Corten-Dolan criteria

d	The exponent which appears in the C-D damage equation.
db	Decibel
D	Fatigue damage
e	Natural or Naperian logarithm base
E( )	Expected value of some function
f	Frequency. Dimensions in cps.
f_e	The frequency of the equivalent sine dwell test vibration component
f_n	Resonant frequency of specimen
f_1	Frequency component of field vibration tests associated with highest stress.
f_{ij}	The $_j$th frequency component of the $_i$th field vibration test.
F( )	Fourier transformation symbol
g	Gravitational acceleration: 386 inches/sec^2.
$G(\omega)$	Fourier transform of the vibration input
$H(\omega)$	The complex transfer function
i	The imaginary number $\sqrt{-1}$
k	The elastic restoring coefficient used in the equations of motion.
K_1	The proportionality constant between stress and deflection
ln	Natural or Naperian logarithm symbol
m	Mass
M_i	The factor used in correlation testing to relate the actual specimen vibration characteristics to the hypothetical specimen characteristics.
n	The number of cycles the specimen experiences
n_i	The number of cycles that the specimen experiences at the $_i$th stress level.
N	The expected number of cycles to failure that a specimen will experience.

N_g	The expected number of cycles to failure that a specimen will experience in a multilevel test.
N_i	The expected number of cycles to failure that a specimen would experience if stressed at the ith stress level.
$p(a)$	The probability density function of peak stress at stress level a.
Q	Resonant magnification
R	The logarithmic sweep rate: $\ln f_2/f_1/t_{ss}$
$S(\omega)$	The theoretical spectral density at $\pm\omega$. Dimensions in g^2/radian.
t	Test time in seconds
t_{ss}	Sine sweep test time
t_{sd}	Sine dwell test time
t_e	Equivalent test time
t_r	Random test time
$W(f)$	The experimental spectral density at f. Dimensions in g^2/cps.
α_i	The fraction of the total number of cycles to failure which were conducted at the ith stress level.
$\Gamma(\ )$	The gamma function symbol
ϵ	Material strain
η	A measure of specimen damping: $1/2Q$
θ	A generalized damage exponent used in the derivation of equations.
Σ	Summation symbol.
σ	Stress symbol. Dimensions in psi. Where dealing with distribution of random stress peaks, it is the r.m.s. level.
σ_r	Random stress. Dimensions in r.m.s. psi
σ_s	Sine stress. Dimensions in peak psi
ϕ	An approximation term used in the damage expression due to sine sweep testing.

Ω Ohms of electrical resistance

ω Angular frequency. Dimensions in radians/sec.

APPENDIX B

DERIVATION OF EQUATIONS

The following analysis is based upon the Palmgren-Miner[1][2] (P-M) and Corten Dolan[3] (C-D) fatigue damage accumulation hypotheses. It deals with vibration environments whose descriptive parameters remain constant and are applied sequentially. The model is a linear single degree of freedom oscillator. The principle goal of this analysis is to equate fatigue damages using vibration input parameters rather than terms of stress or strain.

It is assumed that any complex equipment may be represented by a combination of non-interacting single degree of freedom oscillators and that the damage due to combined vibration types may be handled by considering the various types of vibration separately. The case of non-stationary or time varying vibration will be treated by breaking that environment into a series of sequential environments each of which has constant parameters.

The method of solution is outlined at this point. Let the field vibration which the specimen experiences in its effective life time be presented as three types of vibration envelopes:

1) W_i The ith random vibration envelope
2) $A_{sd,i}$ The ith sinusoidal dwell vibration envelope
3) $A_{ss,i}$ The ith sinusoidal sweep vibration envelope

The first operation is the reduction of all the envelopes of one type of vibration into one envelope of that type. As a result, one random envelope W_e with the same damage potential as all of the use vibration random envelopes will have been derived. This is repeated for each of the other types of vibration.

The second operation is the scaling of damage resulting from one type of vibration to an equal damage resulting from the type of vibration which is desired to use for testing purposes in the lab.

Symbolically:

$$W_e \Rightarrow A_{sd,r}$$

$$W_e \Rightarrow A_{ss,r}$$

$$A_{ss,e} \Rightarrow W_{ss}$$

$$A_{sd,e} \Rightarrow W_{sd}$$

$$A_{sd,e} \Rightarrow A_{ss,sd}$$

$$A_{ss,e} \Rightarrow A_{ss,ss}$$

The final subscripts on the right hand terms indicate the initial equivalent test. The first equivalent test which results from summing damages of one type of vibration is scaled in the second operation to a second equivalent test.

The third and final operation is a summation of the three equivalent tests into one final equivalent test. Since all tests are by this stage transformed into the final desired type of vibration, this is a summation like that used in the first operation. The overall process may be presented in the following manner for an equivalent random test:

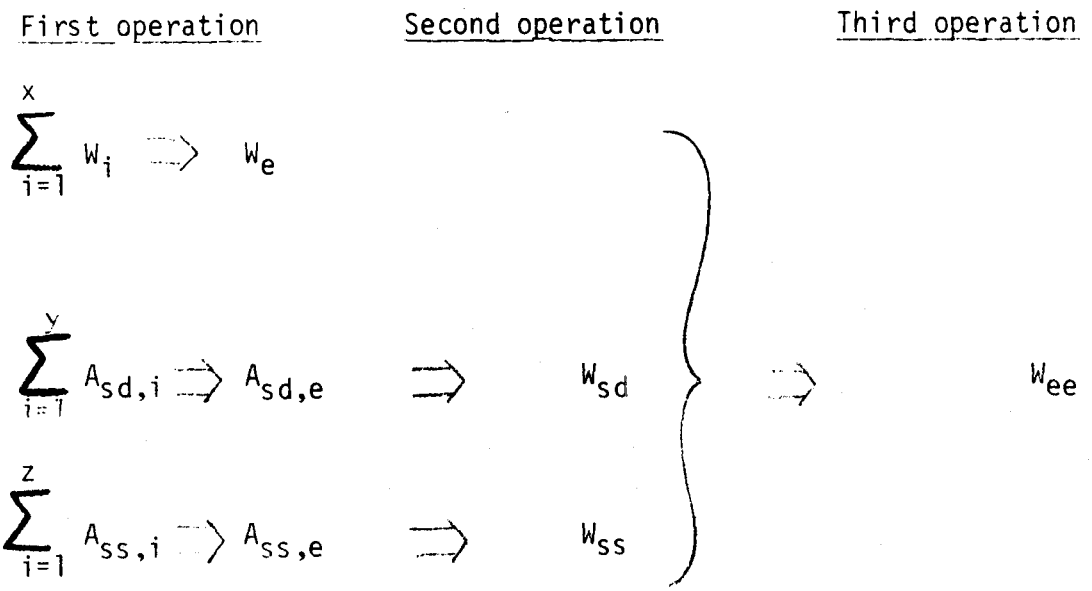

The first step of the detailed development of the equivalence equations involves altering the basic form of the C-D equation to obtain a form similar to the P-M equation. This simplifies many of the later manipulations. The P-M hypothesis is usually presented as:

$$D = \sum_{i=1}^{m} n_i / N_i \qquad (1)$$

When D is unity, the specimen is assumed to have failed. This is a linear damage equation; the N_i term is the life from an S-N plot and the change in D is proportional to a change in n_i. On a log-log plot of stress vs. cycles to failure for specimens run at a constant stress level, the locus of failure points is approximately a straight line, the slope of which is $-1/b$.

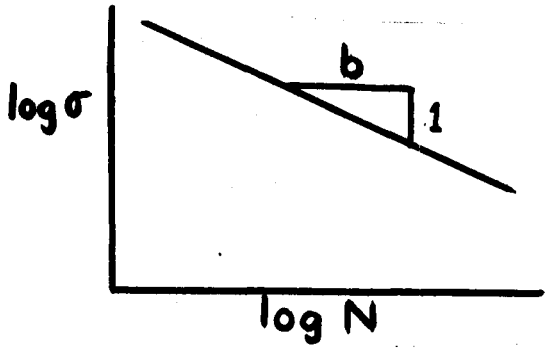

Figure 1

The equation of this failure curve is:

$$N\sigma^{b} = C \tag{2}$$

Although the curve is a locus of failure points, the accumulation of damage, or cycle ratio, for a specimen is considered to occur with the N_i defined by this line regardless of the ordering of stress levels.

The (C-D) hypothesis is usually expressed as:

$$\frac{N_g}{N_1} = \frac{1}{\sum_{i=1}^{m} \alpha_i \left(\frac{\sigma_i}{\sigma_1}\right)^{d}} \tag{3}$$

This may also be expressed as:

$$N_1 \sigma_1^{d} = \sum_{i=1}^{m} n_i \sigma_i^{d} \tag{4}$$

where n_i is $N_g \times {}_i$, the number of cycles occurring at the $_i$th stress level.

$$1 = \sum_{i=1}^{m} \frac{n_i}{N_1} \left(\frac{\sigma_i}{\sigma_1}\right)^{d} \tag{5}$$

This can be transformed to a (P-M) type form by letting $N_i' = N_1\left(\frac{\sigma_1}{\sigma_i}\right)^{d}$. This results in the equation:

$$1 = \sum_{i=1}^{m} \frac{n_i}{N_i'} \tag{6}$$

Besides being similar to the P-M equation, the plot of the damage accumulation curve shows the similarity of the two hypothesis.

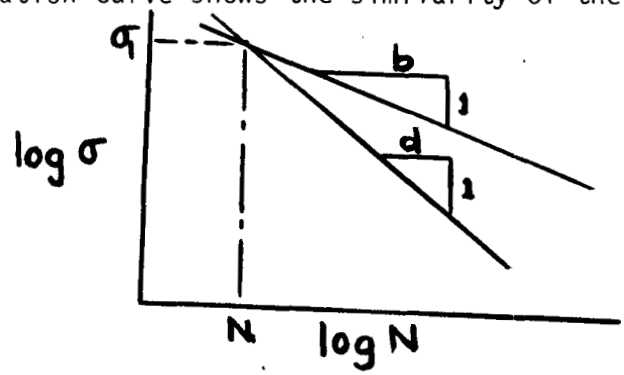

Figure 2

The curve with the slope - $1/d$ and intersecting the S-N curve at σ_1, N_1 is the (C-D) damage curve. In general $d < b$[3] so the slope is steeper than for the S-N curve. It can be observed that the high stress σ_1 causes the lower stresses σ_i to have greater damage potential than if σ_1 had not occurred. The two criterias become equivalent when d = b. In order to simplify the derivations, the damage exponent will be referred to as θ until it is desired to specify which hypothesis to use.

$$D = \sum_{i=1}^{m} n_i / N_i = \sum_{i=1}^{m} \frac{n_i}{N_1} \left(\frac{\sigma_i}{\sigma_1} \right)^{\theta} \tag{7}$$

The structural model will be represented by the Voight model in Figure 3.

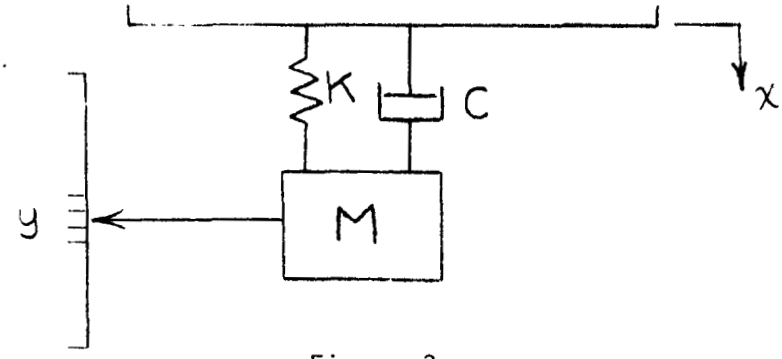

Figure 3

The differential equation of motion in terms of y, the relative displacement, and x the absolute input displacement, is:

$$M\ddot{y} + C\dot{y} + Ky = -M\ddot{x} \tag{8}$$

which is the equivalent of:

$$\ddot{y} + 2\eta\omega_n\dot{y} + \omega_n^2 y = -\ddot{x} \tag{9}$$

The complex transfer function representing the system is defined as

$$H(\omega) = \frac{F[\text{output}]}{F[\text{input}]} \tag{10}$$

where F is the Fourier Transformation

$$\begin{aligned} F[f(t)] &= \int_{-\infty}^{+\infty} f(t)e^{-i\omega t}\,dt = F(\omega) \\ F\left[\frac{d^n f(t)}{dt^n}\right] &= (i\omega)^n F(\omega) \\ G(\omega) &= \int_{-\infty}^{+\infty} \ddot{x}(t)e^{-i\omega t}\,dt \end{aligned} \tag{11}$$

Transforming the differential equation (9) and solving for $H(\omega)$.

$$\left[(i\omega)^2 + 2\eta\omega_n(i\omega) + \omega_n^2\right]F(\omega) = -G(\omega)$$

$$H(\omega) = \frac{F(\omega)}{G(\omega)} = \frac{-1}{\omega_n^2 - \omega^2 + 2i\eta\omega_n\omega} \tag{12}$$

It is useful when dealing with magnitudes to use the absolute value of $H(\omega)$.

$$|H(\omega)| = \frac{1}{\sqrt{\omega_n^4 + \omega^4 - 2\omega^2\omega_n^2(1-2\eta^2)}} \tag{13}$$

The maximum $|H(\omega)|$ for a system with a Q=20 occurs at $\omega = .9987\ \omega_n$ For practical purposes the maximum $|H(\omega)|$ occurs at $\omega = \omega_n$.

$$|H(\omega_n)| = \frac{Q}{\omega_n^2} \tag{14}$$

When dealing with frequency expressed in units of cps, the expressions become

$$|H(f)| = \frac{1}{4\pi^2\sqrt{f_n^4 + f^4 - 2f^2f_n^2(1-2\eta^2)}} \tag{15}$$

$$|H(f_n)| = \frac{Q}{4\pi^2 f_n^2} \tag{16}$$

To express stress, σ , in terms of acceleration input, the following development is used.

$$\sigma = K_1 y \tag{17}$$

For a given deflection shape the proportionality constant K_1 is defined. It is a constant for all frequencies in a single degree of freedom model and nearly constant for the resonant frequency region in a distributed mass system. By the previous derivation it can be shown that

$$\sigma = K_1 |H(\omega)| \ddot{x} = K_1 |H(f)| \ddot{x} \tag{18}$$

which is the basic formula for stress in sinusoidal sweep and sinusoidal dwell tests.

For the case of random vibration the rms stress is

$$\sigma_{rms} = K_1 y_{rms}$$

$$y_{rms} = \sqrt{\int_{-\infty}^{+\infty} |H(\omega)|^2 \, S(\omega) \, d\omega} = \sqrt{\int_{0}^{+\infty} |H(f)|^2 \, W(f) \, df} \tag{19}$$

where $S(\omega)$ is the theoretical spectral density in $\left[\frac{(\text{amplitude})^2}{\text{radians per second}}\right]$ and $W(f)$ is the experimental spectral density in $\left[\frac{(\text{amplitude})^2}{\text{cycles per second}}\right]$.

At this stage, the damage due to various types of vibration can be derived. The first and simplest type is sinusoidal dwell. From equations (7), (18), and the equality

$$n_i = f_i t_i \tag{20}$$

$$D = \sum_{i=1}^{m} \frac{n_i}{N_i} \left(\frac{\sigma_i}{\sigma_1}\right)^{\theta} = \sum_{i=1}^{m} \sum_{j=1}^{p} \frac{f_{ij} t_i}{N_1} \left[\frac{K_1 |H(f_{ij})| A_{ij}}{K_1 |H(f_1)| A_1}\right]^{\theta}$$

$$D = \sum_{i=1}^{m} \sum_{j=1}^{p} \frac{f_{ij} t_i}{N_1} \left[\frac{|H(f_{ij})|}{|H(f_1)|} \frac{A_{ij}}{A_1}\right]^{\theta} \tag{21}$$

The summation applies to i spectrums or tests each of which could be composed of several acceleration inputs A_{ij}. The particular A_{ij} in the summation which produces the greatest stress in the specimen is A_1, and N_1 is the cycles-to-failure associated with the highest stress, and $|H(f_1)|$ is the transfer function for A_1. When D = 1, a test run for N_1 cycles at A_1 input would result in the same damage as i tests at A_i input. For generality it is assumed that an equivalent test will be performed at resonance. Therefore

$$|H(f_n)| = Q/4\pi^2 f_n^2 \tag{22}$$

$$n_e = f_n t_e \tag{23}$$

where t_e is the equivalent test time.

Now equation (21) for the equivalent test would be

$$D = \frac{f_n t_e}{N_e} \tag{24}$$

since only one level is run. This damage can be equated to the damage caused by the field vibration (equation 21)

$$\frac{f_n t_e}{N_e} = \sum_{i=1}^{m} \sum_{j=1}^{p} \frac{f_{ij}\, t_i}{N_1} \left[\frac{|H(f_{ij})|}{|H(f_1)|} \frac{A_{ij}}{A_1} \right]^{\theta} \tag{25}$$

$$\frac{N_1}{N_e} \left[|H(f_1)| A_1 \right]^{\theta} = \sum_{i=1}^{m} \sum_{j=1}^{p} \left(\frac{f_{ij}}{f_n} \right) \left(\frac{t_i}{t_e} \right) \left[|H(f_{ij})| A_{ij} \right]^{\theta}$$

Now N_1 and N_e are values taken from the SN plot, therefore $N_1\sigma_1^b = N_e\sigma_e^b$

$$\frac{N_1}{N_e} = \left(\frac{\sigma_e}{\sigma_1}\right)^b = \left(\frac{K_1|H(f_e)|A_e}{K_1|H(f_1)|A_1}\right)^b = \left(\frac{|H(f_e)|A_e}{|H(f_1)|A_1}\right)^b$$

$$(|H(f_e)|A_e)^b(|H(f_1)|A_1)^{\theta-b} = \sum_{i=1}^{m}\sum_{j=1}^{p}\left(\frac{f_{ij}}{f_n}\right)\left(\frac{t_i}{t_e}\right)(|H(f_{ij})|A_{ij})^\theta \qquad (26)$$

$$A_e = \frac{4\pi^2 f_n^2}{Q}\left((|H(f_1)|A_1)^{b-\theta}\sum_{i=1}^{m}\sum_{j=1}^{p}\left(\frac{f_{ij}}{f_n}\right)\left(\frac{t_i}{t_e}\right)(|H(f_{ij})|A_{ij})^\theta\right)^{1/b}$$

In the case of the (C-D) hypothesis, θ is d and A_1 is the highest equivalent input occurring prior to i = 1. That is, more explicitly, the summation can only be taken for stresses which do not exceed the highest prior damaging stress which occurred due to A_1. Whenever a more recent high stress occurs, a new value of A_1 is taken and a new summation is taken from that point until a later higher stress. For a case in which the stress levels are monotonically increasing, the equivalent test is equivalent to that determined by a PM damage criteria since there would be only one term in each summation and the $|H(f_{ij})|A_{ij}$ would be the same as the $|H(f_1)|A_1$ which appeared outside the summation sign representing the highest prior stress level. For the Palmgren Miner case θ = b

$$A_e = \frac{4\pi^2 f_n^2}{Q}\left(\sum_{i=1}^{m}\sum_{j=1}^{p}\left(\frac{f_{ij}}{f_n}\right)\left(\frac{t_i}{t_e}\right)(|H(f_{ij})|A_{ij})^b\right)^{1/b} \qquad (27)$$

Here again, of course, the implication is that the equivalent test will be run at the specimen resonance. The value of $|H(f_{ij})|$ can be entered into (27) and simplified

$$A_e = \left(\sum_{i=1}^{m} \sum_{j=1}^{p} \left(\frac{f_{ij}}{f_n} \right) \left(\frac{t_i}{t_e} \right) \frac{A_{ij}^{\,b}}{\left(Q^2 \left(1 + \left(f_{ij}/f_n \right)^4 \right) - \left(f_{ij}/f_n \right)^2 \left(2Q^2 - 1 \right) \right)^{b/2}} \right)^{1/b} \tag{28}$$

Next, the random vibration equivalent tests will be derived. The case of scaling several sequential tests to one equivalent test is based on a similar development to that for the sine dwell tests.

The first assumption is that the specimen has a narrow band response so that a Rayleigh distribution of peak stresses will occur. The relatively narrow band pass also implies that only the random spectrum in the immediate frequency region of resonance produces any significant response. Therefore random stresses will be based upon the spectral density at resonance.

To obtain the rms deflection, one must refer again to the complex transfer function $|H(\omega)|$. Mean square response can be defined as:

$$E(y^2) = \int_{-\infty}^{+\infty} S_y(\omega)\, d\omega = \int_{-\infty}^{+\infty} S_x(\omega) \left| H(\omega) \right|^2 d\omega \tag{29}$$

Since $S_y(\omega)$ will not be referred to again, $S_x(\omega)$ will be referred to as $S(\omega_n)$, the input at resonance.

$$E(y^2) = S(\omega_n) \int_{-\infty}^{+\infty} \frac{d\omega}{\left(\omega_n^4 + \omega^4 - 2\omega^2 \omega_n^2 (1 - 2\eta^2) \right)} \tag{30}$$

The solution of this integral is:

$$E(y^2) = \frac{\pi Q S}{\omega_n^3} \tag{31}$$

The theoretical spectral density is related to the actual spectral density W, by the relation:

$$S = \frac{W}{4\pi} \tag{32}$$

and using the relation, $\omega = 2\pi f$, we get:

$$E(y^2) = \frac{Q W}{32\pi^3 f_n^3} \tag{33}$$

The relation between rms stress and rms deflection remains the same as for the sinusoidal case so that the expression for stress becomes:

$$\sigma_{rms} = K_1 y_{rms} = K_1 \sqrt{E(y^2)} = K_1 \left(\frac{Q W}{32\pi^3 f_n^3} \right)^{1/2} \tag{34}$$

Referring back to (7) for the expression for damage,

$$D = \sum_{i=1}^{m} \frac{n_i}{N_{1,r}} \left(\frac{\sigma_i}{\sigma_1} \right)^{\theta} = \sum_{i=1}^{m} \frac{n_i}{N_{1,r}} \left(\frac{W_i}{W_1} \right)^{\theta/2} \tag{35}$$

The damage expression or cycle ratio for random vibration is expressed as:

$$D = f t \int_0^{\infty} \frac{p(a)}{N(a)} da$$

The frequency term is the mean frequency occurring in time t and is most accurate for narrow band random vibration where $f \approx f_n$. The number of stress peaks occurring in amplitude interval da is $f \cdot t \cdot p(a)\, da$ where $p(a)$ is the probability of a stress peak occurring in interval da. For narrow

band random, a close approximation to the actual distribution can be made with the Rayleigh distribution:

$$p(a) = \frac{a}{\sigma^2} e^{-a^2/2\sigma^2}$$

In this expression a and σ are in terms of stress. The variance is expressed as the rms stress level. The terms N(a) can be expressed in the form of (7) and the final expression for damage is:

$$D = \frac{f_n t}{C_s \sigma^2} \int_0^\infty a^{\theta+1} e^{-a^2/2\sigma^2} da$$

The θ term is the negative reciprocal of the slope of the damage accumulation curve. The solution of the integral gives:

$$D = \frac{f_n t}{C_s} \sigma^\theta 2^{\theta/2} \Gamma(1+\theta/2)$$

From this relation it follows that the random vibration S-N curve should be:

$$N\sigma^\theta = C_s/2^{\theta/2}\Gamma(1+\theta/2) = C_r \qquad (36)$$

It is apparent from (36) that if the (C-D) damage hypothesis is assumed and $\theta = d$, the random S-N slope is different than the sine S-N curve. The separation of the S-N curves at a given value of N is:

$$\frac{\sigma_s}{\sigma_r} = \sqrt{2}\left(\sigma_s^{\theta-b}\Gamma(1+\theta/2)\right)^{1/\theta}$$

This separation is therefore stress dependent as long as the slopes of the random and sine S-N curves are not parallel at a given value of N. The above relation assumes a Rayleigh distribution of peak stresses and for low values of Q this would not be an accurate assumption.

Using (35) one can obtain relations between several random envelopes. The damage for the equivalent random test can be written as:

$$D = \frac{n_e}{N_e} \tag{37}$$

Equating (37) and (35) and using the relation $n_i = f_n t$ the following relations are obtained:

$$\frac{n_e}{N_e} = \sum_{i=1}^{m} \frac{n_i}{N_1}\left(\frac{W_i}{W_1}\right)^{\theta/2} \tag{38}$$

$$\frac{f_n t_e}{N_e} = \sum_{i=1}^{m} \frac{f_n t_i}{N_1}\left(\frac{W_i}{W_1}\right)^{\theta/2} \tag{39}$$

$$\frac{N_1}{N_e} = \sum_{i=1}^{m} \frac{t_i}{t_e}\left(\frac{W_i}{W_1}\right)^{\theta/2} \tag{40}$$

From equation (36) and (34) the following is obtained:

$$\frac{N_1}{N_e} = \left(\frac{\sigma_e}{\sigma_1}\right)^{\theta} = \left(\frac{W_e}{W_1}\right)^{\theta/2} \tag{41}$$

Therefore:

$$W_e = W_1\left[\sum_{i=1}^{m} \frac{t_i}{t_e}\left(\frac{W_i}{W_1}\right)^{\theta/2}\right]^{2/\theta} \tag{42}$$

The same damage criteria is assumed to apply for varying stresses which occur in random vibration and non-repeating blocks of different level vibration. The $2/\theta$ exponent on the outside of the bracket is a function of the slope of the random S-N curve. The $\theta/2$ exponent within the bracket is a function of the damage accumulation for non-repeating blocks of vibration. The final equations used in this report have $\theta = b$. Therefore the equivalent spectral density becomes:

$$W_e = \left[\sum_{i=1}^{m} \left(\frac{t_i}{t_e}\right) W_i^{b/2}\right]^{2/b} \tag{43}$$

The equation for random vibration damage which will be used to equate random to sinusoidal damage is taken from (37), (36) and (34).

$$D = \frac{n_e}{N_e} = \frac{f_n t_e}{N_e} \tag{37}$$

$$N_e = \frac{C_s}{\sigma_e^{\theta}\, 2^{\theta/2}\, \Gamma(1+\theta/2)} \tag{36}$$

$$\sigma_e = K_1 \left(\frac{Q W_e}{32 \pi^3 f_n^3} \right)^{1/2} \tag{34}$$

$$D = \frac{K_1^{\theta}}{C_s} \left(\frac{W_e Q}{16} \right)^{\theta/2} \frac{t_e \, \Gamma(1 + \theta/2)}{\pi^{3\theta/2} f_n^{3\theta/2 - 1}} \tag{44}$$

The sinusoidal sweep vibration damage is developed by starting with (7) once again.

$$D = \sum_{i=1}^{m} \frac{n_i}{N_1} \left(\frac{\sigma_i}{\sigma_1} \right)^{\theta} \tag{7}$$

Since the stress level is continuously varying in this test, the value of m would approach infinity. A differentially small component of damage could be expressed for the damage occurring at the i th stress level.

$$dD_i = \frac{dn_i}{N_1} \left(\frac{\sigma_i}{\sigma_1} \right)^{\theta} = \left(\frac{1}{N_1 \sigma_1^{\theta}} \right) \sigma_i^{\theta} \, dn_i \tag{45}$$

The bracketed value will be considered a constant. The value of n_i can be considered to have occurred within a very short time, dt, as the vibration sweeps thru the i th stress level. Therefore, $dn_i = f_i dt$. The most popular type of sine sweep is one in which the frequency varies logarithmically according to the equation:

$$\frac{df}{dt} = Rf \tag{46}$$

where R is the sweep rate. Solution of (44) gives the following value for R:

$$R = \frac{\ln f_2/f_1}{t_{ss}}$$

where f_2 and f_1 are the extreme frequencies of the sine sweep and t_{ss} is the time required to sweep from f_1 to f_2. Using these relations with (18), equation (45) can be changed.

$$dD_i = \frac{dn_i \sigma_i^\theta}{N_1 \sigma_1^\theta} = \left(\frac{1}{N_1 \sigma_1^\theta}\right) f_i \, dt \left(K_1 |H(\omega)| A_{fi}\right)^\theta$$

$$dt = \frac{df_i}{f_i R}$$

$$dD_i = \left(\frac{1}{N_1 \sigma_1^\theta}\right) \frac{f_i \, df_i}{f_i R} K_1^\theta \left(|H(f_i)| A_{fi}\right)^\theta$$

$$D = \frac{K_1^\theta}{R N_1 \sigma_1^\theta} \int_{f_1}^{f_2} \left(|H(f)| A_f\right)^\theta df = \frac{K_1^\theta t_{ss}}{\ln f_2/f_1 \, N_1 \sigma_1^\theta} \int_{f_1}^{f_2} \left(|H(f)| A_f\right)^\theta df \qquad (47)$$

The term A_f is the table input at frequency f (the subscript i has been dropped). The value t_{ss} is for one sweep but this could be the time for several sweeps to occur if the test lasts an even number sweep durations in time t_{ss}. It is assumed that the highest stress occurs at fn during the first sweep. The case for several sequential sine sweeps is:

$$D = \frac{K_1^\theta}{N_1 \sigma_1^\theta} \sum_{i=1}^{m} \frac{t_{si}}{\ln f_{2i}/f_{1i}} \int_{f_{1i}}^{f_{2i}} \left(|H(f)| A_{fi}\right)^\theta df \qquad (48)$$

Finding an equivalent sweep level (A_{fe}) for several equivalent sine sweeps is done in a manner similar to previous derivations but the assumption must be made that A_{fi} is a constant with respect to frequency so that that term can be taken out of the integral. This assumption is consistant with that made for the random spectrum being constant in the resonant frequency range. Very little damage occurs outside of the half power points of the specimen so this assumption is valid. This assumption also makes it possible to perform another simplification. If the integrals which appear in the summation have different limits but these limits fall reasonably far from the resonance of the specimen, then the damage resulting at the extreme frequencies is of little importance and the extreme frequencies could be changed to coincide with that of the equivalent test frequency range. The resulting equivalent test can be expressed as follows:

$$\frac{t_{se} A_e^{\theta} K_1^{\theta}}{\ln f_{2e}/f_{1e}\, N_e \sigma_1^{\theta}} \int_{f_{1e}}^{f_{2e}} (|H(f)|)^{\theta} df = \frac{K_1^{\theta}}{N_1 \sigma_1^{\theta}} \sum_{i=1}^{m} \frac{t_{si} A_i^{\theta}}{\ln f_{2i}/f_{1i}} \int_{f_{1e}}^{f_{2e}} (|H(f)|)^{\theta} df$$

The values of A_e and A_i are taken at specimen resonance. By cancelling the integrals and regrouping, the resulting equation may be obtained.

$$A_e^{\theta} = \frac{N_e}{N_1} \left(\frac{\sigma_e}{\sigma_1}\right)^{\theta} \sum_{i=1}^{m} \left(\frac{\ln f_{2e}/f_{1e}}{\ln f_{2i}/f_{1i}}\right) \left(\frac{t_{si}}{t_{se}}\right) A_i^{\theta}$$

Since N_e and N_1 lie on the S-N sine curve, the ratio N_e/N_1 can be expressed in terms of stress

$$\frac{N_e}{N_1} = \left(\frac{\sigma_1}{\sigma_e}\right)^{b}$$

$$A_e^{\theta} = \left(\frac{\sigma_i}{\sigma_e}\right)^{b-\theta} \sum_{i=1}^{m} \left(\frac{\ln f_{2e}/f_{1e}}{\ln f_{2i}/f_{1i}}\right)\left(\frac{t_{si}}{t_{se}}\right) A_i^{\theta}$$

At resonance $\frac{\sigma_i}{\sigma_e} = \frac{A_i}{A_e}$

$$A_e = \left(\frac{A_i}{A_e}\right)^{\frac{b-\theta}{\theta}} \left[\sum_{i=1}^{m} \left(\frac{\ln f_{2e}/f_{1e}}{\ln f_{2i}/f_{1i}}\right)\left(\frac{t_{si}}{t_{se}}\right) A_i^{\theta}\right]^{1/\theta} \tag{49}$$

This expression is similar in form to (26). For monotonically increasing test levels this is equivalent to the (P-M) criteria. When $\theta = b$ the (P-M) version of (49) can be found:

$$A_e = \left[\sum_{i=1}^{m} \left(\frac{\ln f_{2e}/f_{1e}}{\ln f_{2i}/f_{1i}}\right)\left(\frac{t_{si}}{t_{se}}\right) A_i^{b}\right]^{1/b} \tag{50}$$

At this stage all three basic types of vibration damage have been derived and the scaling of damage from one type of vibration to another can be made. Since the equations are developed, the algebraic manipulations are omitted and the resulting equivalent level for one type of vibration is presented in terms of the parameters of the field vibration test which is to be scaled.

SINE SWELL FROM SINE SWEEP

GENERAL CASE

$$A_{sd} = \left[\left(\frac{A_{ss} f_n Q}{4\pi^2 f_n^2}\right)^{b-\theta} \left(\frac{t_{ss}}{t_{sd}}\right) \frac{1}{(f_{sd})(\ln f_2/f_1)(|H(f_{sd})|)^b} \int_{f_1}^{f_2} (|H(f)| A_{ss})^{\theta} df\right]^{1/b} \tag{51}$$

In this equation subscript ss denotes sine sweep and sd denotes sine dwell. The term Ass, f_n is the sine sweep input level at resonance and A_{ss} is the sine sweep input at frequency f. f_2 and f_1 are the frequency limits of the sine sweep and f_{sd} is the frequency at which the sine dwell test is conducted. t_{ss} and t_{sd} are the test times of the sine sweep and sine dwell tests. The following equation is the case when $\theta = b$, $f_{sd} = f_n$ and A_{ss} is a constant in the resonant frequency region.

$$A_{sd} = \frac{4\pi^2 A_{ss,f_n}}{Q}\left[\left(\frac{t_{ss}}{t_{sd}}\right)\frac{(f_n)^{2b-1}}{(\ln f_2/f_1)}\int_{f_1}^{f_2}(|H(f)|)^b df\right]^{1/b} \tag{52}$$

SINE SWEEP FROM SINE DWELL GENERAL CASE

$$A_{ss} = A_{sd}\left[\left(\frac{4\pi^2 f_n^2}{Q}\right)^{b-\theta}\left(\frac{t_{sd}}{t_{ss}}\right)\frac{(f_{sd})(\ln f_2/f_1)(|H(f_{sd})|)^b}{\int_{f_1}^{f_2}(|H(f)|)^\theta df}\right]^{1/b} \tag{53}$$

The subscripts have the same meaning as in the previous relation. The assumption has been made that A_{ss} is constant in the resonant frequency region. The simplified equation in which $b = \theta$ and $f_{sd} = f_n$ is presented below:

$$A_{ss} = \frac{QA_{sd}}{4\pi^2}\left[\left(\frac{t_{sd}}{t_{ss}}\right)\frac{(\ln f_2/f_1)}{(f_n^{2b-1})\int_{f_1}^{f_2}(|H(f)|)^b df}\right]^{1/b} \tag{54}$$

RANDOM FROM SINE DWELL GENERAL CASE

$$W = \frac{16\pi^3}{Q}\left[\frac{(f_{sd} f_n^{\frac{3\theta}{2}-1})}{\Gamma(1+\theta/2)}\left(\frac{t_{sd}}{t_r}\right)A_{sd}^b K_1^{b-\theta}(|H(f_{sd})|)^b\right]^{2/\theta} \tag{55}$$

In the above equation the subscript R refers to random test parameters. In this case the stress-deflection ratio K_1 does not cancel out. This is an awkard result of the assumption that the random S-N curve is not parallel to the sinusoidal S-N curve. Experimentally both curves have approximately the same slope. If one assumes that $\theta = b$ and that $f_{sd} = f_n$ then the following equation results:

$$W = \frac{16\pi^2}{Q}\left[\frac{f_n^{\frac{3b}{2}} A_{sd}^{\,b}}{\Gamma(1+b/2)}\left(\frac{t_{sd}}{t_r}\right)\left(|H(f_{sd})|\right)^b\right]^{2/b} \tag{56}$$

SINE DWELL FROM RANDOM GENERAL CASE

$$A_{sd} = \left[\left(\frac{QW}{16\pi^3}\right)^{\theta/2}\frac{\Gamma(1+\theta/2)}{\left(f_{sd}\, f_n^{\frac{3\theta}{2}-1}\right)}\left(\frac{t_r}{t_{sd}}\right)K_1^{b-\theta}\left(|H(f_{sd})|\right)^b\right]^{1/b} \tag{57}$$

All conditions and subscripts for (57) are the same as for (55). Similar simplifications to that made for (56) results in the following:

$$A_{sd} = \left[\frac{QW}{16\pi^3}\right]^{1/2}\left[\frac{\Gamma(1+b/2)}{\left(f_n^{\frac{3b}{2}}\right)}\left(\frac{t_r}{t_{sd}\left(|H(f_{sd})|\right)^b}\right)\right]^{1/b} \tag{58}$$

SINE SWEEP FROM RANDOM GENERAL CASE

$$A_{ss} = \left[\left(\frac{t_r}{t_{ss}}\right)\frac{\Gamma(1+\theta/2)\, f_n^{\left(2b-\frac{7\theta}{2}+1\right)}\, Q^{\frac{3\theta}{2}-b}\ln f_2/f_1\, W^{\theta/2}}{\pi^{\frac{3\theta}{2}}\, 4^\theta\, K_1^{b-\theta}\int_{f_1}^{f_2}\left(|H(f)|\right)^\theta df}\right]^{1/b} \tag{59}$$

Here again the stress deflection ratio K_1 appears. The simplification to the P-M relation is performed by letting $\theta = b$.

$$A_{ss} = \left[\left(\frac{t_r}{t_{ss}}\right)\frac{\Gamma(1+b/2)\, Q^{b/2}\ln f_2/f_1\, W^{b/2}}{f_n^{\frac{3b}{2}-1}\, 4^b\int_{f_1}^{f_2}\left(|H(f)|\right)^b df}\right]^{1/b} \tag{60}$$

RANDOM FROM SINE SWEEP GENERAL CASE

$$W=\left[A_{ss}^{b}\left(\frac{t_{ss}}{t_r}\right)\frac{\pi^{\frac{3\theta}{2}}4^{\theta}K_1^{b-\theta}\int_{f_1}^{f_2}(|H(f)|)^{\theta}df}{\Gamma(1+\theta/2)f_n^{2b-\frac{3\theta}{2}+1}Q^{\frac{3\theta}{2}-b}\ln f_2/f_1}\right]^{2/\theta}$$

The simplification to the (P-M) relation is performed by letting $\theta = b$.

$$W=\left[A_{ss}^{b}\left(\frac{t_{ss}}{t_r}\right)\frac{\pi^{\frac{3b}{2}}4^{b}f_n^{\frac{3b}{2}+1}\int_{f_1}^{f_2}(|H(f)|)^{b}df}{\Gamma(1+b/2)Q^{b/2}\ln f_2/f_1}\right]^{2/b} \qquad (61)$$

This completes the derivation of the basic equivalent equations.

APPENDIX C

COMPUTER PROGRAM

A program was written in Fortran 2 language to generate a family of equivalent curves for a range of Q. This allowed selection of the equivalent test once the test item natural frequencies and Q's are estimated. The program generates a single preselected type of equivalent test.

The sequence of transforming the field or use vibration to an equivalent vibration was broken into three phases. A prior step is the choice of the type of equivalent test, its duration and frequency range, the field vibration inputs, frequency ranges, and durations. In addition, the range of Q's and increments of Q and frequency must be predecided.

Phase I combines all like types of field vibration into one (1) test of that type lasting the same time as the final equivalent test. If only one component of a certain type of vibration existed in the field vibration then its level would be scaled to produce the same damage in the equivalent test time duration. The equations used are (27) (43) and (49) of Appendix B.

Phase II is the transformation of the phase I levels into components of the preselected type of vibration. At the completion of Phase II, a component exists for each type of vibration which was present in the field vibration. Equations (52) (54) (56) (58) (60) and (61) are used with slight modification in Phase II.

Phase III is the combining of these like types of vibration into the final equivalent level using some equations of phase I. A diagram of the process is presented for obtaining a sine sweep equivalent.

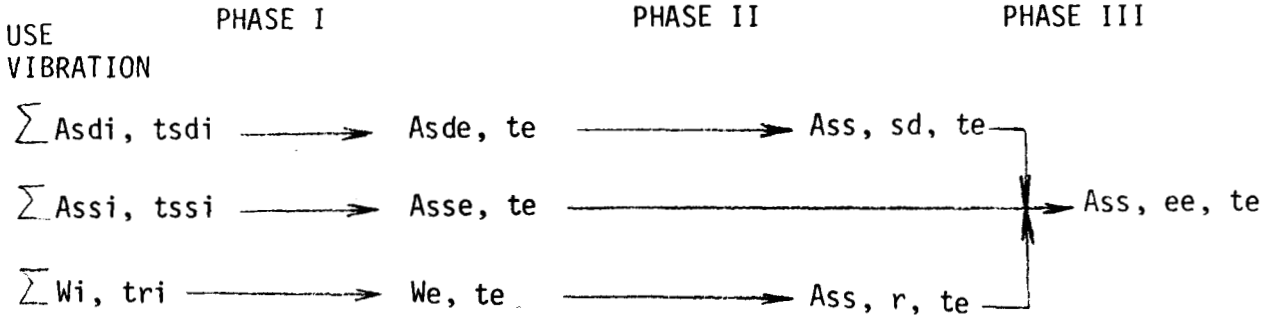

This process is repeated for every change in resonant frequency throughout the equivalent test frequency range. At that point a step is made to the next higher Q and the process is repeated to get a new set of equivalent levels.

The output is in the form of tables of numbers which can be plotted into families of curves. From these curves, interpolations can be made to obtain actual equivalent levels for points which don't fall on the curves.

The transformation equations are modified to minimize the computation time. The integral appearing in the sine sweep equations required major simplification due to the following difficulties:

(1) Scaling of large numbers. As f or fn is changed, the integrand which is raised to the $\theta/2$ power becomes greater than 10^{50} . This is greater than the capacity of the computer causing an accumulator overflow.

The problem of the large number can be helped by expressing the integral in dimensionless ratios. The original form of the damage equations is:

$$D = \left(\frac{f_n^2}{Q}\right)^b \frac{t_{ss}}{\ln f_2/f_1 \, N_1} \int_{f_1}^{f_2} \frac{df}{\left[f_n^4 + f^4 - 2f^2 f_n^2 (1-2\eta^2)\right]^{\theta/2}}$$

This can be changed to the form:

$$D = \frac{t_{ss}}{\ln f_2/f_1 \, N_1} \int_{f_1}^{f_2} \frac{df}{\left[Q^2\left(\left(f/f_n\right)^4 + 1\right) - \left(f/f_n\right)^2 \left(2Q^2 - 1\right)\right]^{b/2}}$$

(2) Time for solution. It required one minute for an IBM 7074 to solve 8 integrals of this nature. Since this computation is repeated on the order of a thousand times in an overall scaling program, it becomes necessary to approximate this integral by some means so that the computer time is kept to a practical minimum.

The problem of excessive computation time is solved by using an approximation for the integral in sine sweep transformations.

A dimensionless function Φ is defined as being:

$$\Phi = \frac{Q}{f_n} \int_{f_1}^{f_2} \frac{df}{\left[Q^2\left(\left(f/f_n\right)^4 + 1\right) - \left(f/f_n\right)^2\left(2Q^2-1\right)\right]^{\theta/2}}$$

so that:

$$D = \frac{\Phi f_n t}{\ln f_2/f_1 \, N_i Q}$$

The function Φ can be approximated by a simple function of θ since the function Φ varies less than 2% when f_n is in the range of 10 to 1500 cps and Q is in the range of 10 to 30.

These plots are shown in Fig. C-1. A plot of the variation of Φ with respect to b shows this to be nearly a straight line on log log paper Fig. C-2. This feature makes it possible to approximate the function by the equation: $\Phi = 1.89\ b^{-.645}$. The use of this approximation reduces the computer time by about a factor of a thousand with respect to the determination of the sine sweep damage.

It is assumed that Q varies by less than an order of magnitude over the frequency range of 5 to 2000 cps. It is, therefore, desirable to have a logarithmic step size to obtain the same relative resolution over the entire frequency range. The computer program uses $f_i = f_{i-1} \cdot (f_2/f_1)^{1/n}$ where f_1 and f_2 are the extreme frequencies and n is the desired number of frequency increments.

A change in step size was made to prevent difficulty arising when sine dwell field vibration was superimposed with sine sweep on random field vibration While the change in level of the random and sine sweep inputs was gradual (or of a low Q nature) the sine dwell component is a discrete single frequency and any equivalent transformation of this will change greatly as the specimen resonant frequency varies in the region of the sine dwell frequency. For the

field vibration in this project a logarithmic frequency stepping of 100 intervals had sufficient resolution to make accurate curves. When sine dwell components were superimposed in the field vibration at low frequencies, the resulting equivalent curve plots were very irregular in the region of the sine dwell frequency. This was most pronounced for high Q equivalent curve plots. As the specimen resonance changed gradually in the sine dwell frequency region to coincide with it, an equivalent Q curve took on the appearance of a single degree of freedom response. When the step spacing was greater than the response bandwidth, the response was completely missed. A finer stepping was necessary for sine dwell components, but outside the frequency region of the sine dwell component where the effect of that component was negligible, the fine step size is detrimental in that too many points are generated resulting in a long computer run. Therefore it was desired to have the step size change to a finer spacing in the frequency region of a field vibration sine dwell component and change back to the normal spacing in the rest of the frequency region. The change in step size was chosen to be by a factor of 10.

At this point a flow chart and operational description are presented:

BASIC FLOW DIAGRAM

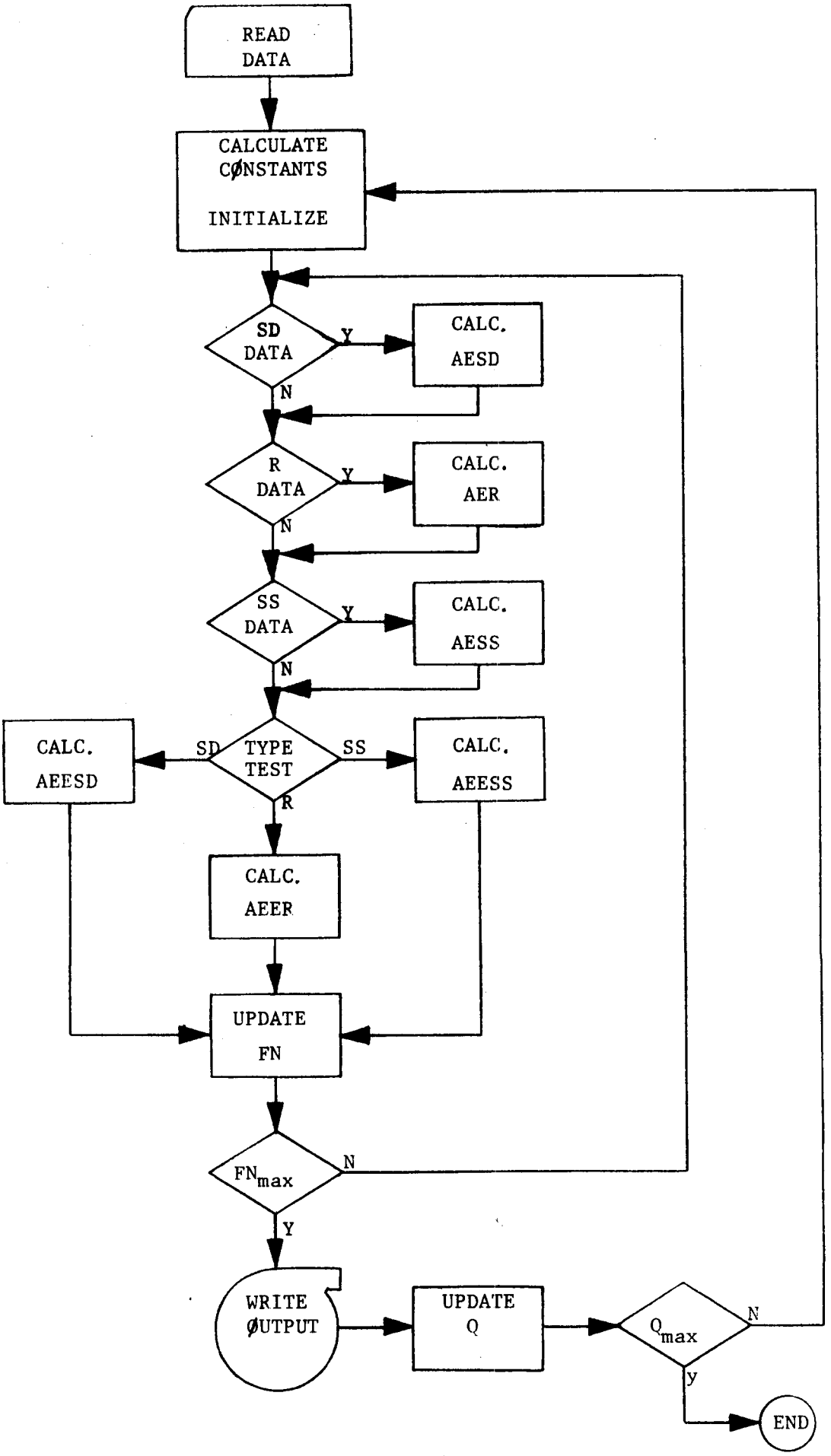
READ DATA
CALCULATE CØNSTANTS
INITIALIZE
SD DATA
Y
CALC. AESD
N
R DATA
Y
CALC. AER
N
SS DATA
Y
CALC. AESS
N
CALC. AEESD
SD
TYPE TEST
SS
CALC. AEESS
R
CALC. AEER
UPDATE FN
FNmax
N
Y
WRITE ØUTPUT
UPDATE Q
Qmax
N
y
END

DETAILED FLOW DIAGRAM

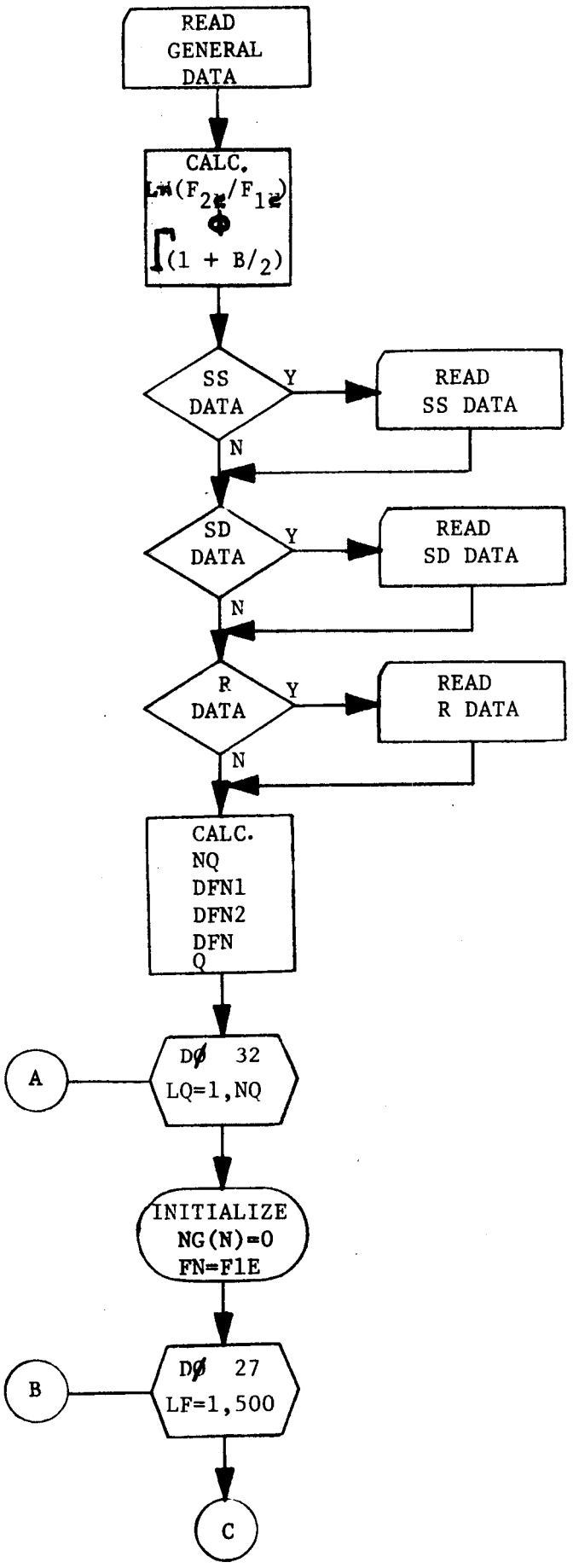
READ GENERAL DATA
CALC. Ln(F2E/F1E) / (1 + B/2)
SS DATA
Y
READ SS DATA
N
SD DATA
Y
READ SD DATA
N
R DATA
Y
READ R DATA
N
CALC. NQ DFN1 DFN2 DFN Q
A
DØ 32 LQ=1,NQ
INITIALIZE NG(N)=0 FN=F1E
B
DØ 27 LF=1,500
C

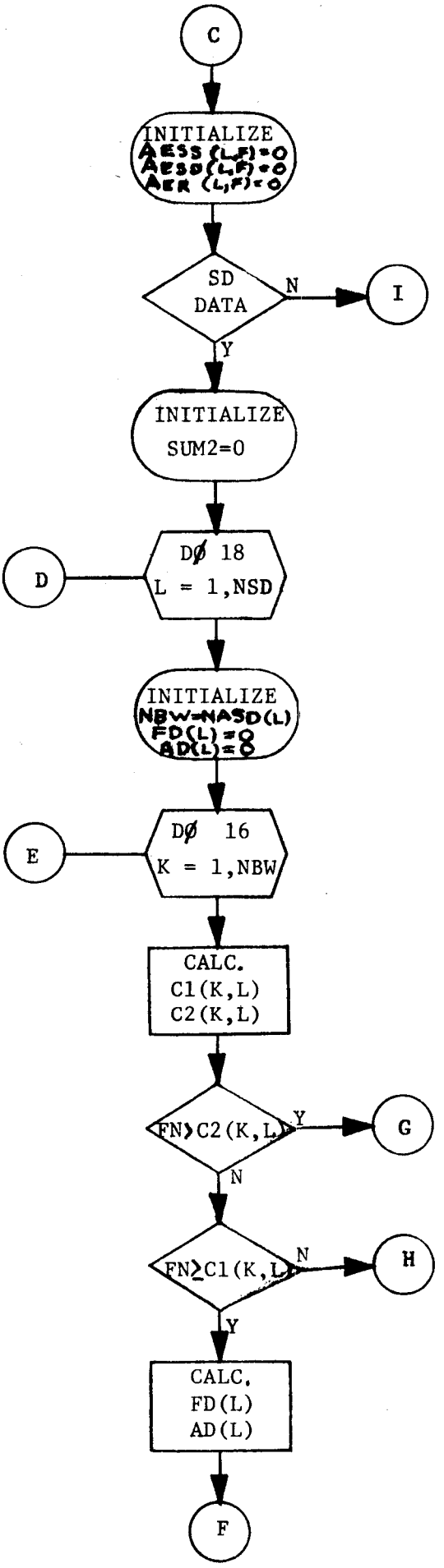
C
INITIALIZE
AESS(L,F)=0
AESD(L,F)=0
AER(L,F)=0
SD DATA
N
I
Y
INITIALIZE
SUM2=0
D
DØ 18
L = 1,NSD
INITIALIZE
NBW=NASD(L)
FD(L)=0
AD(L)=0
E
DØ 16
K = 1,NBW
CALC.
C1(K,L)
C2(K,L)
FN>C2(K,L)
Y
G
N
FN≥C1(K,L)
N
H
Y
CALC.
FD(L)
AD(L)
F

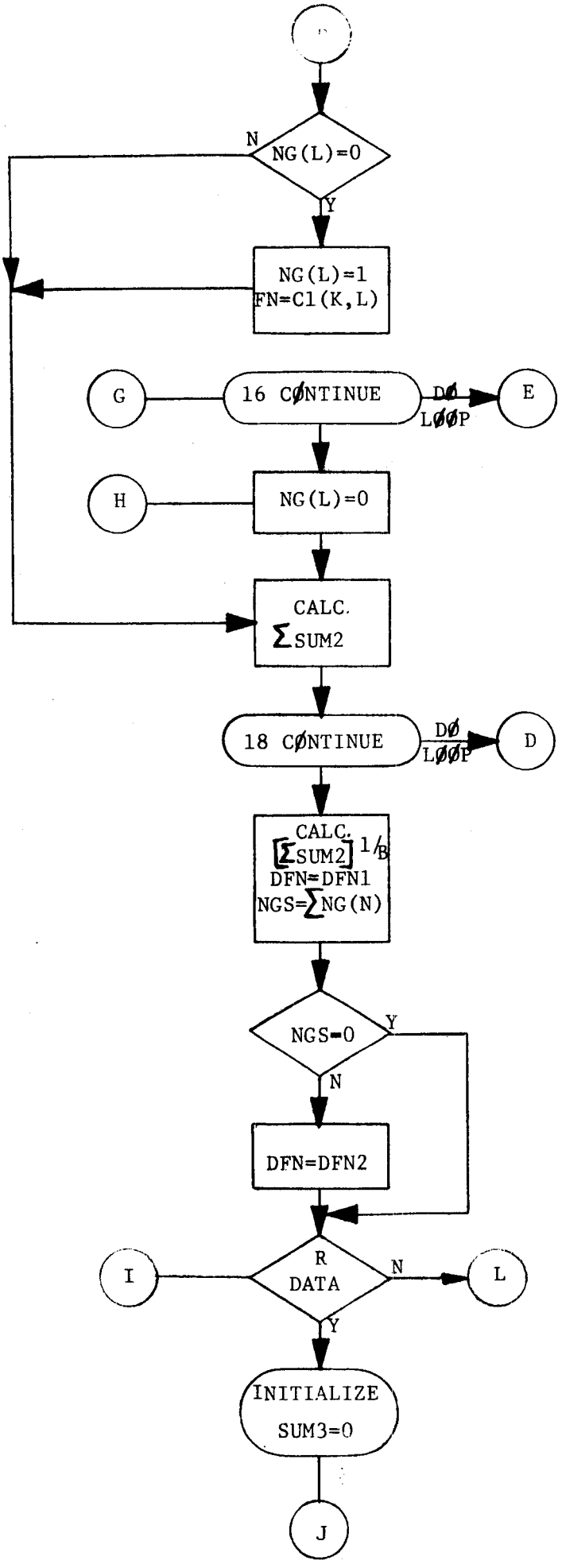
N
NG(L)=0
Y
NG(L)=1
FN=C1(K,L)
G
16 CØNTINUE
DØ LØØP
E
H
NG(L)=0
CALC.
ΣSUM2
18 CØNTINUE
DØ LØØP
D
CALC.
[ΣSUM2]^1/B
DFN=DFN1
NGS=ΣNG(N)
NGS=0
Y
N
DFN=DFN2
I
R
DATA
N
L
Y
INITIALIZE
SUM3=0
J

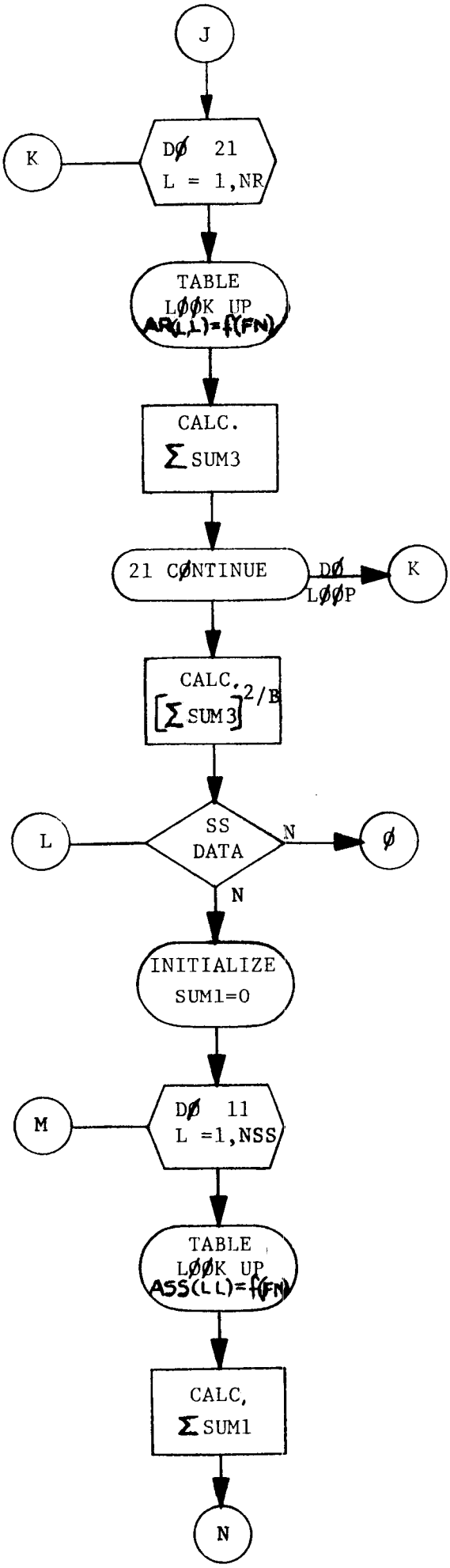
J
K
DØ 21
L = 1,NR
TABLE
LØØK UP
AR(L,L)=f(FN)
CALC.
Σ SUM3
21 CØNTINUE
DØ
LØØP
K
CALC.
[Σ SUM3]2/B
L
SS
DATA
N
Ø
N
INITIALIZE
SUM1=0
M
DØ 11
L =1,NSS
TABLE
LØØK UP
ASS(LL)=f(FN)
CALC,
Σ SUM1
N

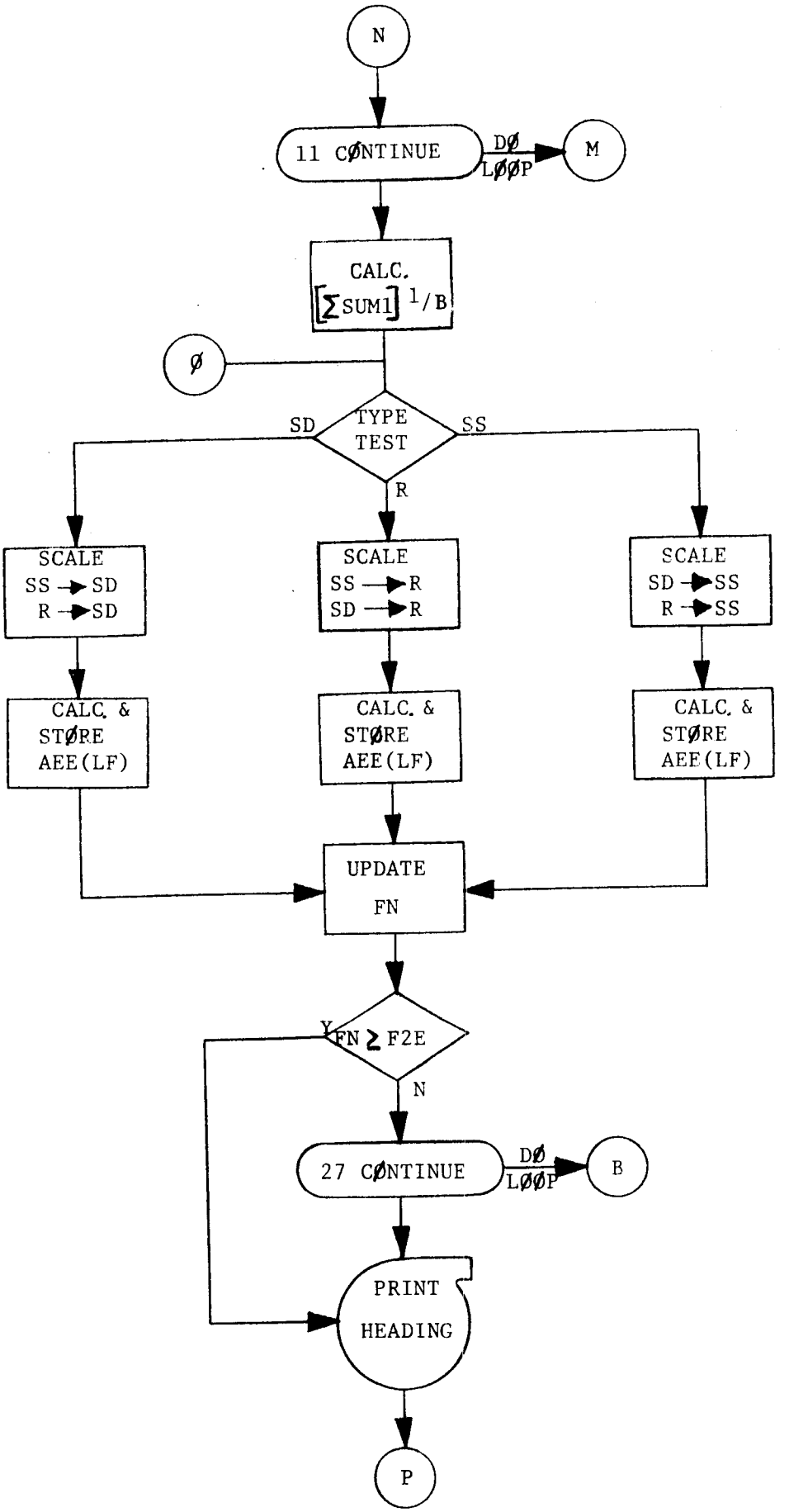
N
11 CØNTINUE
DØ LØØP
M
CALC. [ΣSUM1] 1/B
Ø
TYPE TEST
SD
SS
R
SCALE SS → SD R → SD
SCALE SS → R SD → R
SCALE SD → SS R → SS
CALC. & STØRE AEE(LF)
CALC. & STØRE AEE(LF)
CALC. & STØRE AEE(LF)
UPDATE FN
Y
FN ≥ F2E
N
27 CØNTINUE
DØ LØØP
B
PRINT HEADING
P

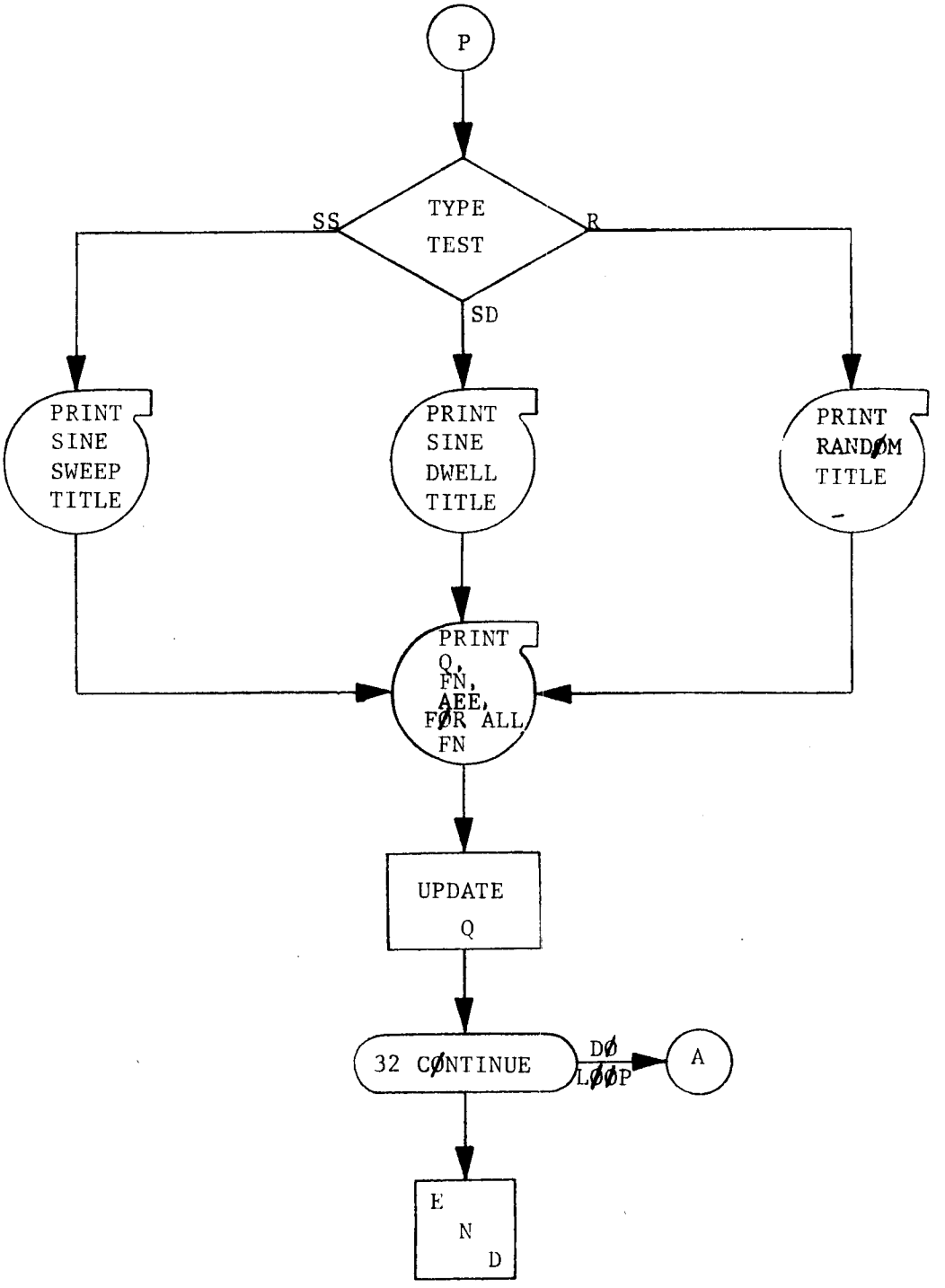
P
TYPE TEST
SS
R
SD
PRINT SINE SWEEP TITLE
PRINT SINE DWELL TITLE
PRINT RANDØM TITLE
PRINT Q, FN, AEE, FØR ALL FN
UPDATE Q
32 CØNTINUE
DØ LØØP
A
E N D

PROGRAM PRINT-OUT

```
C      VIBRATION SCALING
       DIMENSION TSS(10),F1SS(10),F2SS(10),ASS(99,10),NASS(10),
      1TSD(10),ASD(99,10),FSD(50,10),NASD(10),
      2TR(10),AR(99,10),NAR(10),
      3C1(10,10),C2(10,10),FD(10),AD(10),AESS(500),AESD(500),
      4AER(500),SFN(500),A(500),NG(10)
       READ(2,1000)NTYP,NSS,NSD,NR,Q1,Q2,DQ,F1E,F2E,DN,
      1B,TE
       FLN=LOGF(F2E/F1E)
       PH=1.89/B**.645
       BGAM=GAMF(1.+B/2.)
       PI=3.14159
       IF(NSS)1,3,1
1      DO 2 L=1,NSS
       READ(2,1001)MASS,TSS(L),F1SS(L),F2SS(L),(ASS(N,L),N=1,MASS)
       NASS(L)=MASS
2      CONTINUE
3      IF(NSD)4,6,4
4      DO 5 L=1,NSD
       READ(2,1002)MASD,TSD(L),(ASD(N,L),FSD(N,L),N=1,MASD)
       NASD(L)=MASD
5      CONTINUE
6      IF(NR)7,9,7
7      DO 8 L=1,NR
       READ(2,1002)MAR,TR(L),(AR(N,L),N=1,MAR)
       NAR(L)=MAR
8      CONTINUE
9      NQ=(Q2-Q1)/DQ+1.0
       DFN1=(F2E/F1E)**(1./DN)
       DFN2=DFN1**.1
       SFN=DFN1
       Q=Q1
       DO 52 LQ=1,NQ
       DO 53 N=1,NSD
53     NC(N)=0
       FN=F1E
       DO 27 LF=1,500
       NFN=LF
       AESS(LF)=0.0
       AESD(LF)=0.0
       AER(LF)=0.0
       IF(NSD)13,19,13
13     SUM2=0.0
```

```
      ...,NSD
      FD(L)=...
      AD(L)=...
      NOW=NASD(L)
      DO 18 K=1,NBW
      C1(K,L)=FSD(K,L)*(    Q-1.)/(    Q)
      C2(K,L)=FSD(K,L)*(    Q+1.)/(    Q)
      IF(FN-C2(K,L))14,14,16
14    IF(FN-C1(K,L))42,15,15
15    FD(L)=FSD(K,L)
      AD(L)=ASD(K,L)
      IF(NG(L))41,40,41
40    NG(L)=1
      FN=C1(K,L)
41    CONTINUE
      GO TO 17
16    CONTINUE
42    NG(L)=0
17    XSUM2=(FD(L)/FN)*(TSD(L)/TE)*AD(L)**B/
     1(Q*Q*(1.+(FD(L)/FN)**4)-(FD(L)/FN)**2*
     2(2.*Q**2-1.))**(B/2.)
      SUM2=SUM2+XSUM2
18    CONTINUE
      AESD(LF)=SUM2**(1./B)
      DFN=DFN1
      NGS=0
      DO 51 N=1,NSD
51    NGS=NGS+NG(N)
      IF(NGS)52,19,52
52    DFN=DFN2
19    IF(NR)20,22,20
20    SUM3=0.0
      DO 21 L=1,NR
      LL=1+99*(L-1)
      CRR=CVRDF(AR( LL),NAR(L),1,1,2,FN)
      XSUM3=TR(L)/TE*CRR**(B/2.)
      SUM3=SUM3+XSUM3
21    CONTINUE
      AER(LF)=SUM3**(2./B)
22    IF(NSS)10,12,10
10    SUM1=0.0
      DO 11 L=1,NSS
      LL=1+99*(L-1)
      CRSS=CVRDF(ASS( LL), ASS(L),1,1,2,FN)
```

```
      XSUM1=FLN*TSS(L)*CRSS**B/(TE*
     1(FSSS(L)/F1SS(L)))
      SUM1=SUM1+XSUM1
   11 CONTINUE
      AESS(LF)=SUM1**(1./B)
   12 GO TO (23,24,25),NTYP
   23 A1=SQRTF(PI*   AER(LF)*FN/Q)*(FLN*Q*BGAM/PH)**(1./B)
      A2=AESD(LF)*(Q*FLN/PH)**(1./B)
      A(LF)=(AESS(LF)**B+A1**B+A2**B)**(1./B)
      GO TO 26
   24 A1=AESS(LF)*(PH/(Q*FLN))**(1./B)
      A2=SQRTF(PI*FN*AER(LF)/Q)*BGAM**(1./B)
      A(LF)=(AESD(LF)**B+A1**B+A2**B)**(1./B)
      GO TO 26
   25 A1=     AESD(LF)**2*Q/(FN*PI)  *(1./BGAM)**(2./B)
      A2=AESS(LF)**2*Q/(FN*PI)*(PH/(FLN*Q*BGAM))**(2./B)
      A(LF)=(AER(LF)**(B/2.)+A1**(B/2.)+A2**(B/2.))**(2./B)
   26 CONTINUE
      SFN(LF)=FN
      FN=FN*DFN
      IF(FN-F2E)27,27,45
   27 CONTINUE
   45 WRITE(2,1003)
      GO TO (28,29,30),NTYP
   28 WRITE(2,1004)
      GO TO 31
   29 WRITE(2,1005)
      GO TO 31
   30 WRITE(2,1006)
   31 WRITE(2,1007)(Q,SFN(K),A(K),K=1,NFN)
      CALL DUMP ONE
      Q=Q+DQ
   32 CONTINUE
 1000 FORMAT(411/(3E10.0))
 1001 FORMAT(I2,3E10.0/(2E10.0))
 1002 FORMAT(I2,E10.0/(2E10.0))
 1003 FORMAT(1H1,13X,18HVIBRATION SCALEING//)
 1004 FORMAT(4X,1HQ,8X,2HFN,6X,30HEQUIVALENT SINE SWEEP (PEAK G)//)
 1005 FORMAT(4X,1HQ,8X,2HFN,6X,30HEQUIVALENT SINE DWELL (PEAK G)//)
 1006 FORMAT(4X,1HQ,8X,2HFN,6X,26HEQUIVALENT RANDOM (G2/CPS)//)
 1007 FORMAT(F6.0,F11.1,F12.4)
      END
```

CURVE READ SUBROUTINE PRINT-OUT

```
A     ORIGIN    CNTRL1000
A     EXECUTE   CNTRL7
A               DC
A                    @CVRDF     @
A                    +0
A                    +0
A                    +1000
A                    +0
A                    +9100000002
A     ORIGIN    CNTRL1000
A     CVRDF     SMSC
A               ZA1   2(4,5)+X94
A               STD1  HAHAYY(4,5)
A               ZA1   3(4,5)+X94
A               STD1  HAHAXX(4,5)
A               ZA1   0(2,3)+X94
A               STD1  *(6,9)+2
A               ZA1   0(6,9)+X94                                    INTP
A               AA    *(2,5)
A               STD1  TABLEWORD(2,5)                                INTP
A               ZA1   1+X94
A               STD1  *(2,9)+1
A               ZA1   *(6,9)
A               S1    +1                                            INTP
A               AA    TABLEWORD(2,5)
A               STD1  TABLEWORD(6,9)                                INTP
A               ZA1   4+X94
A               STD1  *(2,9)+1
A               ZA1   *
A               STD1  WORDXX1(6,9)                                  INTP
A               XLIN  IWRD,2+X94                                    INTP
A     HAHAYY    ZA1   0+IWRD                                        INTP
A               STD1  WORDXX2(2,3)                                  INTP
A               XLIN  IWRD,3+X94                                    INTP
A     HAHAXX    ZA1   0+IWRD                                        INTP
A               STD1  WORDXX2(4,5)                                  INTP
A               XLIN  IWRD,5+X94
A               MSP   IWRD
A               ZA3   0+IWRD
A               BLX   RETURN,INTP                                   INTP
A     WORDXX1   DRDW  +TABLEWORD,TABLEWORD                          INTP
A     WORDXX2   NOP   UGYUGY                                        INTP
A               ZA1   UGYUGY                                        INTP
```

```
A                B       6+X94
A     UGYUGY     NOP     *
A     TABLEWORD  HP      *
A     CCOM       DA      1
A                        ØØ,199
A     INTP       MSM     *+8Ø        SET EXT SW TO NOP=OFF      INTPØ1    ØØØØØ
A                MSM     *+16        SET TLU SW TO NOP=OFF      INTPØ2    ØØØØØ
A                ZST3    CCOM        SAVE ARGUMENT              INTPØ3    ØØØØØ
A                XL      98,Ø+RETURN PUT RDWLOC AND A IN 98     INTPØ4    ØØØØØ
A                ZAA     Ø+X98       GET +RDW OF TABLE          INTPØ5    ØØØØØ
A                S1      98(8,9)     LAST FUNCTION ADDRESS      INTPØ6    ØØØØØ
A                A1      *(Ø)        MINUS A + 1 IS XN ADDR     INTPØ7    ØØØØØ
A                ZST1    CCOM+1      SAVE XØ AND XN ADDRES      INTPØ8    ØØØØØ
A                LEH     Ø+X98       LOOK UP. IF ARG IS GRTR    INTPØ9    ØØØØØ
A                MSP     *+8         TBL,SET TLU SW TO BR=ON    INTPIØ    ØØØØØ
A                XLIN    98,98       SET 98 = +A,FOUND          INTP11    ØØ/SØ
A                ZA3     1+RETURN    IS THIS LAST FUNCTIONN     INTP12    ØØØØØ
A                CSM     9993        TO BE INTERPOLATED         INTP13    ØØØØØ
A                BH      *+3                                    INTP14    ØØØØØ
A                MSP     *+66        SET EXT SW TO BR = ON      INTP15    ØØØØØ
A                MSP     9993        CHANGE SIGN OF LAST DRDW   INTP16    ØØØØØ
A                ZST3    CCOM+4      NO,SVE DRDW OF CALLING     INTP17    ØØØØØ
A                B       *+18        SEQ AND GO THRU TLU SW     INTP18    ØØØØØ
A                S1      9991        IF OFF, GET XØ LOC         INTP19    ØØØØØ
A                ZA2     CCOM(4,5)+4 GET K                      INTP2Ø    ØØØØØ
A                D       *(Ø)-1      DIVIDE BY 2                INTP21    ØØØØØ
A                S2      *(Ø)-3      ADD 1 TO QUOTIENT          INTP22    ØØØØØ
A                ZS3     9992        MAKE SUM MINUS             INTP23    ØØØØØ
A                M       98(4,5)     TIMES A                    INTP24    ØØØØØ
A                A2      98(6,9)     ADD TLU FOUND LOC          INTP25    ØØØØØ
A                ZST2    CCOM+2      SAVE XØ LOCATION           INTP26    ØØØØØ
A                C2      CCOM(2,5)+1 COMPARE WITH TABLE XØ      INTP27    ØØØØØ
A                ZA3     CCOM(4,5)+4 GET K IN AC3               INTP28    ØØØØØ
A                BL      *+12        BR IF XØ IS BEFORE TBL     INTP29    ØØØØØ
A                M       98(4,5)     IF XØLOC IS IN TBL, GET    INTP3Ø    ØØØØØ
A                A2      CCOM+2      K TIMES A PLUS XØ=XNLOC    INTP31    ØØØØØ
A                C2      CCOM(6,9)+1 IS XN LOCATION             INTP32    ØØØØØ
A                BH      *+4         OUTSIDE THE TABLE          INTP33    ØØØØØ
A                ZA2     CCOM+2      NO. PICK UP XØ LOC         INTP34    ØØØØØ
A                B       *+7         GO TO INTERPOLATE          INTP35    ØØØØØ
A                ZA3     CCOM(4,5)+4 YES. GET K                 INTP36    ØØØØØ
A                M       98(4,5)     TIMES A                    INTP37    ØØØØØ
A                MSM     9992        MAKE MINUS                 INTP38    ØØØØØ
A                A2      CCOM(6,9)+1 ADD TABLE XN LOC TO GET    INTP39    ØØØØØ
```

```
A       B       *+2                 XØ LOC GO TO EXTRAPLTE      INTP40    ØØØØØ
A       ZA2     CCOM(2,5)+1         GET TBL XØ.GO TO EXTRPL     INTP41    ØØØØØ
A       STD2    *(6,9)+12           STORE XØ LOC                INTP42    ØØØØØ
A       A2      CCOM(2,3)+4         ADD NUMBER OF FUNCTION      INTP43    ØØØØØ
A       STD2    *(6,9)+13           STORE YØ LOC                INTP44    ØØØØØ
A       ZA2     *(6,9)-2            CCOM+4                      INTP45    ØØØØØ
A       A2      9993                PLUS K                      INTP46    ØØØØØ
A       A2      *(Ø)                PLUS 2 IS FIRST CCOM        INTP47    ØØØØØ
A       STD2    *(6,9)+1Ø           USED TO STORE Y             INTP48    ØØØØØ
A       STD2    *(6,9)+2Ø           VALUES.                     INTP49    ØØØØØ
A       STD2    *(6,9)+22           INSERT THIS LOC IN          INTP5Ø    ØØØØØ
A       STD2    *(6,9)+24           INSTRUCTIONS                INTP51    ØØØØØ
A       XL      IIWA,9993           SET IIWA = Ø,K              INTP52    ØØØØØ
A       XZA     IIWB,Ø              SET IIWB = Ø                INTP53    ØØØØØ
A       ZA1     Ø+IIWB              GET XI                      INTP54    ØØØØØ
A       FS      CCOM                MINUS X AND SAVE IN         INTP55    ØØØØØ
A       ZST1    CCOM+5+IIWA         C+5 THRU C+5+K              INTP56    ØØØØØ
A       ZA1     Ø+IIWB              GET YI AND SAVE IN          INTP57    ØØØØØ
A       ZST1    Ø+IIWA              C+6+K THRU C+6+2K           INTP58    ØØØØØ
A       XA      IIWB,Ø+X98          INCRMT IIWB BY A            INTP659   ØØØØØ
A       BIX     IIWA,*-6            LOOP K+1 TIMES              INTP6Ø    ØØØØØ
A       ZA3     CCOM(4,5)+4                                     INTP61    ØØØØØ
A       S3      *(Ø)+3              GET K-1                     INTP62    ØØØØØ
A       XL      IIWB,9993           SET IIWB = Ø,K-1            INTP63    ØØØØØ
A       XZA     IIWA,1              SET IIWA = 1,K              INTP64    ØØØØØ
A       ZA1     CCOM+5+IIWA                                     INTP65    ØØØØØ
A       FS      CCOM+5+IIWB         DO                          INTP66    ØØØØØ
A       ZST1    CCOM+2                                          INTP67    ØØØØØ
A       ZA1     CCOM+5+IIWB         AITKEN                      INTP68    ØØØØØ
A       FM      Ø+IIWA                                          INTP69    ØØØØØ
A       ZST1    CCOM+3              INTERPOLATION               INTP7Ø    ØØØØØ
A       ZA1     CCOM+5+IIWA                                     INTP71    ØØØØØ
A       FM      Ø+IIWB                                          INTP72    ØØØØØ
A       FS      CCOM+3                                          INTP73    ØØØØØ
A       FD      CCOM+2                                          INTP74    ØØØØØ
A       ZST1    Ø+IIWA                                          INTP75    ØØØØØ
A       BIX     IIWA,*-11                                       INTP76    ØØØØØ
A       XZA     IIWA,2+IIWB                                     INTP77    ØØØØØ
A       BIX     IIWB,*-13                                       INTP78    ØØØØØ
A       XLIN    IIWA,CCOM+4         GET STORE ADDRS IN IWA      INTP79    ØØØØØ
A       ZST1    Ø+IIWA              STORE INTP VALUE            INTP8Ø    ØØØØØ
A       B       2+RETURN            SW IS BR OR NOP             INTP81    ØØØØØ
A       XA      RETURN,1            IF OFF, UP RETURN. GO       INTP82    ØØØØØ
A       B       *-71                TO PROCESS NEXT DRDW        INTP83    ØØØØØ
```

```
A       [illegible]     EQU   43,X
A       IIWB            EQU   44,X
A       IWRD            EQU   45,X
A       RETURN          EQU   46,X
A       IIWARN          EQU   47,X
A       IIWBRN          EQU   48,X
A       END             CNTRLCVRDF
```

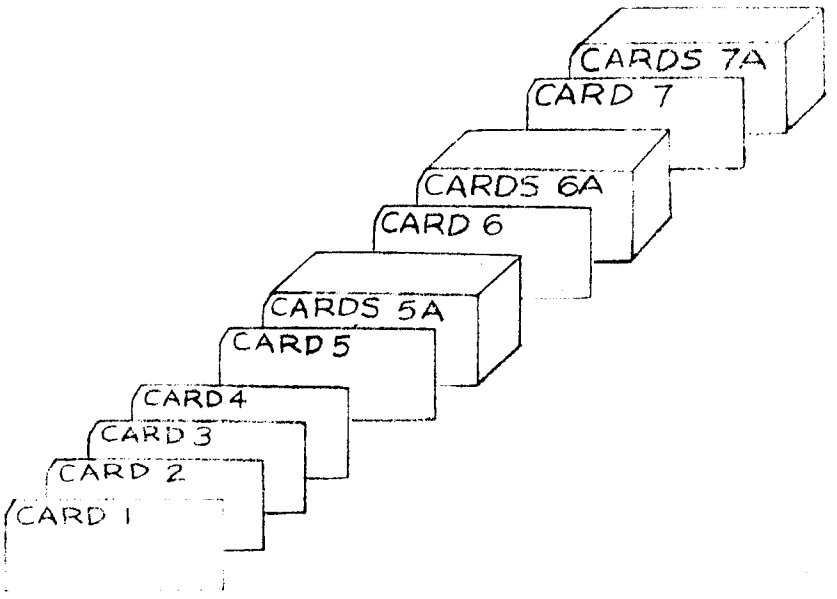

ORDER OF
INPUT DATA

INPUT DATA

CARD 1 (must be present)

COL. 1 Type of Equivalent Test

a. Enter "1" for Sine Sweep

b. Enter "2" for Sine Dwell

c. Enter "3" for Random

COL. 2 Number of Use Sine Sweep Tests (maximum of 9)

COL. 3 Number of Use Sine Dwell Tests (maximum of 9)

COL. 4 Number of Use Random Tests (maximum of 9)

CARD 2 (must be present)

COL. 1-10 Q_1 Lowest Q (floating point number)

COL. 11-20 Q_2 Highest Q (floating point number)

COL. 21-30 Q Step Size (floating point number)

CARD 3 (must be present)

COL. 1-10 F_{1e} Lowest frequency of Equivalent Test (floating point number)

COL. 11-20 F_{2e} Highest frequency of Equivalent Test (floating point number)

COL. 21-30 N Number of Points Defining Equivalent Test (maximum of 500) (FPN)

CARD 4 (must be present)

COL. 1-10 B Fatigue Curve Slope On Log Log Plot (FPN)

COL. 11-20 T_E Equivalent Test Time in Sec. (FPN)

CARD 5 Optional - Only Required For Use Sine Sweep Tests

COL. 1-2 Twice the number of cards defining us Sine Sweep Spectrum (cards 5A). This number must be right justified. Maximum number of cards is 49.

COL. 3-12 T_i Time for ith Use Sine Sweep Test in Secondary (FPN)

COL. 13-22 $F1_i$ Lowest frequency for above test (FPN)

COL. 23-32 $F2_i$ Highest frequency for above test (FPN)

CARDS 5A Optional - Only required for Use Sine Sweep Test.

COL 1-10 A_i Shaker amplitude in peak G's (FPN)

COL 11-20 f_i Shaker frequency for A_i (FPN)

COMMENTS! Cards 5A are used to define a curve. A first order interpolation and extrapolation is used with this curve. The program can easily be changed to give up to 99th order interpolation and extrapolation.

For each Use Sine Sweep test there will be a Card 5 and Cards 5A that will follow.

CARD 6 Optional - Only required for Use Sine Dwell Tests

COL 1-2 The number of Cards defining use Sine Dwell Spectrum (Cards 6A). This number must be right justified. Maximum number of Cards is 49.

COL 3-12 T_i Time for ith Use Sine Dwell Test in Seconds (FPN)

CARDS 6A Optional - Only required for Use Side Dwell Test

COL 1-10 A_i Shaker amplitude in peak G's (FPN)

COL 11-20 f_i Shaker frequency for above test (FPN)

COMMENTS! For each Use Sine Dwell Test there will be a Card 6 and Cards 6A that will follow.

CARD 7 Optional - Only required for Use Random Test

COL 1-2 Twice the number of Cards defining use Random Spectrum (Cards 7A). This number must be right justified. Maximum number of Cards is 49.

COL 3-12 T_i Time for ith Use Random Test in Seconds (FPN)

CARDS 7A Optional - Only required for Use Random Test

COL 1-10 W_i Shaker amplitude in G^2/cps (FPN)

COL 11-20 f_i Shaker frequency for W_i

COMMENTS! All comments for 5A apply here. For each random test there will be a card 7 and Cards 7A that will follow.

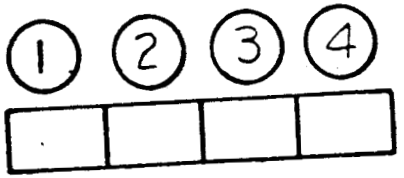

CARD 1

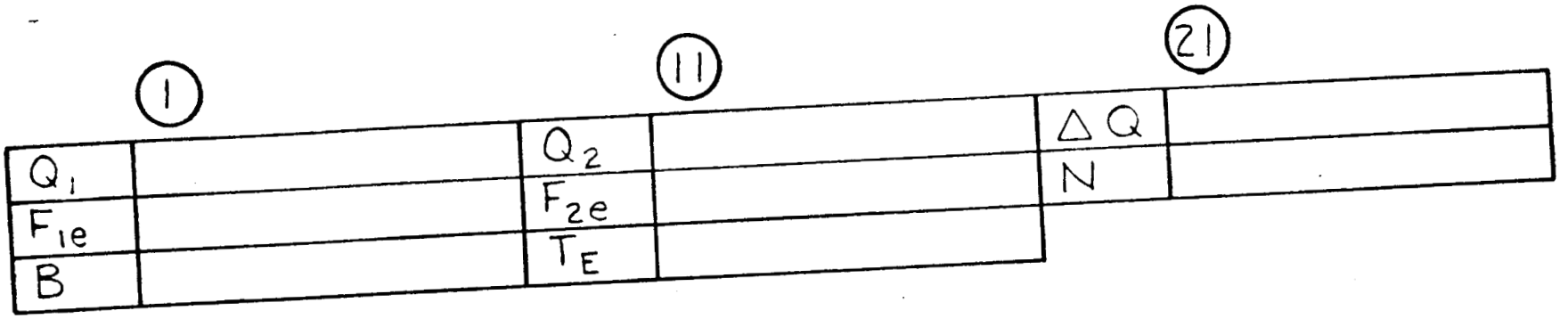

CARD 2
CARD 3
CARD 4

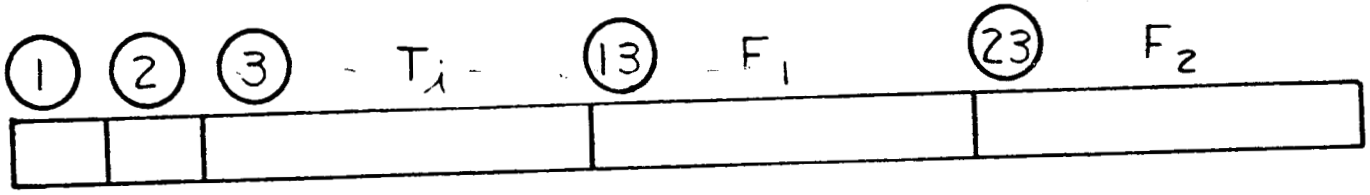

CARD 5

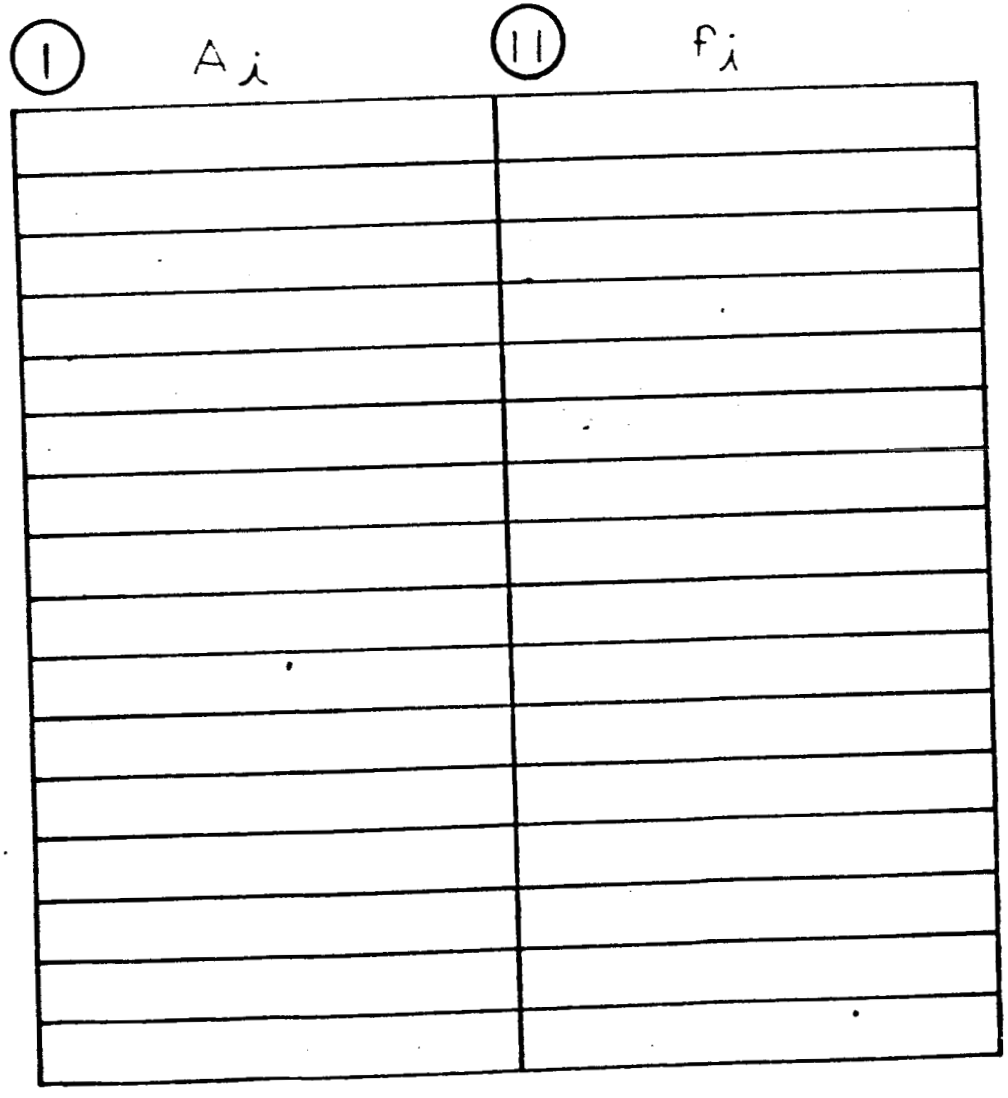

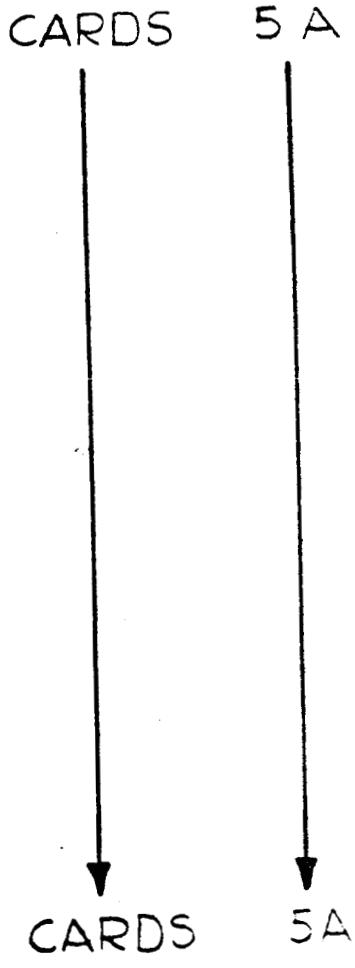

(1)	(2)	(3) T_i

CARD 6

(1) A_i	(11) f_i

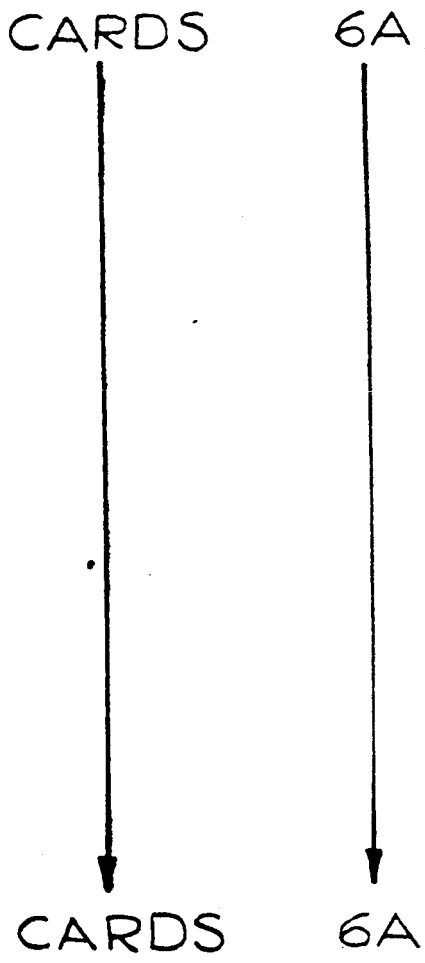

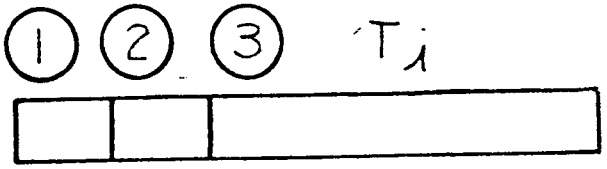

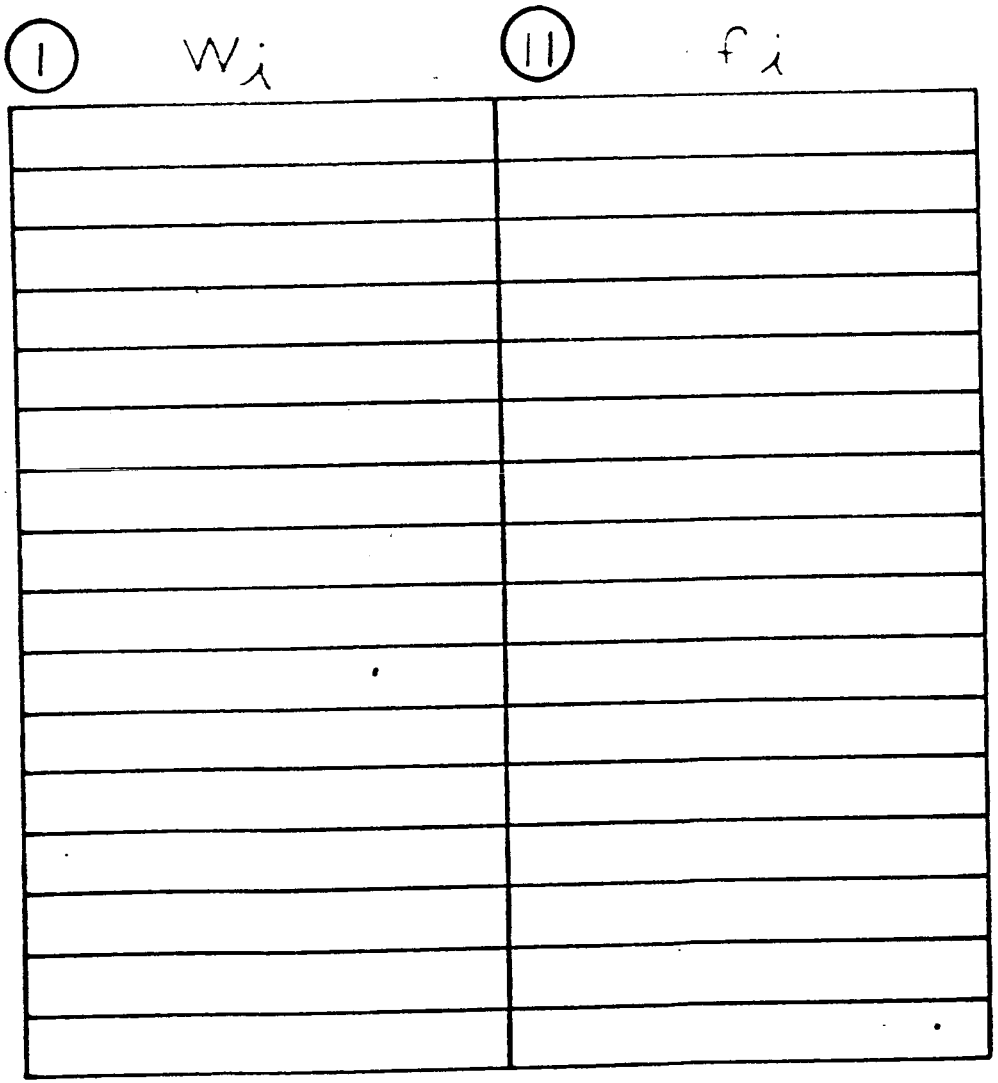

CARD 7

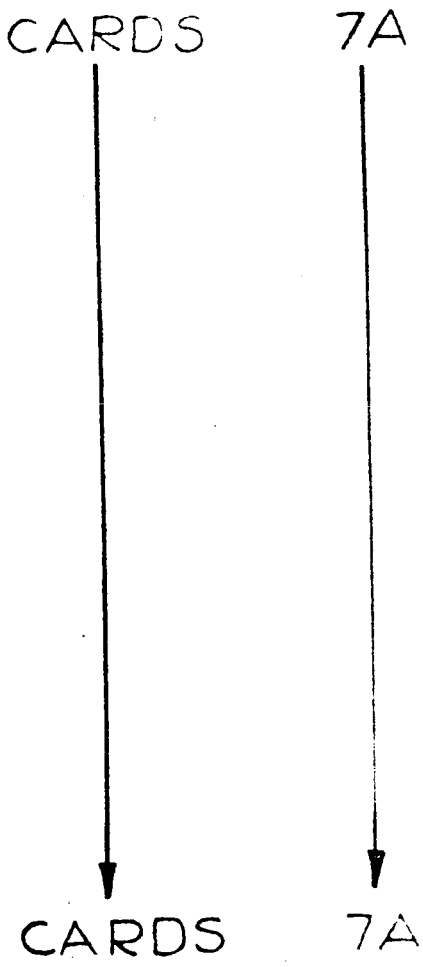

FIG. C-1

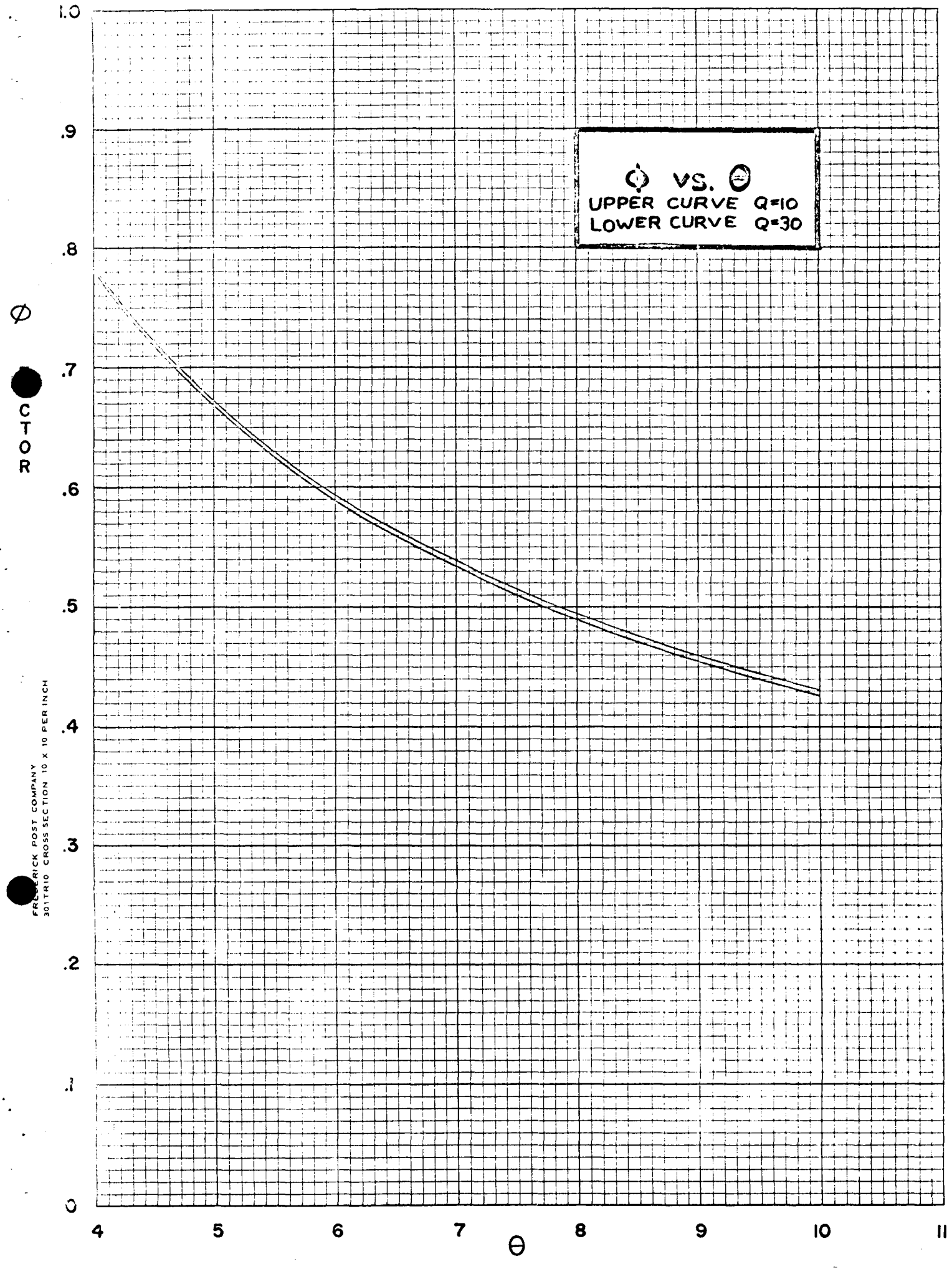
Φ VS. Θ
UPPER CURVE Q=10
LOWER CURVE Q=30
1.0
.9
.8
.7
.6
.5
.4
.3
.2
.1
0
Φ
C
T
O
R
4
5
6
7
8
9
10
11
Θ
FREDERICK POST COMPANY
301TR10 CROSS SECTION 10 X 10 PER INCH

FIG. C-2

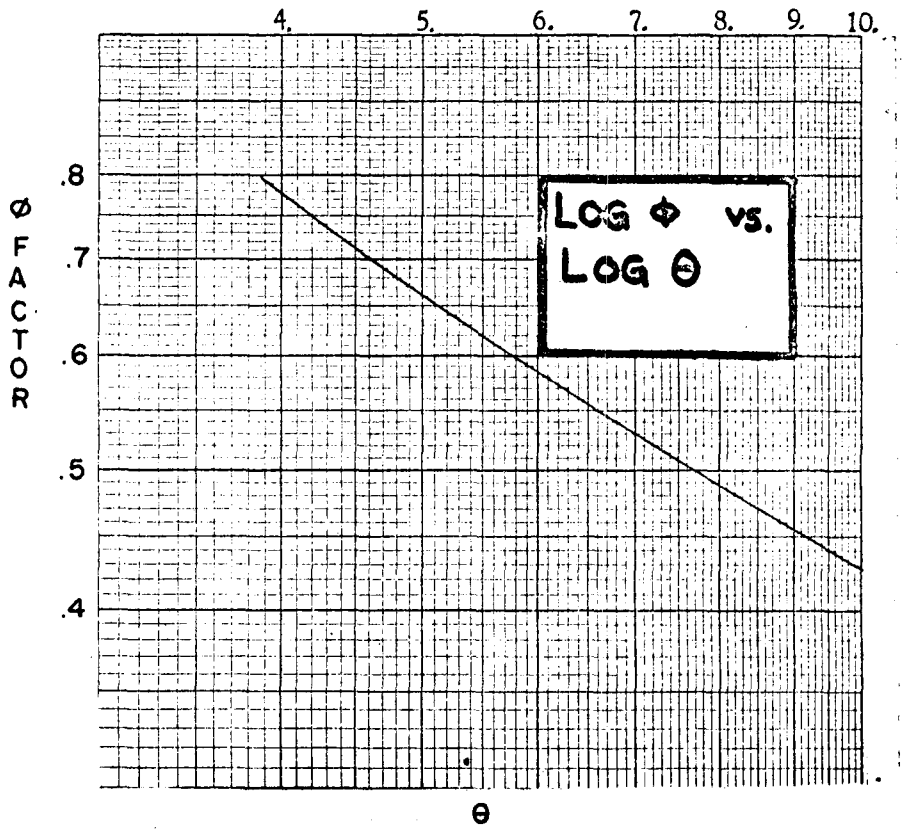

APPENDIX D

TEST PROCEDURE

This appendix presents a discussion of the variables to be measured and the development of adequate testing techniques. Various unsuccessful attempts to instrument the tests revealed physical measurement problems, which once identified, may be avoided.

The objective of the test procedure was to establish the test sequence and measurement techniques to be employed in gathering of data in alignment with project objectives.

The test procedure consists of a twelve-step sequence which was used on the final set of multibeam tests:

1. Mount accelerometers on the table for input control, and on the tip of the specimen beam. Calibrate the accelerometers against a known standard at 300 cps.
2. Apply a thin coating of silicone grease to the specimen beam root area and mount on the vibration fixture. Using an ohm meter, check to assure that the specimens are insulated from the test fixture. The specimen must be positioned such as to achieve proper spacing between the beam tip and the sensing capacitor.
3. Determine undamped beam resonance frequency by supplying sinusoidal input to the specimen. Input level shall be adjusted to yield 100 g's output as measured by the beam tip accelerometer.

4. Position rubber columns on the beams and secure by use of an adhesive. The beam tip static deflection shall be measured before and after installing rubber columns. The columns shall be allowed to relax for several hours prior to measurement.

5. Trim the columns as each beam is calibrated again. When the Q is within 2 of being 20 the low level calibration is ended.

6. Based on the type of test to be run, and the pre-test characteristics of the beams, an estimate of damage due to the correlation test shall be made. It is attempted to get at least .3 damage on all beams. If needed, the rubber columns are trimmed further or completely replaced to meet this minimum damage level.

7. Start the test and monitor the resonant frequency and acceleration for each type of test in the following manner:

   7.1 Sine Dwell: Acceleration is measured by voltmeter reading of capacity transducer. Resonance is read from frequency meter connected to shaker oscillator. The specimen is peaked to resonance.

   7.2 Sine Sweep: Peak acceleration is measured by peak voltmeter reading of capacity transducer. Value of Q and resonance frequency is determined from oscillographic trace.

   7.3 Random: RMS acceleration is measured by damped TRMS voltmeter reading of capacity transducer output. Value of Q and f_n is determined by spectral analysis of 20 sec. tape loop.

8. After the first readings, a second damage calculation shall be made and the time duration of the correlation test is altered if needed. If a change in time duration is not practical then a change in level must be made.

9. Readings of acceleration and frequency shall be repeated during the correlation test along with visual inspection of the specimens.
10. At the finish of the correlation test, the static deflection of the specimen must be measured before and after removal of the rubber columns.
11. The calibration shall be checked and, one at a time, the beams are run out to failure with sine dwell input.
12. The calibration is checked at the end of the test along with the accelerometer calibration.

As described in Appendix E, the test specimens were cantilever beams of fixed dimension and end mass.

The failure criteria was defined as being the cycle ratio to produce macro cracks of sufficient size to shift the specimen resonance frequency 0.5%. The definition of failure criteria is based on previous work at Collins[5] Radio Company and knowledge that fatigue cracks of sufficient magnitude to cause greater shifts in resonance frequency result in no predictible relationship between stresses and test input levels.

An inspection device was desired which would sense the crack without interrupting the test. It was decided to try an eddy current detector. The theory of operation is that the mutual inductance between two inductors, in this case we used an induction coil in close proximity to the beam root and the aluminum of the beam in the beam root area as indicators, is changed by crack formation in the root of the beam. A series of tests with progressively

more efficient coils indicated that this could have been developed into something workable but at the stage at which work was abandoned, the sensitivity was marginal and the amount of instrumentation needed for a multibeam test would have been prohibitive.

A parallel effort was the attempt to make a truly viscous damper. The first type of damper (Figure D-1) considered was based on the fact that a force proportional and opposite to the beam tip velocity results from the interaction of the DC magnetic field and the induced eddy current field. The damper was successful with no end mass but gave insufficient damping on the actual test specimen.

The next two attempts at a viscous damper used oil dash pots in which a small paddle blade was attached to the end mass of the beam and moved in a small slot filled with oil. The damper (figure D-2) would not maintain a constant Q at high g level due to oil splatter. The damper (figure D-3) gave a deteriorating wave shape due to pivot wear.

A number of viscoelastic materials were tried prior to obtaining a workable damper. Shear plates were put on top and bottom surfaces of the beam; a commercial viscoelastic sheet material was glued to top and bottom surfaces; strips of nylon or high damping rubber were clamped from base to beam tip, but none of these would last for the duration of the test at high g levels, or the Q and f_n were very dependent upon input level. The final damper was in the form of two 1" x 1/2" x 1/2" columns of soft silicone rubber as shown in figure (D-4). The silicone rubber columns were glued to the beam tip and the fixture and top support. Problems which were encountered with this type of damper are listed here:

1. Relaxation of the rubber column caused the Q to drift from the initial setting.
2. The dynamic modulus was not greatly changed by the amount of compression of the columns. The amount of compression was limited by the tendency of the column to buckle. It was necessary later to make columns with oversized areas and compress them to get a Q of about 15. Then the column was trimmed with a knife to get a Q of 20.
3. The Q's were set at a low input to minimize damage to the specimens. When high levels were applied, the Q was observed to change. Contributing factors included:
   - 3.1 Buckling of the columns at high g levels.
   - 3.2 Partial failure of the adhesive points.
   - 3.3 Heating of the columns due to increased energy dissipation at higher g levels.
   - 3.4 Differencies between the top and bottom mount resulted in differences in the dynamic strain.
4. The static compression of the columns varied if one column had a smaller cross sectional area or its hardness was greater than the other column. This resulted in a case of combined static and dynamic stresses. It was necessary to measure the static position of the rubber to determine how much static prestress each beam was experiencing.

Although the viscoelastic columns presented problems, they were better than any the other dampers tested due to the following characteristics:

1. The viscoelastic material did not fatigue or deteriorate during high level tests. Once the damper temperature had stabilized and any unbonding of the columns had occurred, the characteristics remained nearly constant throughout the test.
2. The amplitude linearity of the specimen with this damper was better than for any previous damper.
3. The change in frequency due to changes in input level were small.

An effect occurred at this phase which changed the procedure significantly. It was observed that on long duration fatigue tests which were interrupted over night that the fatigue life was lengthened. After this effect was noticed repeatedly, a series of checks were conducted to determine if this observation was valid. These checks were for:

1) possible calibration drift,
2) frequency variation due to 20°F temperature variation in shaker room,
3) biased readings due to different operators and,
4) healing of fatigue damage in fatigue tests having long interruptions.

Some random calibration drift was discovered in the amplifier which was the early FM unit. This drift led to some additional scatter in results but did not account for the observed increase in life for the interrupted tests. The test procedure was rewritten to include additional calibration checks in order to minimize possible scatter.

The temperature induced variation in the natural frequency due to a 30°F change was found to be 0.05% with the variation being completely reversible upon return to initial temperature. This accounted for a small part of the observed variation in the resonant frequency. A small amount of the variation is also attributable to operator characteristics.

During this time more tests were performed to determine quantitatively how significant the healing effect was. Time and sample limitations prevented a thorough test of this effect but it was determined that at least several hours were required to notice a singificant degree of healing. In addition, the earlier in the test the interruption occurred, the more pronounced was the healing. In general this is in disagreement with the results of similar studies.[10]

Due to the healing effect, the last procedure was modified. All beams were to be vibrated simultaneously to a flat random input in the run-out-to-failure portion of the test. Small tuning masses were added to the beams so that variation in beams resonances was less than 0.1 cps. The failure check was made with a 5 cps bandwidth filter set slightly above the original resonance. When the resonance fell below the lower frequency range of the filter, no response was noticed and a sinusoidal frequency check was made.

The original procedure was impractical due to the interaction of the beams with the shaker table. Since the beams had an undamped Q of slightly less than 2000, a sharp notch in the shaker spectrum resulted at the specimen resonance in conjunction with an equally high spike about a hundredth of a cps above the notch. As one beam would fail, its resonance would drop and it would move out of the large notch caused by the other beams causing accelerated failure. The

other beams would occupy a shallower notch due to the absence of the one failing beam which would also accelerate their failure. This interaction caused all the beams to fail at once. Three times, a multiple beam test displayed this effect and therefore this form of run-out-to-failure test was abandoned.

The final impact on the test procedure of the healing effect and the interaction during multiple tests was that a sine dwell run-out-to-failure had to be performed on the beams one at a time with a minimum delay after the correlation test. The overall number of specimens in one multibeam test was reduced from 10 to 6. This resulted in a shorter average interruption between the correlation portion and run-out-to-failure portion.

During the summer the humidity of the laboratory increased to the point where it was felt that some change in fatigue life might occur. Therefore the last two sets of beams were coated with Dow Corning DC-11 silicone grease in the root area. This was to prevent moist air from getting into the fatigue crack, but since it kept air from the root, additional effects resulted. It was first determined that the grease increased the fatigue life by a significant amount and then it was observed that the increase was probably dependent upon the thickness of the grease coating. The most repeatable way of applying a nearly uniform thickness of grease was by squeezing the excess grease away with one's finger. This was done for all beams of the last set tested by one technician so that some uniformity existed. Although the grease was very viscous, the vibration levels were high enough to cause the grease on the top surface to puddle in the horizontal portion of the beam

root run out. On the bottom surface, the puddling caused an excess of grease to collect on the vertical pertain of the beam root run out. Despite this unsymmetrical coating, no preferential surface for crack initiation was noticed.

FIGURE D-1

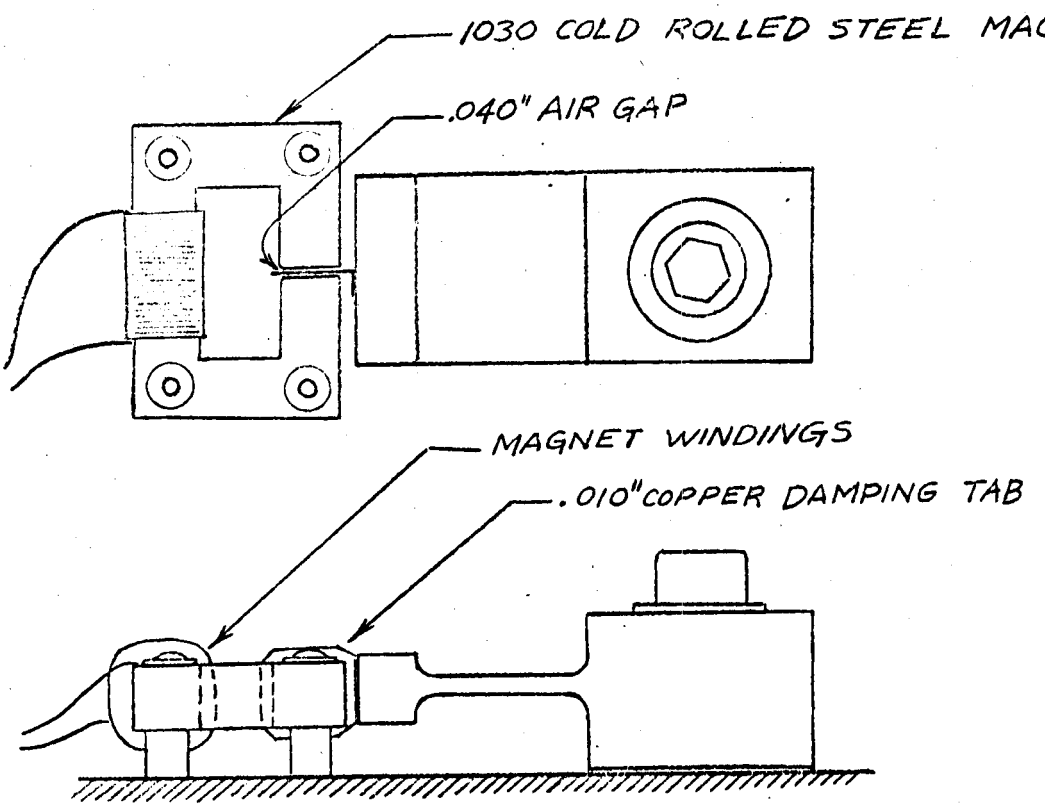

MAGNETIC HYSTERESIS DAMPER

FIGURE D-2
VISCOUS OIL DAMPERS

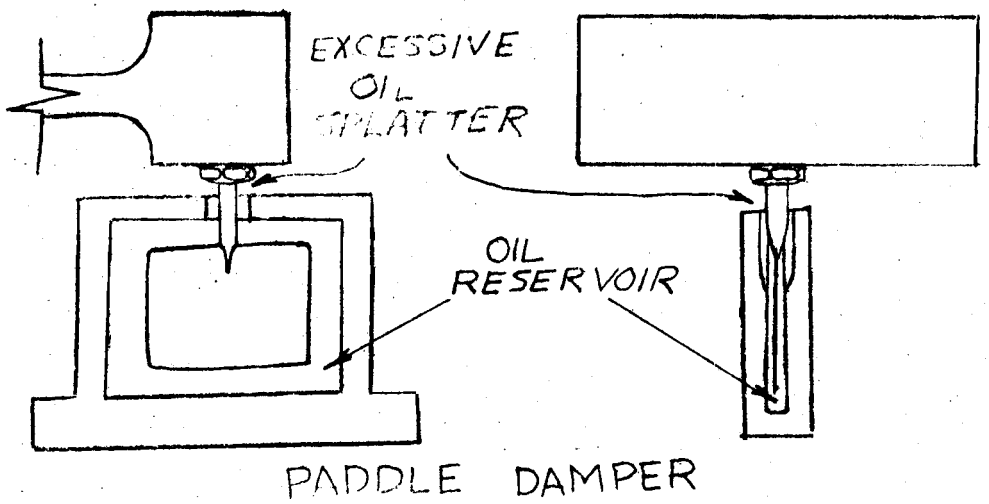

PADDLE DAMPER

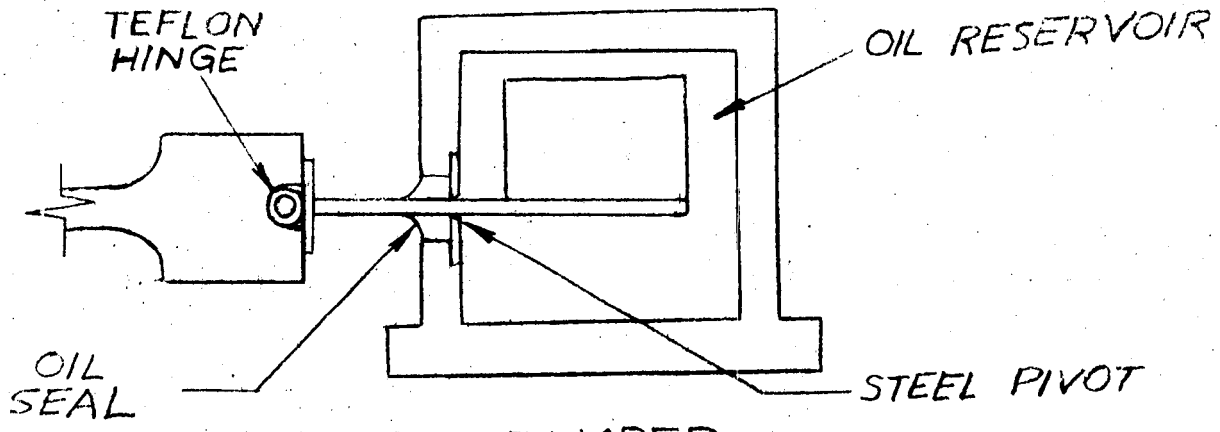

PIVOT DAMPER

FIGURE D-3

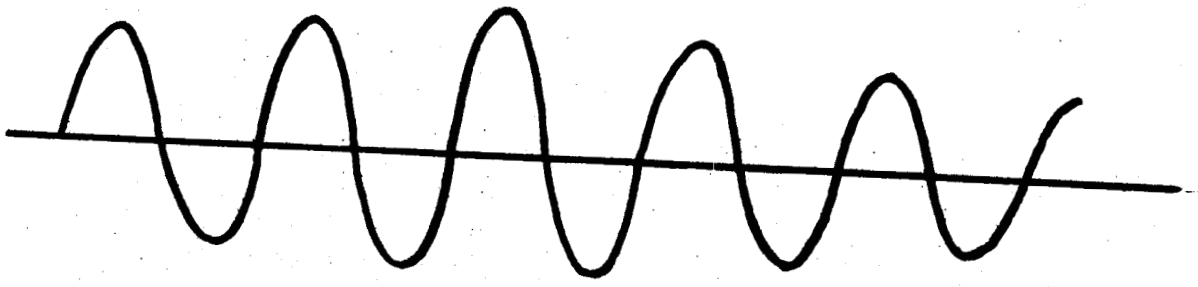

VARYING AMPLITUDE OF PADDLE DAMPED SPECIMEN DUE TO ENTRAPPED AIR IN OIL RESERVOIR

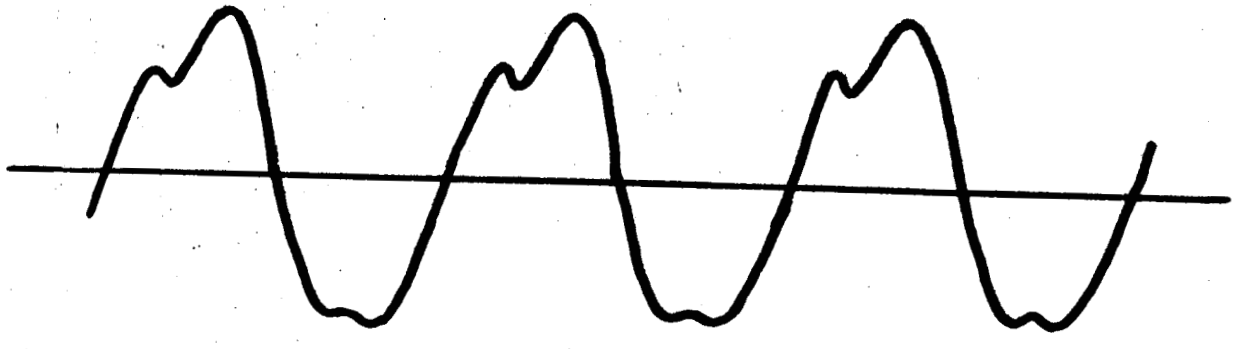

DISTORTED WAVE SHAPE OF PIVOT DAMPED SPECIMEN DUE TO WEAR ON HINGE AND PIVOT

FIGURE D-4

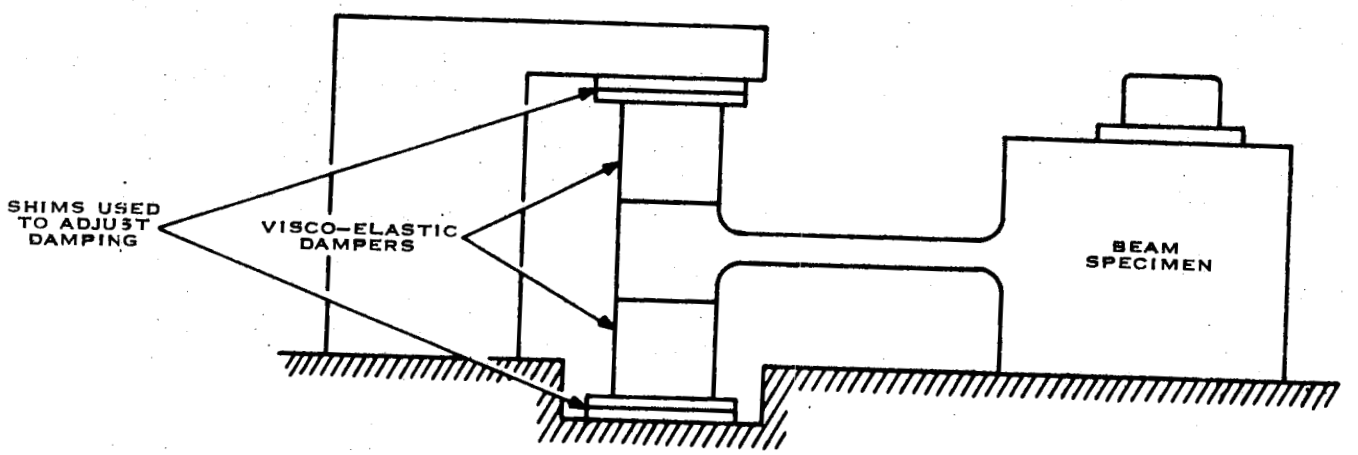

SILICONE RUBBER DAMPER

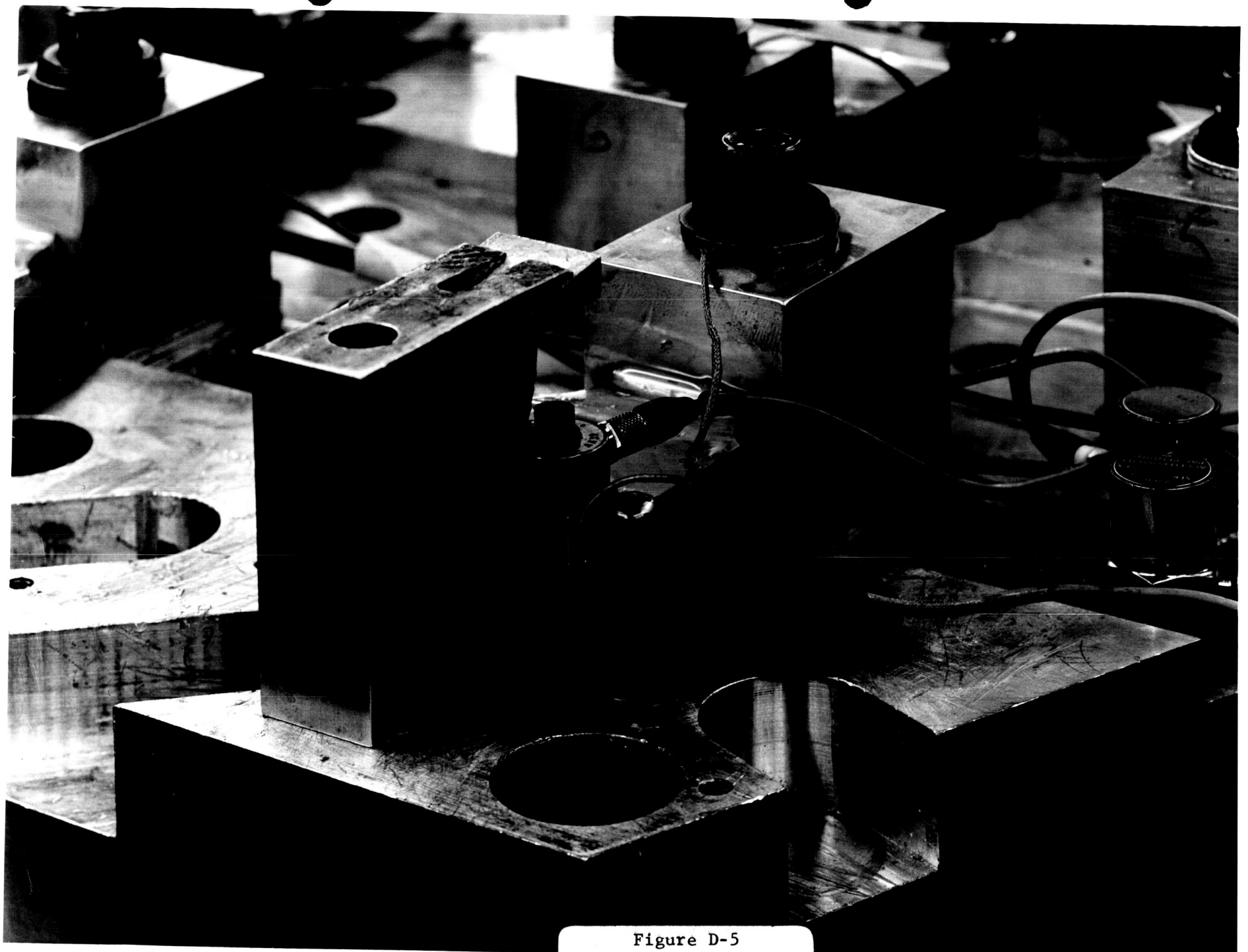

Figure D-5
Calibration Config.
For Capacity Probe
Transducer

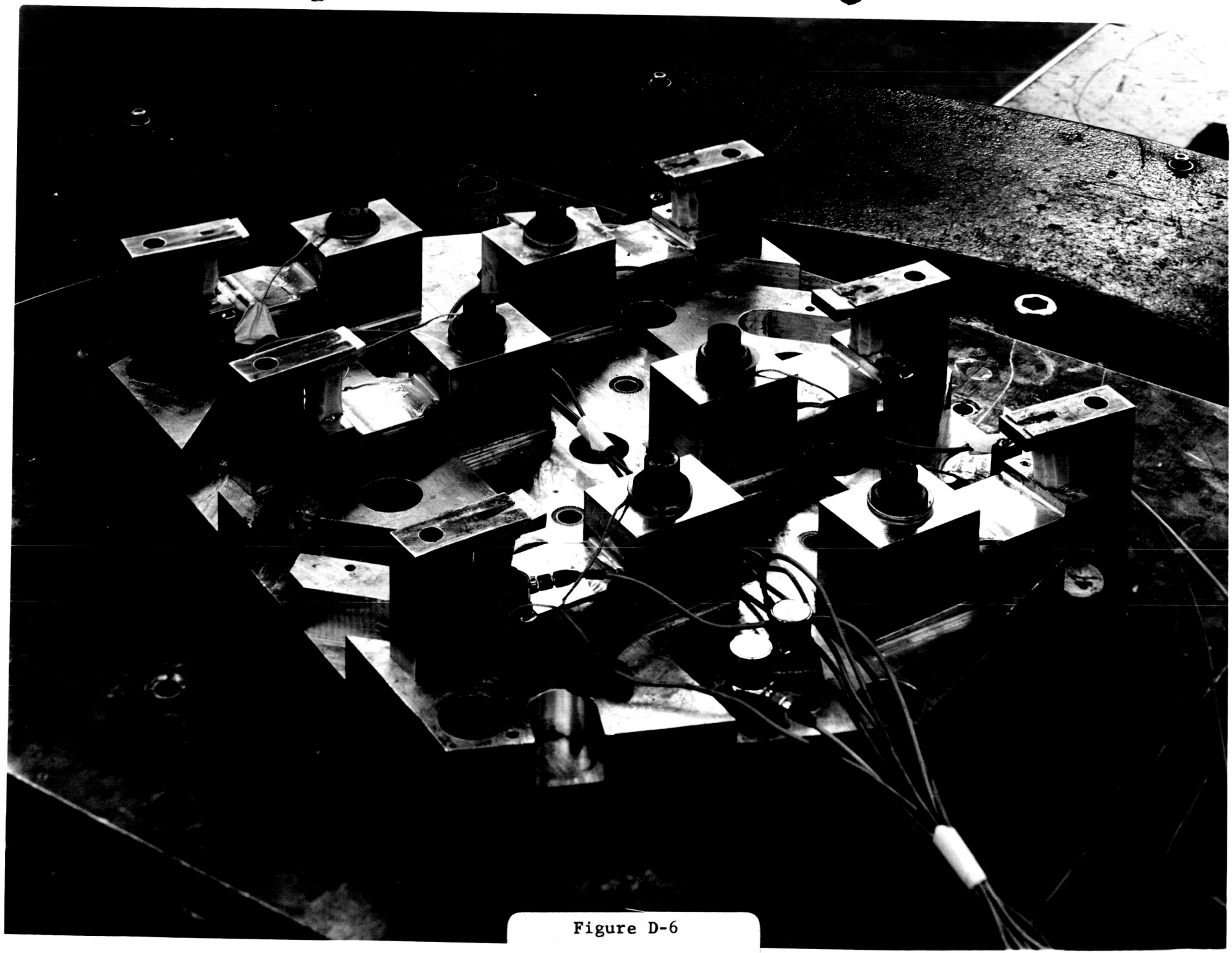

Figure D-6

Multibeam Test Setup

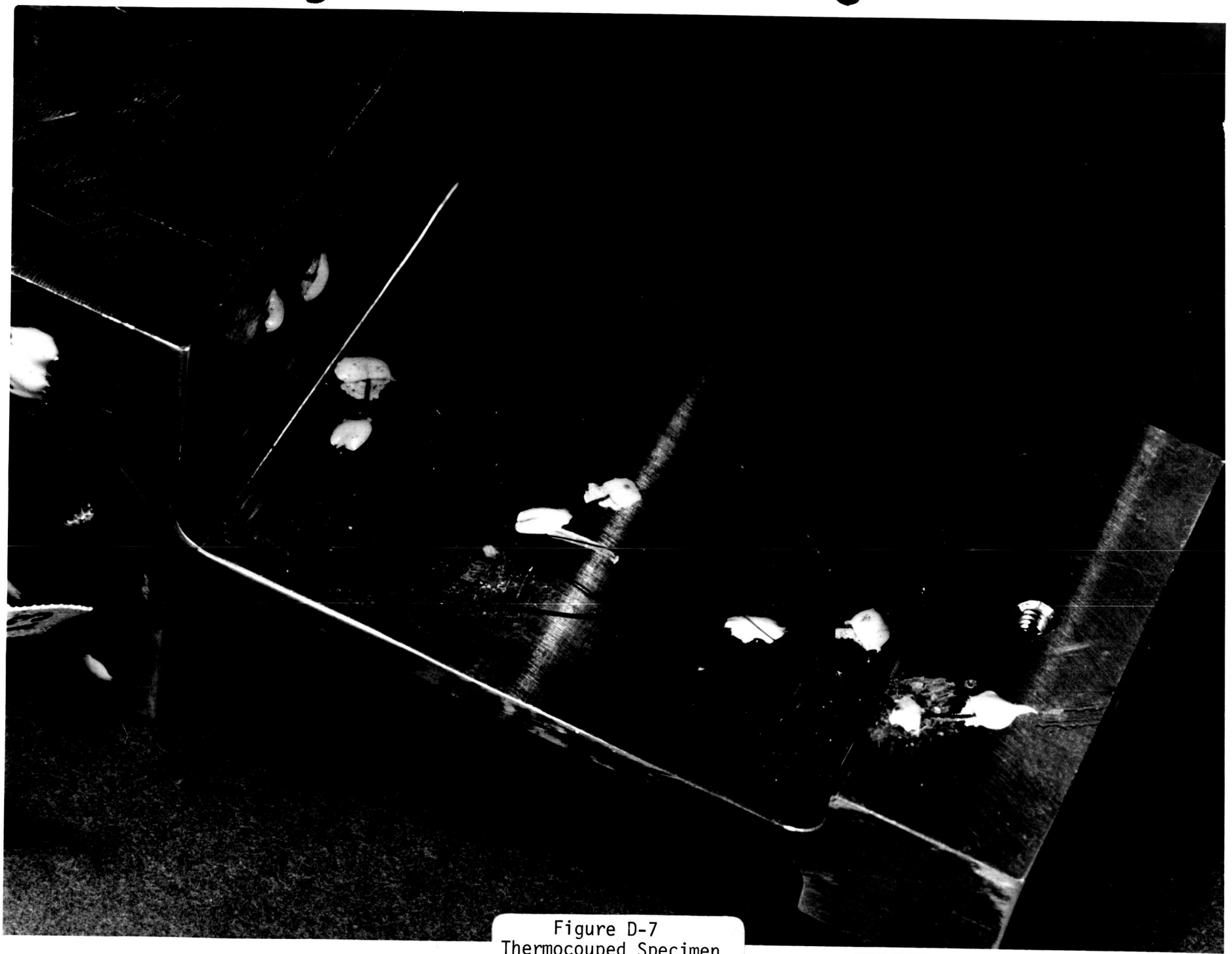

Figure D-7
Thermocouped Specimen
in F_n vs. Temp. Test

APPENDIX E

MEASUREMENT TECHNIQUES

The importance of accurate amplitude measurement can be gained by observing that a ±3% error in a stress measurement on a material with a b = 7.8 will result in a ±26% change in mean life. If this measurement error is a random error, then the inherent fatigue life scatter will be superimposed on this measurement scatter to produce an even larger scatter of specimen lives. It is estimated that the one sigma error in stress measurement for this project was about ±3.5%.

Two ways of measuring beam root stress were considered. The most direct means was to strain gage the point of highest stress and monitor it during the test. This was found to be impractical. The gages which were small enough to fit in the region of high stress failed due to:

(1) Fatigue of the lead in wires at the junction of the gage.

(2) Failure of the bond between the gage and the beam.

(3) Fatigue of the foil gages.

The mean life of the gages tested were so much shorter due to the above failures that that approach was abandoned. A more indirect means of measuring stress is involved in the second approach. Based on the assumption that the beam deflection curve is the same in the immediate region of resonance, the ratio of beam tip deflection to beam root stress should be a constant. This approach is implied in the analysis in that the single degree of freedom model has a constant stress deflection ratio. Strain gaged specimens were vibrated with the tip motion measured by an accelerometer and the assumption of a constant ratio was found to be true.

The first attempt to monitor tip motion was with an accelerometer. The problems which occurred with this approach were:

(1) Excessive connector and cable failure at tip motions of 400 to 600 g's.

(2) The length of cable was critical in determining beam resonance in the undamped state.

(3) The problem of switching all the monitoring accelerometers to one amplifier.

The second attempt to measure tip motion was by the use of a capacity transducer. The sensing capacitor consisted of one side of the end mass of the beam tip separated by an air gap from the other plate of the capacitor which was mounted to the fixture by an isolator post. The fixture side of the capacitor was of the same size as the side of the end mass of the beam tip. Leads from the two surfaces to a circuit at the amplifier input were insulated and shielded. The size of the sensing capacitor was about 1/3 $\mu\mu$f. During vibration, the change of capactance was about 1/10 $\mu\mu$f for high g levels.

$C = \epsilon\, A/d$ where C is capacitance, A is plate area, d is the plate separation and ϵ is a constant. The change in A (side of the beam end mass) is proportional to the change in capactance. If A is rectangular, $dC/dt = V$ where V is the relative velocity of the beam tip with respect to the fixture plate. For small deflections the tip motion of the beam is nearly vertical and the change in capacitance is proportional to the total displacement of the beam tip. At large displacements, the beam tip moves thru a nearly circular arc so that the total acceleration at the extreme swing of the beam has a horizontal and vertical component of motion. The change in relative area of the two plates is not proportional to acceleration of the beam tip for large displacements with the output of the capacity probe reading less at large deflections than an accelerometer located on the beam tip.

Another distortion which is likely to occur with this type of capacity probe is a frequency doubling effect. When the plates of the sensing capacitor are mutually centered at the rest position, two cycles of capacity change occur for one cycle of mechanical motion. By offsetting the plates of the sensing capacitor somewhat more

than the maximum expected displacement of the beam tip, one cycle of capacity change results from one cycle of mechanical motion. The offset reduces the sensitivity of the transducer to about 60% of that in its centered position.

The most severe type of distortion resulted from non-parallel motion of the two plates of the sensing capacitor. It was prohibitively difficult to align every beam so no variation of gap width occurred during a cycle of motion. It can be shown that the error component of the signal due to changes in the gap distance results in harmonic distortion. This distortion can be eliminated by filtering out the harmonics with a low pass filter but the frequency response is adversely effected by the filter response. An electronic automatic tracking bandpass filter with a very flat peak was the best means of removing the harmonic distortion but this was unavailable to the project. The harmonic distortion was reduced to negligible levels by increasing the sensing capacitor gap. The amplitude of the error components of the signal are inversely proportional to the square of the gap dimension while the signal level due to parallel motion is inversely proportional to the gap dimension. The error can then be reduced by increasing the gap size. Not only does this reduce the signal level but it increases the fringing effect of the electrostatic field at the edge of the capacitor.

The capacity variations due to changes in the dielectric constant of the air is negligible since the variation in dielectric constant between air, water vapor and a vacuum are negligibly small.

Although the output of the capacity transducer is proportional to the relative displacement which the two plates of the sensing capacitor experience, it is also nearly proportional to the absolute acceleration of the beam end mass. This is most easily shown by the quations of motion of the beam end mass.

$$m\ddot{y} + c(\dot{y}-\dot{x}) + k(y-x) = 0$$

$$\ddot{y} = -\frac{c}{m}(\dot{y}-\dot{x}) - \frac{k}{m}(y-x) \qquad \text{E-1}$$

In the case of the undamped beams, $c\omega \ll k$ and can be neglected.

$$\ddot{y} = -\omega_n^2 (y-x) \qquad \text{E-2}$$

The constant of proportionality is the square of the resonance in radians, but it is also evident that the equation is not frequency sensitive. The relative displacement of beam tip is proportional to the acceleration for all frequencies. Since this is a result of assuming a single degree of freedom, the actual specimen might not be a good accelerometer. A test was constructed in which the output of an accelerometer on the beam tip was monitored simultaneously with the capacity transducer. This was a sinusoidal sweep test. From 100 cps to 800 cps the undamped beam's relative displacement was proportional to acceleration. Above 800 cps it is considered that the beam began to bend in its second mode shape. In the case of the damped beam with a Q of 20, the effect of the damping can be estimated. The coefficient c/m is identical to ω_n/Q. The value of $(\dot{y} - \dot{x})_{max}$ is $\omega (y - x)_{max}$ but the maximum velocity value lags the maximum displacement value by $\pi/2$. This can be represented by letting $(\dot{y} - \dot{x})_{max} = - i\omega(y-x)_{max}$. Equation E-1 now becomes:

$$\ddot{y} = \frac{i\omega\omega_n}{Q}(y-x) - \omega_n^2 (y-x) \qquad \text{E-3}$$

For the case at resonance, the value of ω is ω_n and E-3 becomes:

$$\ddot{y} = \omega_n^2 (y-x)(1/Q - 1) \qquad \text{E-4}$$

The absolute magnitude of the acceleration is:

$$|\ddot{y}| = \omega_n^2 (y-x)\sqrt{1 + 1/Q^2} \qquad \text{E-5}$$

It can be seen that as Q becomes large ($Q > 10$) the damping error is negligible. The damping term was calculated from equation E-3 for a range of ω's. The damping error is insignificant for the range of frequencies and range of Q's used in this project. The result of this analysis is that the capacity transducer measures acceleration of the beam, and that once a calibration has been made at one frequency, it is good for all frequencies and Q's used in this project.

The calibration was performed by using equation E-2. An accelerometer was fixed to the beam tip and vibrated. The resonance was found while the input of the table was kept at a fixed low level. The output of the tip mounted accelerometer was measured along with the voltage output of capacity transducer. The accelerometer was next removed and the beam vibrated with a given table input. The resonance was measured and the output of the capacity transducer was measured at reasonance. Equation E-2 can be written twice, one equation with all terms describing the calibration run with the accelerometer on the beam tip and having a subscript of 1 on all terms. The second equation will have all terms defined except for $\ddot{y}$ which can then be solved. All terms in the test run with no accelerometer on the tip will have a subscript of 2.

$$\ddot{y}_1 = \omega_{n,1}^2 (y-x)_1 \qquad \text{E-6a}$$

$$\ddot{y}_2 = \omega_{n,2}^2 (y-x)_2 \qquad \text{E-6b}$$

The approximation has been made that $\sqrt{1 + 1/Q^2} = 1$

The value of $\ddot{y}_2$ can be found then.

$$\ddot{y}_2 = \ddot{y}_1 \left(\frac{f_{n,2}}{f_{n,1}}\right)^2 \frac{(y-x)_2}{(y-x)_1} \qquad \text{E-7}$$

Relative displacement $(y - x)_2$ is proportional to the capacity transducer output with no accelerometer and $(y - x)_1$ is proportional to the capacity transducer with accelerometer. If the amplifier has a flat frequency response in the beam resonance region ($f_{n1} \leq f \leq f_{n2}$), the proportionality constant is the same for both cases and $(y - x)$ can be replaced by Vc; the voltage output of the capacity transducer.

This calibration was checked at low levels against a strain gage output which measured the root stress. It also checked the assumption that tip motion was directly proportional to root stress. The result was that the strain measurements agreed to within 2% of that predicted by the calibration procedure just described.

The amplifier used in the capacity transducer was the major problem of the project. The requirements for the amplifier are that the sensitivity had to be in the range of 100 volts per peco farad with a flat frequency response ($\pm$1% from 200 cps to 500 cps) and with a good amount of stability with respect to line voltage fluctuations, temperature changes and long duration drift. In addition it could not be microphonic.

The first amplifier was a commercial FM tuner with high quality components and several extra audio stages to get the required sensitivity. It was abandoned for the following reasons:

(1) Critical tuning procedure

(2) Microphonic components in the amplifier and cabling which produced capacity changes under high g loading

A second FM tuner was built in an attempt to get greater gain and better performance. It did not function satisfactorially and was abandoned. A third amplifier was built on the principle of a capacity microphone. It exhibited some of the faults of the FM tuner but its greatest failing was insufficient gain.

The system which was finally used is considered to be a new application for the charge amplifier. A diagram is presented to show the function of the final capacity transducer.

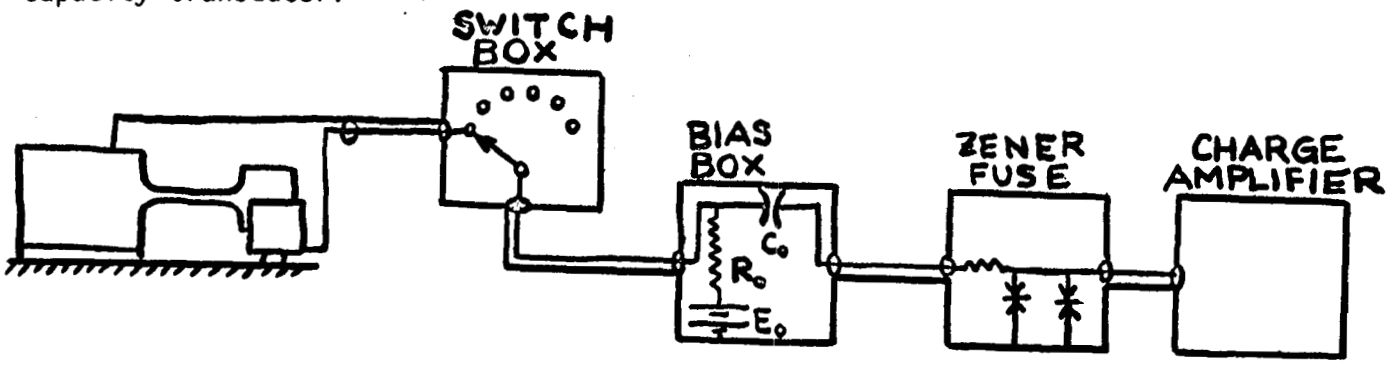

FIGURE E-1

The beam has to be insulated from the fixture as does the fixed capacitor plate. Failure to do this results in eddy currents generated by the shaker magnetic field changing the assumed ground voltage at the beam. The switch box is operated from the console but is located at a convenient distance from the shaker. The most important portion of the circuit is the bias box which contains a 1000 MΩ bias resistor with 200 volt DC source. Because of the low drain, one set of three 66 volt dry cell batteries lasted thru the test program. The coupling capacitor is a .02 uf capacitor with a 250 volt DC bias. The value of the resistor is more critical than the other components. It is important to keep the resistor enclosed and clean to prevent surface conduction. The DC voltage is near the upper limit for discharge across the air gap of the capacitor. The sensitivity is proportional to the voltage bias. The coupling capacitor prevents the DC voltage from reaching the input transistor of the charge amplifier. The zener fuse prevents large voltage spikes from damaging the input transistor.

In handling the specimen it is possible to accidently short the sensing capacitor with one's hand. The large bias resistor limits current to about .2 μ amps which will not result in injury to the operator; but a 200 volt drop occurs on the high voltage side of the coupling capacitor. The resulting -200volts on the negative side of the coupling capacitor is enough to fail the input transistor. The zener fuse is made up of 1.3 volt trigger level zeners in two parallel shunts each consisting of two back to back or front to front zeners. In operation a -10 volt spike appears on the input to the charge amplifier when the sensing capacitor is shorted out. The reason for two parallel fuses is reliability in the event of the failure of one of the zeners. The trigger level of 1.3 volts is sufficiently higher than any expected signal level and the impedance is linear in the range of $\pm$1.3 volts.

An alternate bias box was built which made it possible to use the charge amplifier as a dynamic strain measuring device. This was developed when it was found that strain gages could be mounted higher on the root radius and last for the duration of a test. This became feasible when measurements showed that the stress at the top of the radius, although much less, was proportional to the stress at the highest stress point in the beam root. Development was dropped when the capacity transducer was successful but this strain measuring device had the following advantages:

(1) It did not require a bridge balancing circuit

(2) It did not have zero drift problems associated with DC amplifiers.

(3) It was very sensitive. Strains as low as a few micro inches were measured.

(4) It could be used with simple switching circuitry so that many strain gages could be sequentially monitored on one charge amplifier.

The circuit is shown in Fig. E 2 and the values of the circuit component are:

(1) Bias resistor is same value as strain gage

(2) Bias voltage is twice the recommended voltage for the strain gage.

(3) Once the amount of charge per strain ratio is decided, the value of C_1, the coupling capacitor is determined by the equation:

$$C_1 = \frac{4}{E_o G.F.} \left(\frac{\Delta Q}{\Delta \epsilon}\right)$$

where G.F. is strain gage factor and E_o is the bias voltage.

The transducer amplifier had the following advantages over the earlier type:

(1) The lead length can be made as long as is necessary. Usually the charge amplifier is located in the shaker console, therefore avoiding the problem of microphonic distortion.

(2) The charge amplifier is basically a high gain amplifier and therefore has the desired sensitivity without having to add more stages.

(3) It is more stable with respect to temperatur changes, line voltage regulation and long term drift than the FM tuner. The instrumentation failure in the field vibration test is the only one of that system known to have occurred. Some drift in gain usually occurs for about 2 hours after turning on the amplifier.

The frequency measurements are more straight forward than the amplitude measurements. For sine dwell tests the oscillator output is fed to a frequency counter. That counter is checked against a second counter to check for any differences in measurement. If any difference exists, then both counters are checked against a frequency standard at 100,000 cps. For sinusoidal sweep tests the procedure for measuring resonance is:

(1) Make frequency marks on the oscillographic traces corresponding to markings on the oscillator frequency dial. This is a manual procedure

where the operator presses a margin marker button as a frequency mark on the oscillator dial passes a pointer. This is done for sweeps up and down in frequency.

(2) The true frequency corresponding to the oscillator dial marking is measured with a frequency counter. The resonant frequency from each oscillographic trace is estimated by interpolation from the corrected frequency markings.

(3) The average of all measured resonances for one specimen is taken to compensate for statistical error.

The scatter depends on operator skill. Most of the tests on this project had a 2 to 3 cps scatter.

In the random test, the resonance is measured from the spectral analysis of a tape loop specimen. The resonant frequency check here is most likely to have a greater error due to the following reasons:

(1) Tape loop may stretch

(2) Tape speed may vary. The loop is recorded on one machine and replayed on another.

(3) Due to the short sample time and the reliance on making measurements from one sample, the statistical mean frequency may vary from the true mean (or resonant) frequency for the test.

The frequency marker on the spectral analyzer is checked at 60 cps and 1250 cps prior to the analysis.

The acceleration standard which was used to calibrate the system is checked at the Endevco Corp. every six months. It is estimated that it could be out of calibration by as much as $\pm$5% between checks. A secondary company standard is calibrated just after the primary standard returns from calibration. Both have a separate power supply and read out which comprise a system that is not altered between calibrations. Periodic checks are made between the two standards and at

low frequencies with a microscope. Two working accelerometers are calibrated at 300 cps using one of the company standards. One accelerometer monitors table level. The second, an Endevco 2221 accelerometer is calibrated and is used in turn to calibrate the capacity transducer.

The output of the capacity transducer was measured on a true rms voltmeter. It was not possible to keep one meter for this project due to check out and calibration procedure within the company. One Ballentine 320A true rms meter was obtained for exclusive use of the vibration lab. This was modified so that the meter movement could be highly damped. The damping capacitors had a total shunt capacity of .072 farad. This high capacity was necessary because of the low resistance of the meter. The total time constant was on the order of 45 sec to 1 minute. For random tests the time allowed for the meter to come to equilibrium was 2 minutes. Usually no reading was made until the meter began to fluctuate about some mean voltage. The fluctuation over a several minute period varied about $\pm 5\%$. The mean of the fluctuation was estimated by eye over about a 30 second period after the end of the two minute equilibrium time. Repeated readings were made throughout the random test to determine any change in Q.

The peak count measurements were made on a counter which was modified for this project. The threshold level was set by this procedure:

> A precision oscillator in parallel with the counter and a peak reading meter was set to produce a sine signal of the same frequency and at a peak level which was desired for the threshold. The first stage of the counter was an amplifier. The gain was changed until the counter began to register. The signal was then played into the counter and the measurement made for that threshold. There was a reaction time for this counter for which the signal duration had to exceed at a given level before a count would register. Therefore the oscillator had to be set at approximately the same frequency as the signal to set the threshold level.

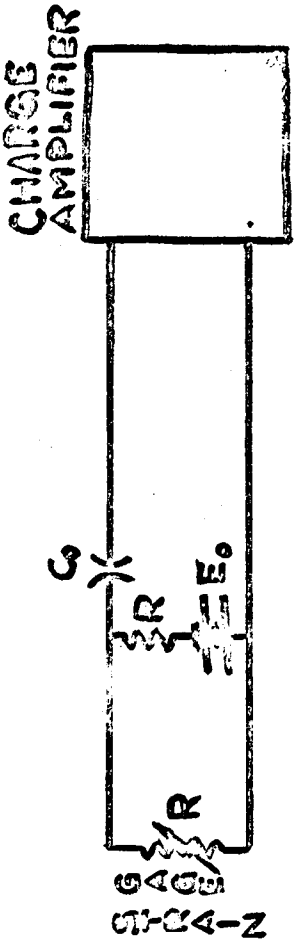

FIGURE E-2
STRAIN GAGE, CHARGE AMPLIFIER CONFIGURATION

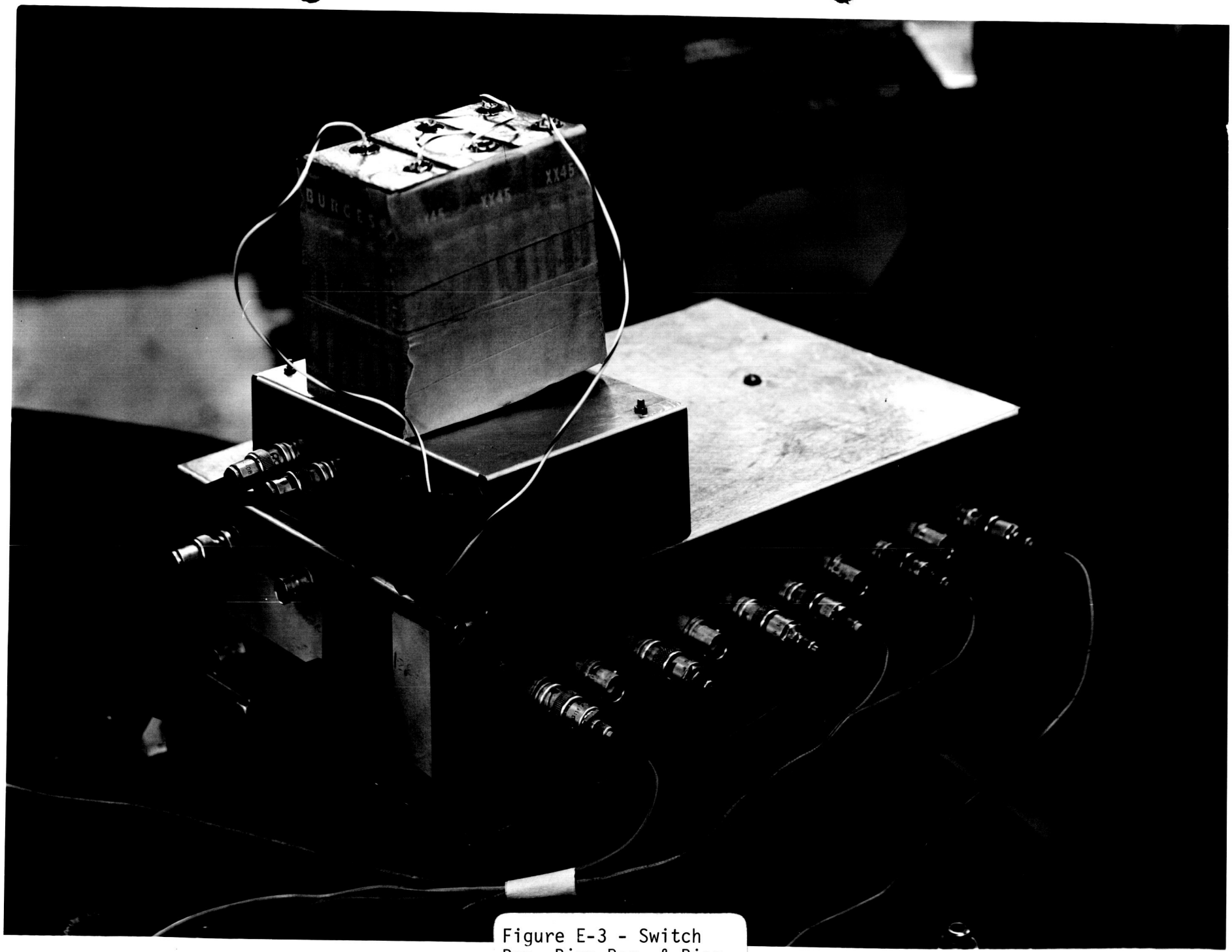

Figure E-3 - Switch Box, Bias Box, & Bias Batteries on Shaker

APPENDIX F

TEST SPECIMEN

This section briefly describes the specimen, the stress at the failure region and its fatigue characteristics.

The specimen is shown in figure F-1 . It is machined from 6061T6 aluminum cold rolled 1 1/2" thick plate. Each set of specimens was aligned similarly with respect to the grain and the same machinist machined each specimen of one set. A special endmill cutter was made for machining the beam root region and end run out region. Successively lighter cuts were made until the dimensions were within tolerance. This reduced the tendency of large residual surface stresses. To produce a smooth surface in the failure region, the root was polished with a rouge impregnated cloth fitted to a rotating mandrel. The final process was the degreasing of the specimen after which each was stored in a plastic bag.

No post machining heat treatment was performed and this is one criticism of the specimen. The machining and polishing undoubtedly induced surface stresses but these were not relieved by annealing and further heat treatment. The grain structure in the root region is characteristically enlogated in the longitudinal direction (figure F-2) so some recrystallization probably did occur due to polishing. The temperature attained during polishing and degreasing was estimated at less than 200°F which is too low for any annealing. Hardness tests were performed as long as six months after fabrication with no change in hardness noted (values were in the upper T-6 range with no difference noted between the root region and the unpolished region). No excessive scatter was noted in the fatigue curves so that it can be assumed that the effect on the fatigue life of the surface

treatment was fairly uniform over a set of specimens. The specimens were not stored in oil which is a standard fatigue test practice. No adverse effects were noticed due to this type of storage. During testing the root region of the last two sets of beams was coated with silicone grease to prevent moisture from entering the crack. This coating reduced the air corrosion of the crack. It was necessary to obtain S-N curves for the specimens of each set since the variations in machining and raw material could lead to poor repeatability of the S-N curves.

The fatigue crack formed in the center of the root region of the beam. The specimen is more a plate than beam and therefore the maximum stress at the center higher than that at the edge of the beam. When it became necessary to add side notches to the specimen, the stress gradient in the root region became very distorted. The notches were varied until the same crack configuration occurred as before the notches were added. A photo elastic study was made of the beam root with notches and appears in figure F-3. Although the highest stress occurs close to the edge of the beam the gradient here is very high while the stress is more uniform in the central region of the root region. It is believed that the first cracks form at the high stress points and propagate inwardly to the central portion of the beam. Outwardly propagating cracks are stopped by the steep negative stress gradient.

In the specimens used in this project, the crack began to enlarge significantly at about .6 to .8 total damage. It was assumed that the crack which resulted in failure did not propagate individually but that many small cracks (which had the highest density in the high stress region) linked together to form one large crack.

Several micro graphs were taken of the failure region of a failed beam with no side notches. In figure F-2 the cracks are shown at 140X after they have been etched and plastically strained to open the cracks. The first picture shows a typical fatigue crack changing direction at a grain boundry. The second picture shows a high density of cracks running parallel to the final failure crack (the specimen was fractured manually after failing in a test). This was at the central portion of the beam where the highest stresses occurred. The third picture shows two smaller cracks in the process of linking together about 1 mm from the final failure crack. These micro graphs tend to confirm the hypothesis that the phases of damage (intercrystal damage, micro crack, and macro crack) are separated to some degree. If the first phase of damage does last for about .4 total damage then the hypothesis that recovery due to relaxation during an interruption seems reasonable since no significant cracks have formed.

A different configuration of stress riser was tried which incorporated 1/8" diameter hole drilled transversely at the center of the root. The stress gradient around the hole was so great that a crack was started almost immediately. This crack propagated very slowly. It was presumed that since the stress ahead of the crack tip was low, no small cracks were present which would link with the large crack. Therefore since the only mechanism of crack propagation was the stress riser at the tip of the crack it propagated more slowly than in the normal beams. This is an indirect additional verification that the final failure crack did propagate by linking of smaller crakcs in the normal beams.

FIGURE F-1

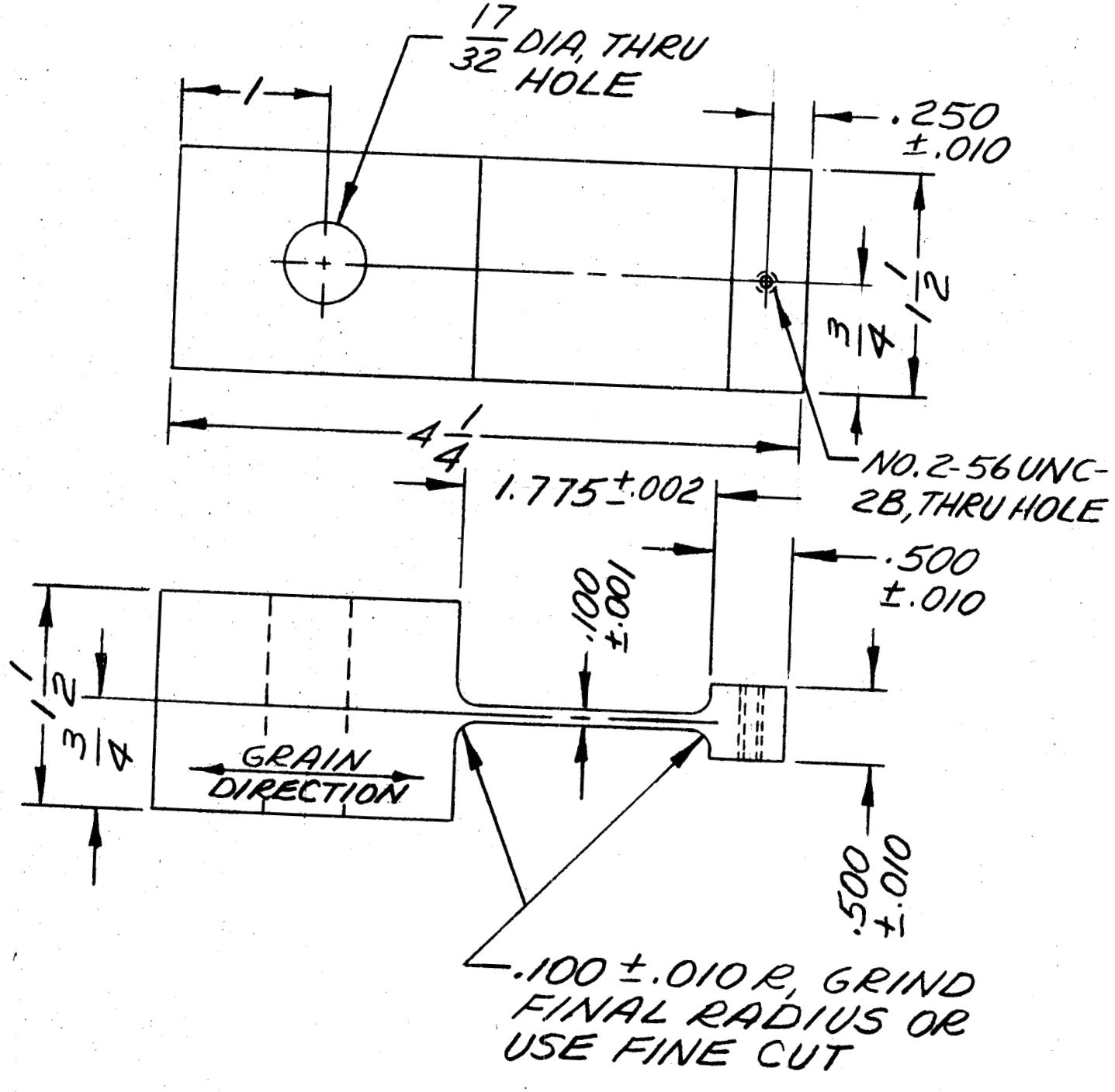
17/32 DIA, THRU HOLE
1
.250 ±.010
1 1/2
3/4
4 1/4
NO. 2-56 UNC-2B, THRU HOLE
1.775±.002
.500 ±.010
.100 ±.001
1 1/2
3/4
GRAIN DIRECTION
.500 ±.010
.100 ±.010 R, GRIND FINAL RADIUS OR USE FINE CUT

FIG F-2 MICRO PHOTOGRAPHS OF FATIGUE CRACKS 140X

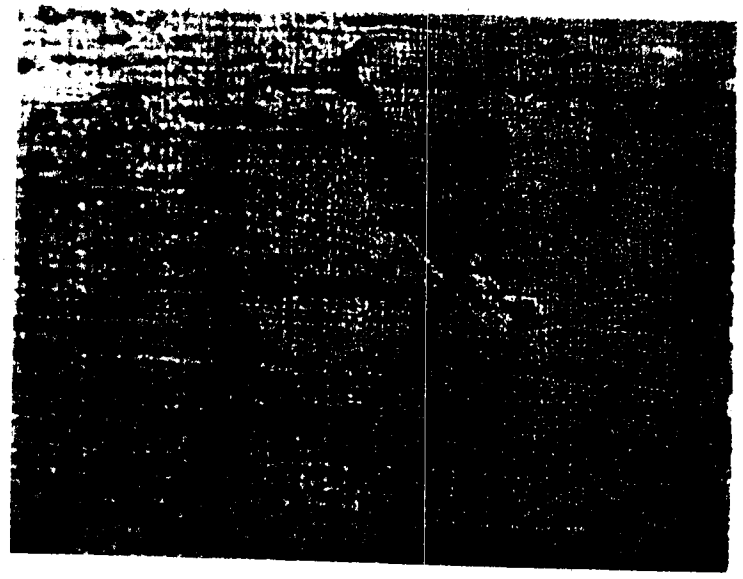

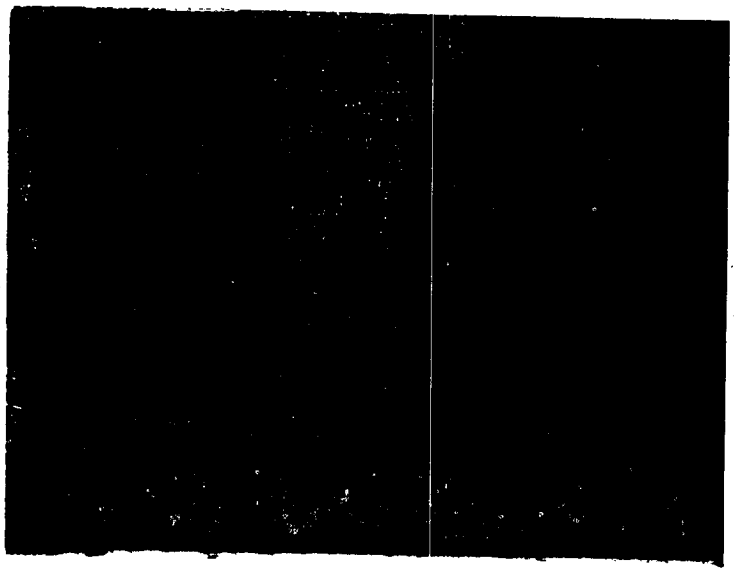

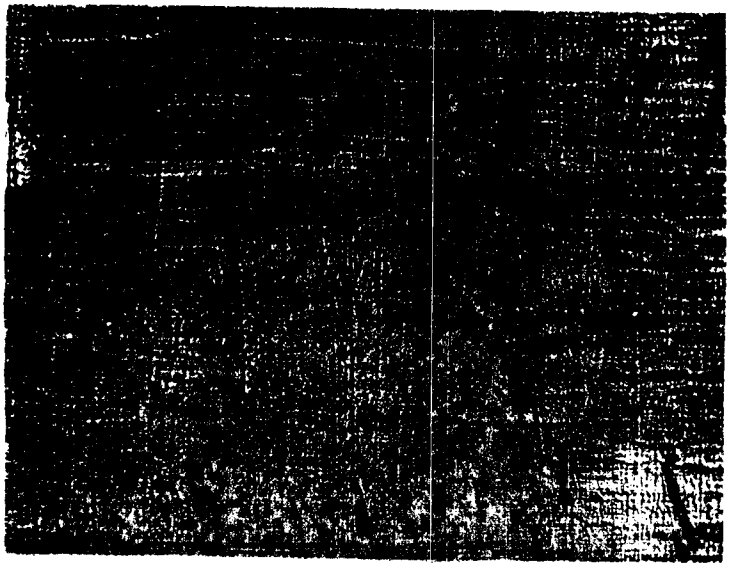

FIGURE F-3

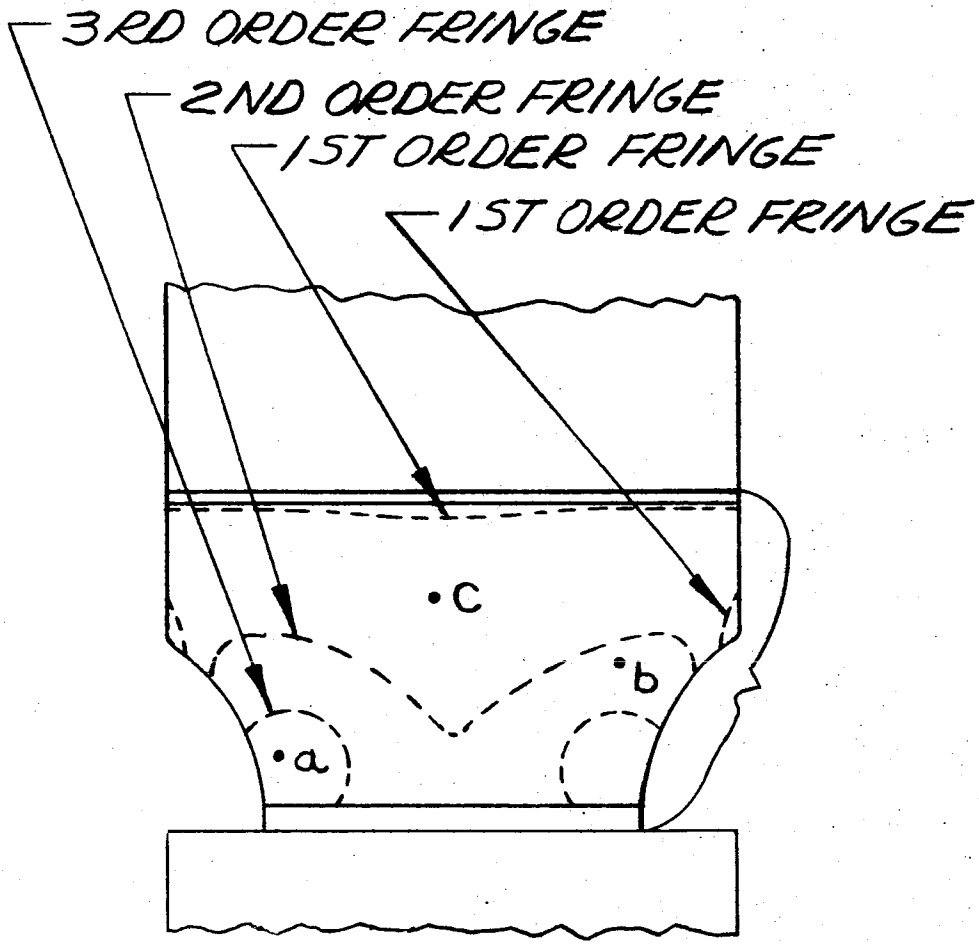

AREA COVERED BY PLASTIC
POINT a: $h = 3.65$
POINT b: $h = 2.46$
POINT c: $h = 1.65$

FIGURE 1
SCALE 2/1

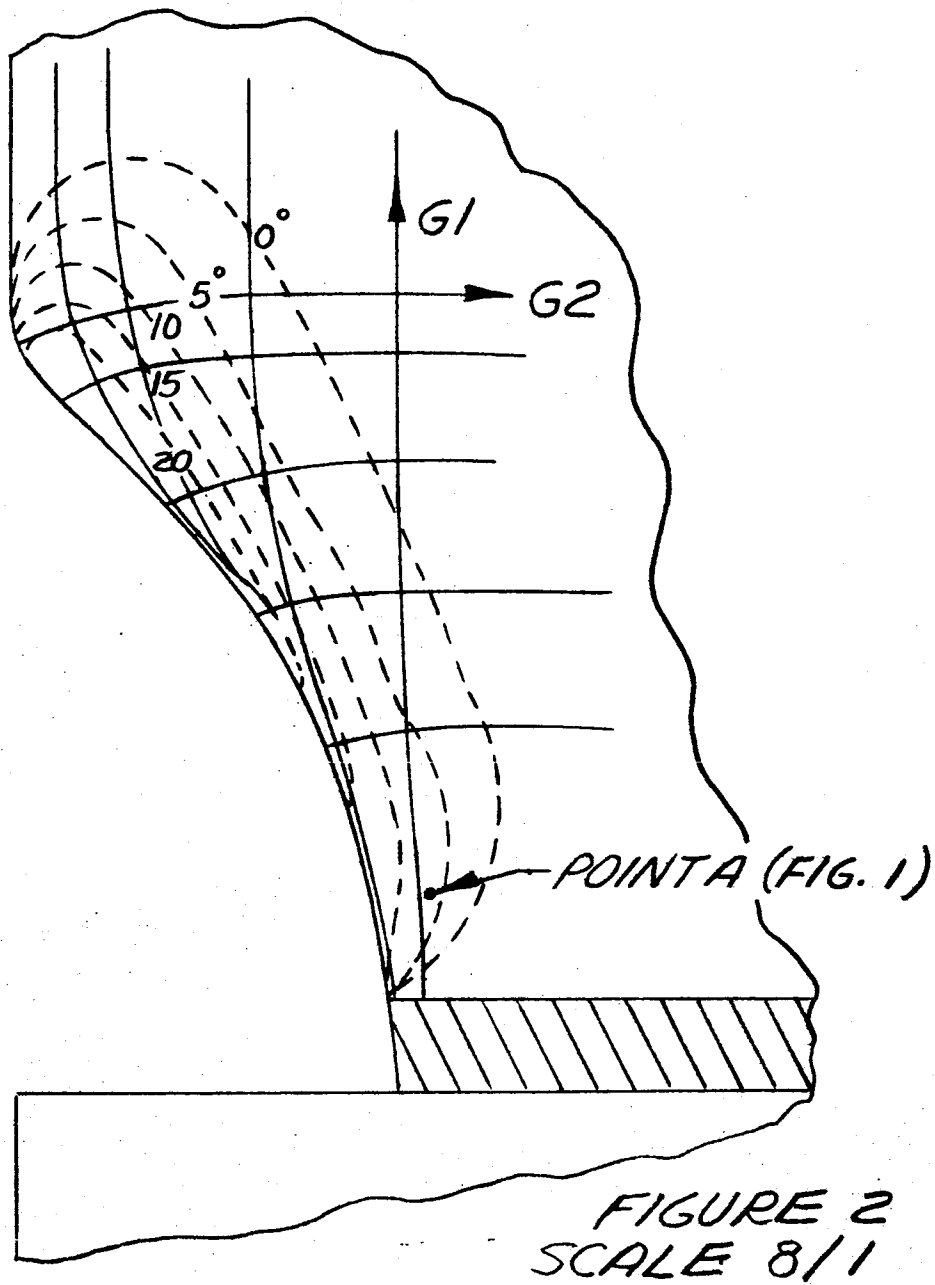

FIGURE 2
SCALE 8/1

STRESS PATTERN IN NOTCHED BEAM ROOT

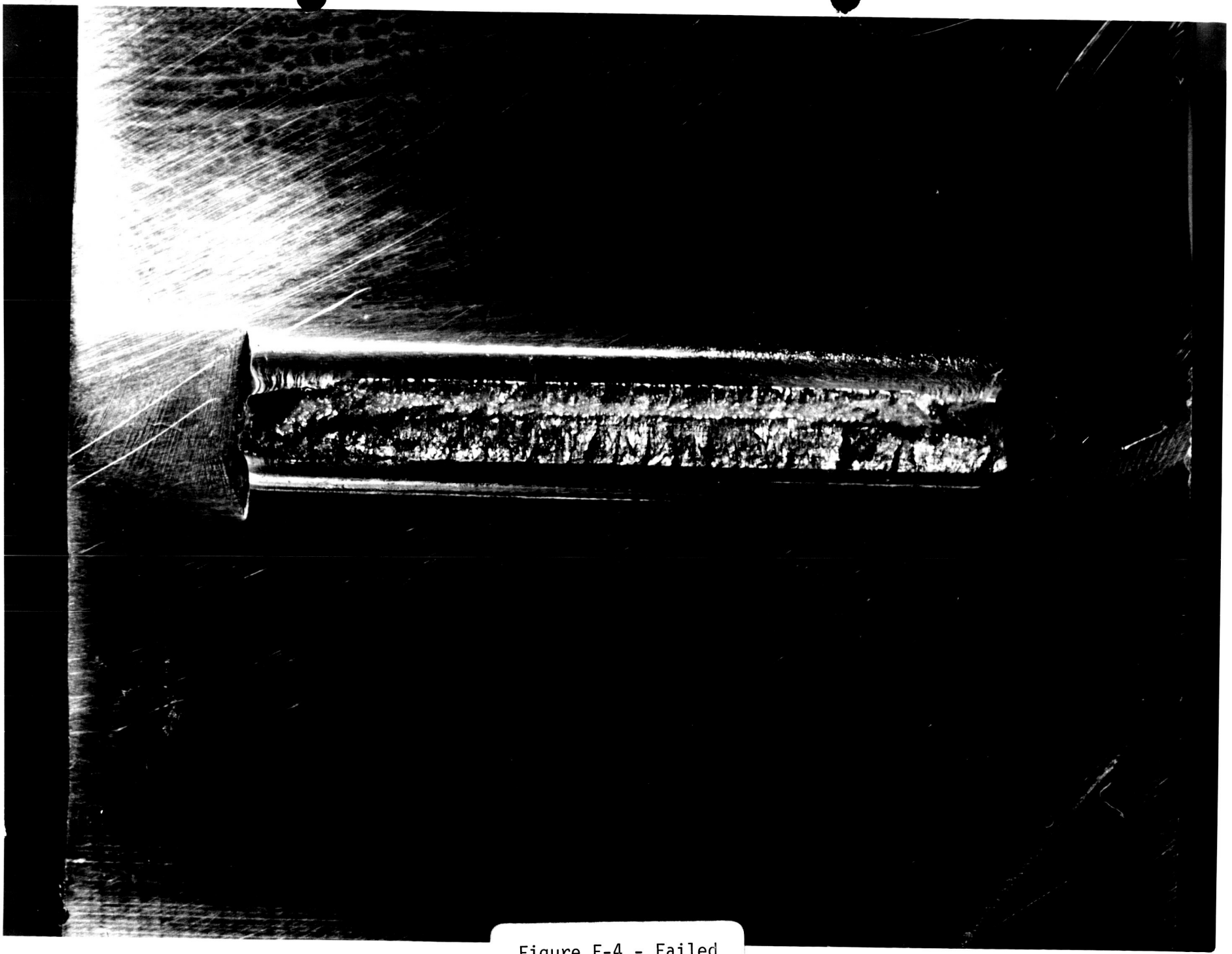

Figure F-4 - Failed Specimen Showing Fretted Surface

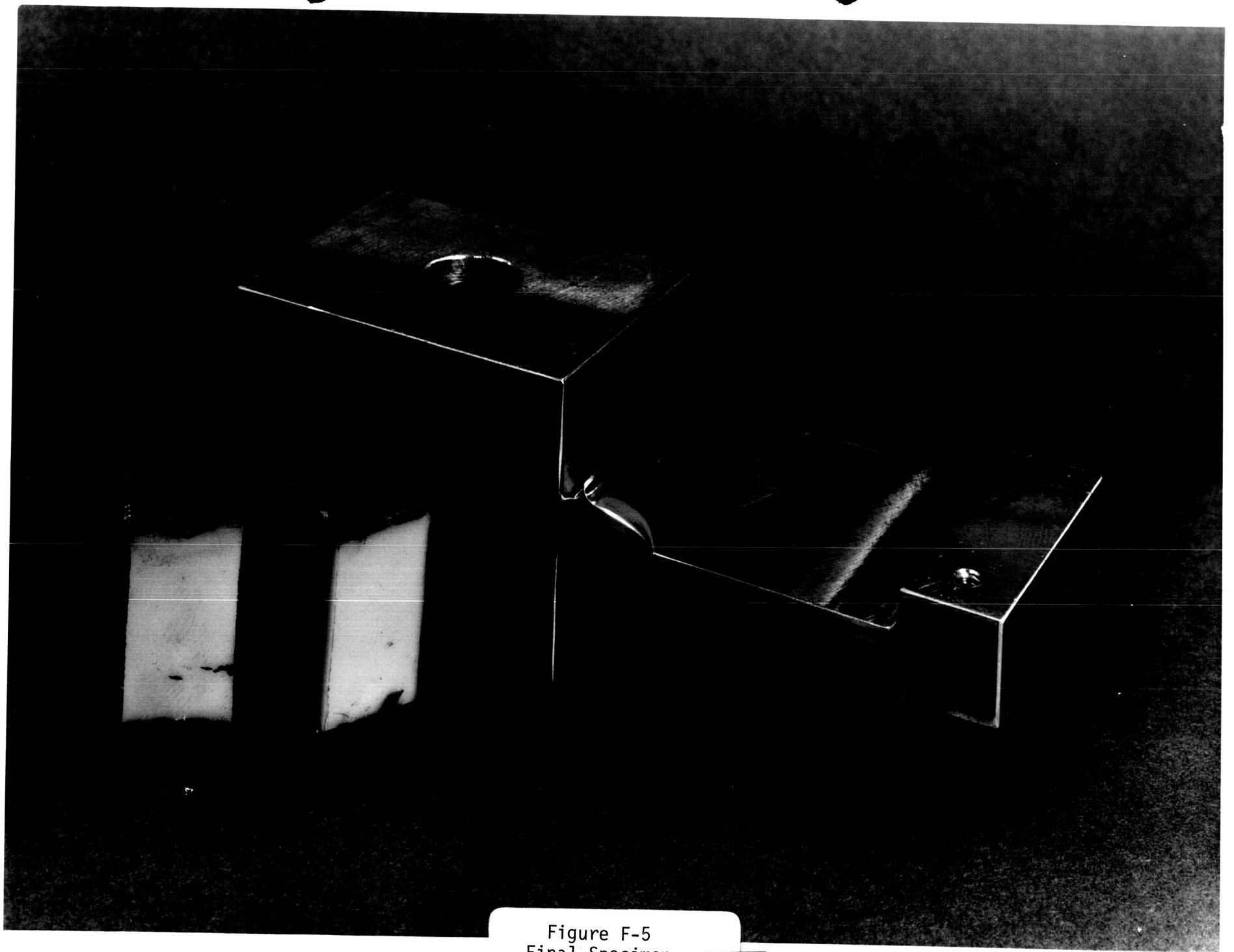

Figure F-5
Final Specimen
and Damper

APPENDIX G

ANALYSIS OF DATA

This section contains the data, the manner in which the data was reduced, some of the reasons for the particular form of reduction and some conclusions based on data reduction. Results of tests involving the first capacity probe amplifier are in general omitted because of its poor performance. The one exception is that data from the sine dwell tests obtained with this amplifier is used but it is considered valid for these reasons:

(1) These tests were conducted in May before the temperature drift became a bad problem.

(2) The correlation tests are normally multibeam tests, but since this test is a resonant dwell test and each beam has a different resonance, a test must be run for each beam separately. Therefore the drift which would skew the results of a multibeam test all in one direction would probably vary from one test to another so that the overall effect of the drift for several tests is an increase in scatter.

For all multibeam tests it is necessary to take the data from each beam and reduce this data separately to account for the different f_n and Q of the individual beams. The variations in f_n and Q from beam to beam is great enough to cause a range in damages of about 20 to 1 to occur in the specimens for one multibeam test. If the data reduction is performed with consideration taken for these individual differences, the range of values for predicted damage at actual failure becomes about 4 to 1.

For cases where f_n and Q changed during the test, some consideration of these changes were made in the calculations. If the changes in Q and f_n were slight (stress changes of less than 5%), then the average value was used. If the stress changes were greater than 5% the test was broken into segments in which the stress level changed less than 5%.

An important consideration which must be taken into account before any data reduction can be made is the determination and calculation of an accurate calibration. The data and calculation for one test are presented here. Due to reasons innumerated in Appendix E, several repetitions of the pretest calibration are necessary to obtain statistical confidence in the g-level to voltage sensitivity. The amplifier used in the capacity probe transducer may occassionally be changed or some overall wiring changes made so that the sensitivity of the transducer will change. It is desirable to use data from all calibrations to get an estimate of the relative sensitivities. The calibration procedure will be described and an example will be presented. This example was chosen to be the calibration from the field vibration test which failed to correlate with the predicted damage. This is presented to show that instrumentation drift may have been responsible for the lack of correlation.

Five repetitions of the calibration were made. Three were made on one day and two were made the next. Changes were made after the first day which affected the sensitivity. The sensitivities for each beam are presented in Fig. G-1, with compensations made so that it is correct for the resonance of the specimen during the test.

SENSITIVITY $\left(\frac{\text{mv-rms}}{\text{peak g}}\right)$

BEAM	Run 1	Run 2	Run 3	Run 4	Run 5
1	1.057	1.038	1.015	.908	.903
2	1.000	.990	.994	.908	.833
3	1.580	1.590	1.635	1.520	1.400
4	.566	.577	.559	.544	.511
5	1.230	1.250	1.221	1.140	1.008
6	.981	.960	.947	.899	.803
SUM	6.414	6.385	6.371	5.919	5.458

FIGURE G-1

From the presented data it can be seen that the calibration varied from beam to beam within one calibration run. If one assumes that the fluctuations in the sensitivity of one beam between calibration runs are of a random nature, then the sum of all the sensitivities of one run should be very nearly equal to the sum from another run. For the first three runs made on the day prior to the field vibration test, the sums of the first three calibration runs do not vary by more than .7%. It is concluded that practically no drift occurred in the amplifier for that set of three calibration runs. On the day of the test, two calibration runs were made (runs 4 and 5). It is apparent that the amplifier drift resulted in an overall decrease in sensitivity which is noticeable in the sums of runs 4 and 5. It was initially assumed that the 8% drop in the sum of run 5 from the sum of run 4 was due to the stabilization of the amplifier gain since run 4 was made just after the amplifier had been turned on. Because of the lack of correlation in predicted damages, it is now considered probable that the change in sum of runs 4 and 5 was due to amplifier drift which continued during the test and did not stabilize after warm up. With respect to the field vibration, it can be seen by the sums for each calibration run that if the amplifier continued to drift in the same direction (lower sensitivity) that this is consistent with the type of error which occurred in the damage accumulation for that test.

Using the original assumption that run 5 was stable, it is desired to correct sensitivities for amplifier drift and to estimate the mean sensitivity for each beam. The first step is to multiply every sensitivity of a given run by the ratio of the sum of run 5 to the sum of that given run. This in effect corrects for the amplifier drift. Then the only remaining step is to average each beam sensitivity for all runs.

CALIBRATION RUN

BEAM	Run 1	Run 2	Run 3	Run 4	Run 5	AVG.
1	.899	.888	.869	.837	.903	.879
2	.851	.847	.851	.837	.833	.844
3	1.344	1.360	1.400	1.401	1.400	1.381
4	.481	.477	.479	.501	.511	.490
5	1.046	1.069	1.046	1.051	1.008	1.044
6	.835	.821	.811	.829	.803	.820
SUM	5.456	5.462	5.456	5.456	5.458	5.458

FIGURE G-2

The average sensitivity listed in the last column of Figure G-2 is used in the reduction of data. All the test data was reduced using sensitivities found in this manner.

The equivalent test formulas were rederived in terms of damage with the tests being indirect proofs of the formulas as given in the summary. The formula for the run-out-to-failure portion of the test was the same for each test.

$$D = \frac{f_n\, t}{N} \qquad \text{G-1}$$

The test was conducted at the resonant frequency f_n and the time t was that required to lower the initial resonance 1/2%. The value of N was taken from an S-N curve once the value of stress was determined. This was determined by the equation:

$$\sigma = K_1\,(y-x)$$

where (y-x) is the relative motion of the beam tip. The capacity probe amplifier gives a voltage proportional to the relative displacement. The derivation of the

formula used for data reduction to obtain stress is based on the assumption that the specimen is a single degree of freedom model with negligible damping.

$$m\ddot{y} + k\,(y-x) = 0$$

$$(y-x) = -\frac{m}{k}\,\ddot{y}$$

$$\sigma = K_1\,(y-x) = -\frac{K_1\,\ddot{y}}{W_n^2} \qquad \text{G-2}$$

The value of K_1 is measured to be 3.82×10^5 psi per inch of tip deflection for a beam with no side notches cut in the beam. The final equation used is:

$$\sigma = \frac{6.04\,\ddot{y}\,10^6}{f_n^2} \quad ** \qquad \text{VI (3)}$$

where $\ddot{y}$ is expressed in g's. It is apparent from the above derivation that the f_n term results from the ratio of k and m and is not frequency dependent. The stress which the specimen experiences during run-out-to-failure should be compared with the peak stress which occurs during the correlation portion of the test. The stress should be higher during the final run-out-to-failure portion of the test so that the predicted damage for this phase will be the same for the (C-D) as for the (P-M) hypothesis.

The equations used in the correlation phase of the tests are now presented. They vary from the equations used in the summary by containing terms related to stress levels such as C_s and N_1 . These equations are:

(1) Sine dwell - This damage equation is the same as for the run out to failure, equation G-1. Equation G-3 is used to determine stress with K_1 being the same for Q=20 as for Q=2000.

(2) Random - This damage equation is also equation G-1. The only difference is that the N in this equation is taken from a random S-N curve and not a sine S-N

**For the sine dwell test, the root geometry resulted in different stress riser so constant was 5.72 instead of 6.04.

curve. Equation G-3 is used also to obtain the rms stress level. The value of $\ddot{y}$ used here must also be in rms measure. The frequency f_n may be obtained from the response by counting zero crossings or from the spectral analysis.

(3) Log sine sweep. The form of the damage equation used in this section is:

$$D = \frac{\Phi f_n t_{ss}}{\ln f_2/f_1 \, N_1 Q} \qquad \text{G-4}$$

where the derivation of Φ is described in Appendix C. An approximate equation for Φ is:

$$\Phi = 1.89/\theta^{.645} \qquad \text{G-5}$$

In this study the (P-M)b term is 7.8 so that Φ = .50. The (C-D) d term is 4.9 so that Φ = .67. The values of Q and f_n during the test are taken from oscillographic traces of the beam response. The resonant amplification was taken as the maximum amplitude which occurred during one sweep. The shape of the response curve was measured during the sine sweep from the oscillographic trace and value of Q used in G-4 was obtained by the equation:

$$Q = \frac{f_n}{\Delta f} \qquad \text{G-6}$$

where Δf was measured at .707 of the resonant response. The Q which appears in G-4 is used as a measure of the response bandwidth and it is more appropriate to define this Q by equation G-6 than by a resonant amplification since different Q's are obtained by the two methods.

The (C-D) damage accumulation for σ_2 preceded by σ_1 should be:

$$D_2 = \frac{n_2}{N_e} = \frac{f_n\ t_2}{N_e} \qquad \text{G-7}$$

The (P-M) damage prediction is:

$$D_2 = \frac{n_2}{N_2} = \frac{f_n\ t_2}{N_2} \qquad \text{G-8}$$

To convert the (P-M) damage to the (C-D) damage, equation G-8 must be multiplied by $\frac{N_2}{N_e}$ to convert it to equation G-7. The factor $\frac{N_2}{N_e}$ is derived in this manner:

$$N_1 \sigma_1^{\,b} = N_2 \sigma_2^{\,b}$$

$$N_1 \sigma_1^{\,d} = N_e \sigma_2^{\,d}$$

$$\sigma_2 = \sigma_1 \left(\frac{N_1}{N_2}\right)^{1/b}$$

$$\sigma_2 = \sigma_1 \left(\frac{N_1}{N_e}\right)^{1/d}$$

$$N_e = N_1 \left(\frac{N_2}{N_1}\right)^{d/b}$$

$$\frac{N_2}{N_e} = \left(\frac{N_2}{N_1}\right)^{\frac{b-d}{b}} = \left(\frac{\sigma_1}{\sigma_2}\right)^{b-d} \qquad \text{G-9}$$

For the particular case, sinusoidal vibration with a specimen having a constant Q equation G-9 becomes:

$$\frac{N_2}{N_e} = \left(\frac{\sigma_1}{\sigma_2}\right)^{b-d} = \left(\frac{A_{1,1}|H(\omega_1)|}{A_{1,2}|H(\omega_2)|}\right)^{b-d} \qquad \text{G-10}$$

The first subscript denotes frequency. The second subscript on A denotes test. When $\omega_1 = \omega_2$, as would occur in a two level resonant sine dwell test or a sine sweep test, (10) reduces to:

$$\frac{N_2}{N_e} = \left(\frac{A_1}{A_2}\right)^{b-d} \qquad \text{G-11}$$

where the subscript denotes test. A_1 precedes A_2 and $A_1 > A_2$. In the case of random vibration where the input is described in terms of spectral density, G-11 becomes:

$$\frac{N_2}{N_e} = \left(\frac{W_1}{W_2}\right)^{\frac{b-d}{2}} \qquad \text{G-12}$$

In the case of the test specimens for this project, the nonlinearities in Q prevent the use of G-10, G-11 or G-12 in data analysis but they can be used when a linear system is assumed and corrections are wanted to convert (P-M) damage to (C-D) damage. Equation G-9 is used to obtain (C-D) damage in vibration test.

The presentation of data will be in tabular form. All raw data will be presented except for the time to failure in the run-out-to-failure portion of the test. Several checks of resonant frequency are made before the resonance drops 1.55 cps which is the failure criteria. Interpolation or extrapolation must be used in most cases to find the exact time t required to drop the resonance this amount. The rate of change of resonance in the last stages of failure is so high that a slight increase in time duration will result in

a large change in resonance. The time to failure in the table is the calculated time to failure and an example case is shown in Figures G-4 and G-5.

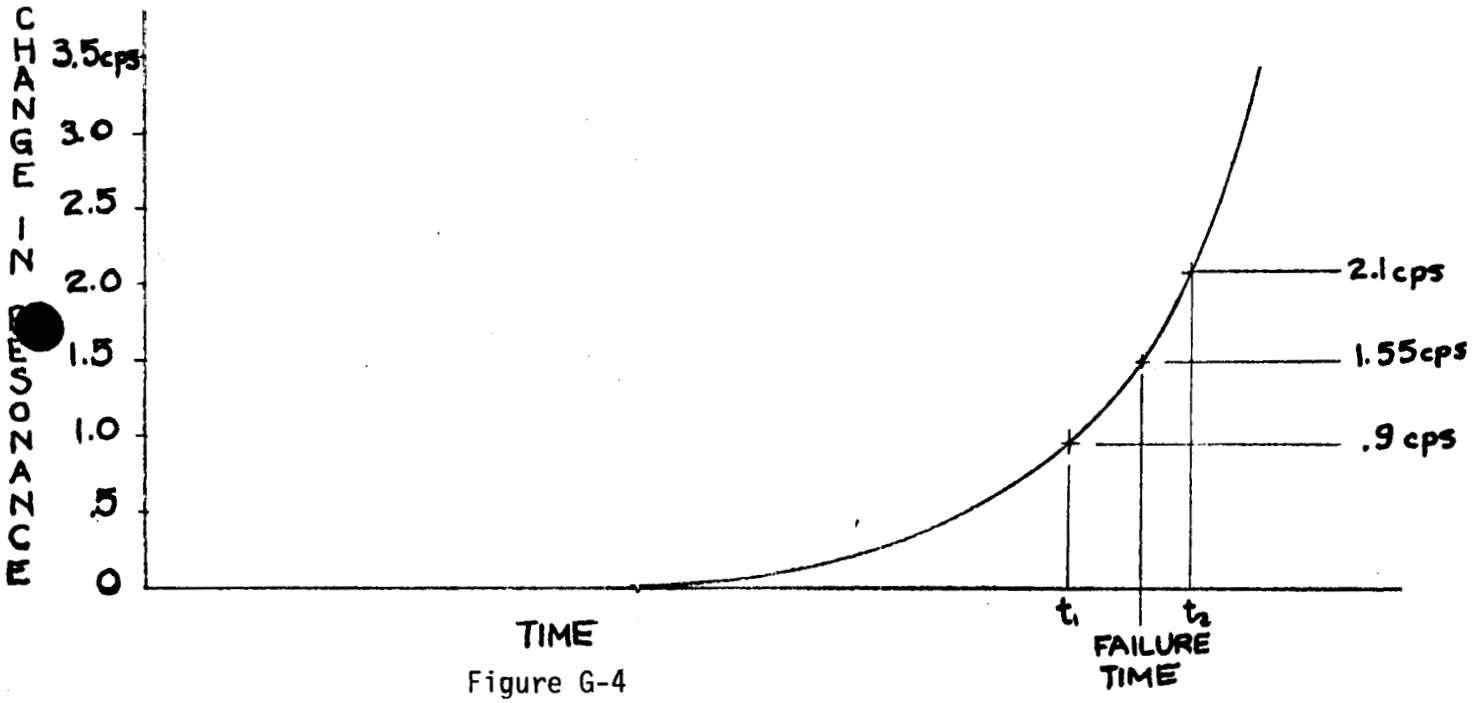

Figure G-4

(1.) Sine Dwell $D_{TOTAL} = \frac{f_{n1} t_1}{N_1} + \frac{f_{n2} t_2}{N_2}$

Beam	f_{n1}	t_1	A_1	N_1	f_{n2}	t_2	A_2	N_2	D_1	D_2	D_{TOTAL}
1	327.5cps	$3x10^3$sec	460g	$6.1x10^6$	311.6cps	$8.05x10^3$sec	460g	$2.9x10^6$	.1607	.8650	1.0257
2	340.4	$7.2x10^3$	460	$10.5x10^6$	316.6	$8.10x10^3$	454	$3.5x10^6$	.2333	.7040	.9373
3	332.0	$7.2x10^3$	460	$7.6x10^6$	317.5	$3.40x10^3$	550	$.94x10^6$	.3145	1.1470	1.4615
4	327.0	$7.2x10^3$	437	$7.3x10^6$	313.1	$7.92x10^3$	437	$3.4x10^6$	.3225	.7290	1.1515
5	335.0	$7.2x10^3$	460	$8.2x10^6$	316.5	$4.80x10^3$	460	$3.2x10^6$	.2940	.4750	.739
6	330.0	$7.2x10^3$	460	$6.6x10^6$	315.4	$4.32x10^3$	460	$3.4x10^6$	.3600	.4010	.761

SUM: 6.076
ARITHMETIC AVG: 1.013
WEIBULL MEAN: 1.028

Figure G-5

Comments on Figure G-5 are mentioned here:

1. The correlation portion of beam 1's test was run for only 3000 seconds because the duration was based on Q's and f_n's measured at low inputs which shifted when the level was raised. Test level characteristics were lower, therefore the rest of the specimens were run for longer times.

2. Specimen 4 in the correlation portion and 2, 3, 4 in the run-out-to-failure portion were run at different levels than the majority of the specimens due to faulty accelerometer calibration which was noticed during a post-test check.

3. The characteristics of Specimen 2 varied during the test. The resonance shifted from 342.4 cps to 339.4 cps during the test due to changes in the damper. The average f_n (340.4 cps) during the test was used.

4. The greatest variation in predicted to actual damage occurred in Specimen 3 which also had the greatest variation is stress level between correlation and run-out-to-failure portions of the test. Other experimenters have recorded greater than the linearly predicted damage for increasing stress levels.

5. The fatigue curve used on these specimens is different from that curve used on later sets of specimens. Each set of specimens had slightly different fatigue properties. The fatigue curve for the set of beams used on this test is defined by the equation:

$$N\sigma^{6.39} = 4.81 \times 10^{34}$$

6. The most significant result of this test with respect to the test procedure is that good prediction is possible on a two part interrupted test.

7. An additional measure of correlation is presented in which only the actual damage which occurs during the correlation portion of the test is compared with the predicted damage for the correlation portion of the test. The actual damage for the correlation protion is defined as $1-D_{(RUN-OUT)}$. The arithmetic average of the ratio of the actual damage to the predicted is then taken as a measure of correlation. See figure G-6.

BEAM	ACTUAL DAMAGE	PREDICTED DAMAGE	D_A/D_P
1	.1350	.1607	.840
2	.2960	.2333	1.269
3	-.1470	.3145	-.467
4	.2710	.3225	.840
5	.5250	.2940	1.786
6	.5990	.3600	1.663
		AVG:	.989

Figure G-6

The reason for choosing the ratio to be D_A/D_P instead of D_P/D_A is that the statistical variation in the run-out-to-failure portion of the test will result in some actual damages being zero or less than zero. When the actual damage is very small, the ratio D_P/D_A becomes very large and is unrealistic. Since D_P always is a positive finite number, the ratio D_A/D_P is a more meaningful number. Another test to use on the validity of the correlation damage is to compare the sum of the actual damage to the predicted damage. In the case of the sine dwell test $\Sigma D_A/D_P = .99$.

(2.) Random Test $D_{TOTAL} = \frac{f_{n_1} t_1}{N_{1R}} + \frac{f_{n_2} t_2}{N_{2S}}$

Beam	f_{n1}	t_1	A_1	N_{1R}	f_{n2}	t_2	A_2	N_{2S}
1	326.5cps	5.4×10^{3}sec	199grms	7.1×10^{5}	314.1cps	6.66×10^{2}sec	586g	4×10^{5}
2	323.1	5.4×10^{3}	207	4.35×10^{6}	308.8	1.35×10^{3}	575	3.4×10^{5}
3	328.5	5.4×10^{3}	199	8.2×10^{6}	313.1	3.18×10^{3}	484	1.6×10^{6}
4	331.5	2.43×10^{3}	254	1.45×10^{6}	314.3	1.02×10^{2}	598	3.3×10^{5}
5	334.9	2.24×10^{3}	278	$.82\times10^{6}$	313.8	0	0	
6	328.4	2.43×10^{3}	221	3.5×10^{6}	314.3	1.059×10^{3}	600	3.3×10^{5}
7	330.7	3.49×10^{3}	227	3.0×10^{6}	314.1	5.8×10^{2}	674	1.25×10^{5}
8	331.5	3.49×10^{3}	201	8.5×10^{6}	314.6	3.84×10^{2}	653	1.7×10^{5}
9	339.6	2.2×10^{3}	288	$.8\times10^{6}$	313.9	0	0	
10	331.8	1.8×10^{3} & $.76\times10^{3}$	257 & 274	1.3×10^{6} & $.8\times10^{6}$	313.5	0	0	
11	330.5	3.49×10^{3}	253	1.35×10^{6}	311.5	5.4×10	674	1.13×10^{5}
12	333.1	3.49×10^{3}	240	2.2×10^{6}	312.2	3.47×10^{2}	610	1.2×10^{5}

FIGURE G-7

Beam	D_r	$D_{run\ out}$	D_{TOTAL}	D_{ACTUAL}	D_A/D_P	$\sum \frac{D_A}{D_P}$ / n	$\sum D_A / \sum D_P$	$\sum D_T / n$
1	.248	.523	.771	.477	1.924	1.04	.99	1.005
2	.401	1.226	1.627	-.226	-.563			
3	.217	.621	.638	1.379	1.746			
4	.555	.097	.652	.903	1.626			
5	.914	0	.914	1.000	1.094			
6	.228	1.008	1.236	-.008	-.035			
7	.384	.552	.936	.448	1.166			
8	.136	.712	.848	.288	2.120			
9	.934	0	.934	1.000	1.071			
10	.459/.316	0	.875	1.000	1.143			
11	.855	.149	1.004	.851	.996			
12	.528	.903	1.431	.097	.184			

FIGURE G-8

Comments on Figures G-7 and G-8

(1) The data consists of results from 12 specimens run in 3 tests. The times and input levels of each test varied depending on what on-the-spot calculations indicated as to the damage levels. The first 3 entries are for the first test while the second three entries are for the second test and the remaining entries are for the third and final test.

(2) The run-out levels are nominally 600 g's peak but have been corrected based on post-test accelerometer calibration checks. If a variation between pre-test and post-test check occurs, a more critical check is then made to determine which is correct.

(3) The Weibull plot (Figure G 16) of the failure points show two distinct curves. Of the three failure points which define the upper curve, each point represents a specimen which came from a different test. No explanation for this effect can be offered. Because of this compound curve and the limited number of samples no Weibull mean was calculated.

(4) Three specimens failed during the correlation portion of the test. They are numbers 5, 9 and 10. When the correlation portion of the test was finished, the changes in resonance were 3.4 cps, 16.2 cps and 5.0 cps respectively, requiring an extrapolation to be made to get the times at failure. Since these times are obtained by extrapolating, they will be excluded for purposes of comparison. An adjusted Weibull plot (Figure G 17) of failure points was made which also showed the compound curve. A table of adjusted test characteristics is shown:

$\sum D_y/n$	$\frac{\sum D_y/D_p}{n}$	$\sum D_y/\sum D_p$
1.038	1.018	.903

Table G-1

The elimination of these three points results in a poorer set of correlation characteristics. The overall predicted damage increased 3.5%. The average predicted damage of the correlation portion of the test increased 10% when compared with the average actual damage.

(5) The important result of this test is that:

Two part tests composed of different types of vibration produce damage which can be predicted by the fatigue hypotheses used in this project.

(6) Specimen (10) changed its dynamic characteristics by more than 5% during the test so therefore the damage accumulation was broken into two time portions rather than taking the average value. This specimen was also one of those which failed during the correlation portion of the test.

Sine Sweep Test $D_{TOTAL} = \frac{\Phi f_{n_1} t_1}{\ln f_2/f_1 N_1 Q_1} + \frac{f_{n_2} t_2}{N_2}$

P-M Hypothesis $\Phi = .50$ and $f_2 = 450 cps$ $f_1 = 250 cps$

$\Phi / \ln f_2/f_1 = .851$

Beam	fnl	$t_{1,1}$	$t_{1,2}$	$t_{1,3}$	$t_{1,4}$	$N_{1,1}$	$N_{1,2}$	$N_{1,3}$	$N_{1,4}$	Q_1	Q_2	Q_3	Q_4
1	320.4	3.6×10^3_s	1.62×10^3_s	9.16×10^3_s	--	2.4×10^6	$.8\times10^6$	1.65×10^6	--	12.7	9.78	9.78	--
2	321.3	3.6×10^3_s	2.34×10^3	8.45×10^3	--	$.91\times10^6$	$.475\times10^6$	$.86\times10^6$	--	19.9	14.85	14.85	--
3	336.4	3.6×10^3_s	1.8×10^3	3.6×10^3	5.4×10^3	6.4×10^6	1.95×10^6	2.0×10^6	2.05×10^6	12.55	11.25	11.25	11.25
4	329.7	3.6×10^3_s	1.08×10^4	--	--	1.5×10^6	$.5\times10^6$	--	--	16.4	16.3	--	--
5	334.0	3.6×10^3_s	1.08×10^3	9.71×10^3	--	2.25×10^6	$.475\times10^6$	$.74\times10^6$	--	13.1	12.64	12.64	--
6	330.2	3.6×10^3_s	1.08×10^4	--	--	$6.\times10^6$	1.65×10^6	--	--	11.62	10.8	--	--
7	323.5	1.33×10^4	--	--	--	2.55×10^6	--	--	--	16.4	--	--	--
8	323.5	1.33×10^4	--	--	--	1.05×10^7	--	--	--	12.7	--	--	--
9	337.0	1.33×10^4	--	--	--	2.20×10^6	--	--	--	13.5	--	--	--
10	338.0	1.33×10^4	--	--	--	$.78\times10^6$	--	--	--	17.1	--	--	--
11	331.5	1.33×10^4	--	--	--	2.35×10^5	--	--	--	18.6	--	--	--
12	331.5	1.33×10^4	--	--	--	7.6×10^5	--	--	--	14.6	--	--	--

FIGURE G-9

Beam	A_1	A_2	A_3	A_4
1	480g's	545g's	504g's	--
2	546	599	550	--
3	467	545	543	540g's
4	535	626	--	--
5	527	649	611	--
6	455	535	--	--
7	484	--	--	--
8	407	--	--	--
9	536	--	--	--
10	618	--	--	--
11	697	--	--	--
12	597	--	--	--

FIGURE G-10

Run-out-to-failure

Beam	fn	t	A	N	$D_{1,1}$	$D_{1,2}$	$D_{1,3}$	$D_{1,4}$	D_1	D_2	D_T	D_A	D_A/D_p
1	312.3cps	1.79×10^3sec	550g	5.6×10^5cy	.0322	.0564	.1545	--	.2431	.993	1.2361	.007	.029
2	308.1	4.2x10	585	2.85×10^5	.0544	.0909	.1810	--	.3263	.0454	.3717	.955	2.930
3	315.8	1.05×10^3	586	4.2×10^5	.0128	.0235	.0458	.0670	.1491	.789	.9380	.211	1.417
4	313.9	1.92×10^2	585	4.1×10^5	.0410	.371	--	--	.412	.147	.559	.853	2.070
5	315.6	9.18×10^2	583	4.3×10^5	.0347	.0511	.2950	--	.3808	.674	1.0548	.326	.856
6	310.0	4.31×10^2	585	3.1×10^5	.0145	.1710	--	--	.1855	.432	.6175	.568	3.060
7	311.4	7.55×10^2	600	2.75×10^5	.0873	--	--	--	.0873	.855	.9423	.145	1.662
8	310.7	9.46×10^2	600	2.75×10^5	.0275	--	--	--	.0275	1.070	1.0975	-.070	-2.550
9	308.2	2.59×10^3	600	2.4×10^5	.1282	--	--	--	.1282	3.32	3.4482	-2.32	-18.100
10	311.8	3.2×10^2	600	2.8×10^5	.286	--	--	--	.286	.356	.642	.644	2.250
11	309.9	7.4x10	788	2.85×10^4	.858	--	--	--	.858	.805	1.663	.195	.227
12	309.5	1.19×10^3	600	2.55×10^5	.338	--	--	--	.338	1.445	1.783	-.445	-1.316

Figure G-11

WEIBULL MEAN: .984 $\sum D_T/n = .99$ $\sum D_A/\sum D_P = 1.03$ $\sum \frac{D_A/D_P}{n} = .97$

The complicated presentation of data in figures G-9, G-10, and G-11 resulted from the fact that in the first sine sweep test the dynamic characteristics of the beams changed more than 5% so the test was broken into four segments. If some specimens did not change enough to warrant more than three breakdowns, for instance, then the fourth space was left vacant. Specific observations include:

(1) The correlation measurements shown above are made without consideration of specimen (9). The total damage of 3.45 is well out of the scatter band of the rest of the data. The run-out-to-failure portion of the test accumulated a damage of 3.32 which is indicative of some gross error. The test calibration was double checked and appeared correct but no comparible deviation was measured on any other test or on the compiling of the fatigue curves. If specimen (9) is included, the correlation measurements are poor.

$\sum D_T/n = 1.20$ $\sum D_A/\sum D_P = .313$ $\sum \frac{D_A/D_P}{n} = -.622$

In addition to this, the Weibull plot (Figure G 18) of all points show specimen (9) far off the line for the other 11 specimens. For these reasons, specimen (9) is omitted.

(2) In the (C-D) damage accumulation, the tabular computations are not shown for the sake of brevity. The correlation measurements are presented for the (C-D) hypothesis with specimen (9) not included:

$\sum D_T/n = 1.09$ $\sum D_A/\sum D_P = .767$ $\sum \frac{D_A/\sum D_P}{n} = .86$

These values show that the (P-M) hypothesis in all comparible aspects yields better correlation than does the (C-D) hypothesis.

(3) This data is the result of two tests. The first test which includes the first six specimens was complicated by changing characteristics. The visco elastic dampers became partially loose as the test progressed due to poor glue bonds. None of them came loose, but the characteristics changed as the test level was increased. After one hour of test time the level was increased to compensate for the unexpectedly low Q's. After this increase, a continued change of characteristics was observed. This change in characteristics was handled by plotting the beam tip g level vs. time and then breaking this up into increments so that the average g level for the increment of time duration was used. This is the way the reduction of data was handled. It is conceded that some error is induced by this non-stationary response and this is reflected in the lower slope of the Weibull failure plot for this test.

Field Vibration: $$D_T = \frac{f_{n_1} t_1}{N_{r,1}} + \frac{f_{n_2} t_2}{N_{r,2}} + \frac{\phi f_{n_3} t_3}{\ln f_2/f_1 \, N_{s,3} Q_3} + \frac{f_{n_4} t_4}{N_{s,4}}$$

P-M hypothesis

$$D_{1,1} = \frac{f_{n_1} t_1}{N_{r,1}}$$

$$D_{1,2} = \frac{f_{n_2} t_2}{N_{r,2}}$$

$$D_{1,3} = \frac{\phi f_{n_3} t_3}{\ln f_2/f_1 \, N_{s,3} Q}$$

$$D_1 = D_{1,1} + D_{1,2} + D_{1,3}$$

$$D_2 = \frac{f_{n_4} t_4}{N_{s,4}}$$

Beam	$f_{n,1,2,3}$	t_1	A_1	$N_{r,1}$	$t_{2,1}$	$t_{2,2}$	$t_{2,3}$	$A_{2,1}$	$A_{2,2}$	$A_{2,3}$	$N_{1,2}$	$N_{2,2}$	$N_{2,3}$	t_3	A_3	N_3	Q_3
1	323.3	1.81×10^3	211g	9.1×10^6	4.31×10^3	4.69×10^3	--	125g	132g	--	2.5×10^8	1.65×10^8	--	3.61×10^3	518g	1.48×10^6	13.7
2	333.2	1.81×10^3	225	9.1×10^6	9×10^3	--	--	140	--	--	1.73×10^8	--	--	3.61×10^3	606	7.0×10^5	13.1
3	329.0	1.81×10^3	219	3.6×10^6	3.6×10^6	3.6×10^3	1.8×10^3	130	135	138	2.48×10^8	1.85×10^8	1.55×10^8	3.61×10^3	628	4.6×10^5	15.2
4	337.3	1.81×10^3	237	2.9×10^6	9×10^3	--	--	166	--	--	5.5×10^7	--	--	3.61×10^3	780	1.18×10^5	18.1
5	331.5	1.81×10^3	196	11.5×10^6	5.4×10^3	3.6×10^3	--	134	141	--	2.25×10^8	1.5×10^8	--	3.61×10^3	656	3.65×10^5	16.1
6	334.4	1.81×10^3	192	16.0×10^6	9×10^3	--	--	130	--	--	3.3×10^8	--	--	3.61×10^3	521	2.50×10^6	12.0

Beam	$f_{n,4}$	t_4	A_4	N_4	$D_{1,1}$	$D_{1,2,1}$	$D_{1,2,2}$	$D_{1,2,3}$	$D_{1,3}$	D_1	D_2	D_T	D_A	D_A/D_1
1	315.6cps	2.87×10^2sec	599g	3.2×10^5cy	.064	$.558\times10^{-2}$	$.917\times10^{-2}$	--	.060	.1388	.283	.4218	.717	5.17
2	316.1	2.1x10	600	3.37×10^5	.066	.017	--	--	.137	.220	.020	.240	.980	4.45
3	312.7	2.155×10^2	602	2.75×10^5	.165	$.476\times10^{-2}$	$.64\times10^{-2}$	$.382\times10^{-2}$	.178	.358	.245	.603	.755	2.11
4	312.5	5.51x10	597	2.85×10^5	.213	.055	--	--	.596	.864	.060	.924	.940	1.09
5	314.0	2.145×10^2	597	3.2×10^5	.052	$.825\times10^{-2}$	$.795\times10^{-2}$	--	.213	.281	.210	.4913	.790	2.81
6	313.6	3.53×10^2	598	3.1×10^5	.038	$.912\times10^{-2}$	--	--	.042	.089	.356	.445	.644	7.23

$$\frac{\sum D_A/D_P}{n} = 3.81 \qquad \sum D_A/\sum D_P = 2.48 \qquad \frac{\sum D_T}{n} = .52$$

FIGURE G-12

Considering figure G-12:

(1) The test was broken up into several portions in the low level random portion of the test. Those portions of the test that varied more than 5% were broken into segments with the average value of that segment being used in computations.

(2) The specimen resonant frequency during the correlation portion of the test was measured during the sine sweep portion and taken from oscillographic records. No measurement was taken during the random vibration portion of the test and it was assumed that the resonance was the same during the random vibration portion of the test as it was during the sine sweep portion.

(3) The calibration of the amplifier for the run-out-to-failure portion of the test was similar enough to the pretest calibration so that it is possible to double check the calibration levels. The results support the possibility that the amplifier drifted during the test. The previous example in this section had the following values which were used during the test:

Beam	Sensitivity (pretest)	Sensitivity (post test)
1	.879 mv/g	1.005 mv/g
2	.844	.928
3	1.381	1.530
4	.490	.550
5	1.044	1.170
6	.820	.917
SUM	5.458	6.100

TABLE G-2

The second column of sensitivities is based on the calibration made after the correlation portion of the test and prior to the run-out-to-failure portion of the test. The sums of sensitivities had been decreasing with each of the last two checks made prior to the test. The post-correlation test calibration indicates

an 11.8% rise in sensitivity had occurred by that time. Therefore, the most probable conclusion is that the amplifier continued to drift throughout the test so that the average sensitivity was about 12% below that sensitivity measured just prior to the test. This is the only test conducted with the second capacity probe in which a calibration drift was observed.

(4) The damage accumulation according to the (C-D) hypothesis was calculated. The only portions of the test which should have been affected by the change of hypothesis is the low level random and the sine sweep. The low level random was preceded by a high level of random so that it should be affected. The sine sweep portion of the test induces the highest stresses in the specimen up to that time, but due to the cycling, the highest stress during one cycle is preceded by lower stresses. The sine sweep test indicated that the (P-M) hypothesis is a better predictor of damage for that type of vibration. Only the altered damage levels for the low level random test and the sine sweep test will be tabularized for the sake of brevity.

Low Level Random

Beam	$(N_2/N_1)_1$	$(N_2/N_e)_2$	$(N_3/N_e)_3$	$D_{1,2,1}$	$D_{1,2,2}$	$D_{1,2,3}$
1	3.43	2.94	--	1.91×10^{-2}	2.7×10^{-2}	--
2	2.99	--	--	.0509	--	--
3	4.84	4.33	4.05	2.31×10^{-2}	2.77×10^{-2}	1.546×10^{-2}
4	2.99	--	--	.1645	--	--
5	3.02	2.60	--	2.49×10^{-2}	2.07×10^{-2}	--
6	3.08	--	--	2.81×10^{-2}	--	--

TABLE G-3

Sine Sweep

Beam	$D_{1,3}$
1	.081
2	.184
3	.239
4	.801
5	.286
6	.056

$\frac{\Sigma D_A/D_P}{n} = 2.80$ $\quad \Sigma D_A/\Sigma D_P = 1.82$

$\frac{\Sigma D_{TOTAL}}{n} = .637$

TABLE G-4

The above correlation measurements are better than those for the P-M hypothesis, but this is only a coincidental circumstance. It is believed that the amplifier drifted in the direction of decreasing sensitivities so that the predicted damage would be lower than the actual damage. Since the (C-D) hypothesis predicts greater damage it would in this case yield better correlation measurements. No value can be obtained from the data for the field vibration since it is felt that the instrumentation was faulty.

It is reasonable at this point to consider how much can be said about the validity of the (P-M) hypothesis or the (C-D) hypothesis.

All tests results indicate that the (P-M) hypthesis is better than the (C-D) hypothesis:

(1) The spacing of the random fatigue curve with respect to the sine fatigue curve is in agreement with the (P-M) hypothesis.

(2) The slope of the random fatigue curve is in close agreement with the (P-M) hypothesis. The slope of the random curve is 7.66 while the slope of the sine fatigue curve is 7.94. This is a 4% difference which is probably within the measurement error range. To satisfy the C-D hypothesis the slope should have been 4.92.

(3) The sine sweep test data correlated better using the (P-M) hypothesis. In this test, repeating blocks of continuously varying stresses were applied to the specimens in a manner similar to the way the (C-D)d term was determined, but still the (P-M) gave a better prediction of the actual damage.

One method of data presentation which is used on this set of tests and which needs clarification is the Weibull Plot in which the absicca is expressed in terms of damage rather than cycles to failure. The graph of per cent failed vs. cycles could have been plotted on probability paper also but it was felt that the Weibull distribution is more realistic for fatigue testing. The tests were conducted at a given input but because of variations in resonance and Q, the stress level was different for each specimen. A failure rate plot is usually made for a given specimen stress therefore it would be unlikely that a very meaningful plot could be made of the raw data unless some effort were made to normalize the stress or the cycles to failure. By the definition of damage used in this report, the normalized cycles to failure, n/N, for a given specimen becomes damage. Now for a rate-of-failure plot in which the stresses are all different, the cycles to failure, n_i, for the ith specimen is normalized on the mean number of cycles, Ni, which would have resulted if all the specimen had been run at this stress. This mean number of cycles comes from the S-N curve for the ith stress. This transformation of the cycles-to-failure-axis into the damage axis also permits plotting the results of multilevel tests such as occurred in this project.

The following illustration and derivation is presented to clarify how the equivalence equations are verified by the indirect approach used in this study.

In the example in Appendix J, the envelope of a random equivalent input is plotted for the field vibration supplied by the Contractor. For a specimen with fn = 340 cps, Q = 20 and a test of one hour, the equivalent random test input is 1.56 g^2/cps at 340 cps region of the spectrum. Using B-34 it can be determined that the stress is 4265 psi. rms. From the S-N curve for these beams in random loading the N term is 1.72×10^{10} cycles. Some scaling up of level is necessary to get any measurable damage in a reasonable time (no experimental data was obtained for this extreme life). Since the actual fn and Q cannot be controlled, scaling of these terms must be made also. In the equivalent random correlation test, values of fn, t and σ can be measured during the test so that scaling factors can be obtained to determine the change in damage due to scaling. A simple derivation is presented to show how actual predicted equivalent test levels can be checked by the tests performed in this project.

Let D_f be the field vibration damage as predicted from the scaled parameters.

$$D_f = \frac{f_{n,f} \cdot t_f \cdot \sigma_f^b}{C_r}$$

where the subscript f denotes parameters scaled from the field vibration. C_r is the random fatigue curve parameter. In the next equation, subscript t stands for the parameters which occur during the correlation test.

$$D_t = \frac{f_{n,t} \cdot t_t \cdot \sigma_t^b}{C_r}$$

The equivalent test parameters are related to the correlation test parameter by some factor M.

$$f_{n,t} = M_1 f_{n,f}$$

$$t_t = M_2 t_f$$

$$\sigma_t = M_3 \sigma_f$$

$$D_t = \frac{(M_1 f_{n,f})(M_2 t_f)(M_3{}^b \sigma_f{}^b)}{C_r} = M_1 M_2 M_3{}^b D_f = M_t D_f$$

where $M_t = M_1 M_2 M_3{}^b$

Now the predicted correlation damage is $M_t D_f$. The actual correlation damage is $1-D_2$ where D_2 is the damage due to the run-out-to-failure portion of the test. If

$$\frac{1}{n}\sum_{i=1}^{n}\left(\frac{1-D_{2,i}}{M_{t,i}D_{f,i}}\right) = 1 \qquad \text{or} \qquad \sum_{i=1}^{n}(1-D_{2i}) \Big/ \sum_{i=1}^{n} M_{t,i}D_{f,i} = 1$$

then the statistically average actual correlation damage is equal to the scaled damage of the equivalent test. The two correlation measurements just shown are no more than $\frac{\sum D_2/D_p}{n}$ and $\sum D_2/\sum D_p$ which were determined for every test. Therefore, once an equivalent test level has been determined, whether it is sine dwell, sine sweep or random, the tests which have been run show that it is possible to predict that damage accurately.

Another measurement was made which is considered important with respect to the basic random damage equation. That is the degree to which the actual peak distribution of stresses are approximated by the Rayleigh distribution. The prediction of the slope and position of the random fatigue curve is based on the assumption of a Rayleigh distribution of peaks and a (P-M) damage accumulation. Close agreement exists for this prediction with the undamped beams. Since with a Q of 2000 a very narrow band random response will occur

and the assumption of a Rayleigh distribution is probably very close. In the correlation tests though, the Q is often close to 10 during the test so some variation could result due to this. Data was taken for all 12 beams of the random vibration test and a plot of a typical response is plotted.

The procedure was to measure the number of times the signal exceeded a certain threshold level. A tape loop of the beam tip response during the test was repeated with the threshold level changed gradually from run to run until the threshold had been changed from the highest positive peaks to the highest negative peaks. The raw data for beam 1 of the random vibration peak count measurement was:

THRESHOLD	COUNTS ABOVE THRESHOLD	PEAKS OCCURING WITHIN INTERVAL
+1.4 volts	0	
		2
1.3 volts	2	
		1
1.2 volts	3	
		1
1.1 volts	4	
		15
1.0 volts	19	
		59
.9 volts	78	
		137
.8 volts	215	
		285
.7 volts	500	
		522
.6 volts	1022	
		753
.5 volts	1775	
		1052
.4 volts	2827	
		1188
.3 volts	4015	
		1143
.2 volts	5158	
		871
.1 volts	6029	
		355
0 volts	6384	

THRESHOLD	COUNTS ABOVE THRESHOLD	PEAKS OCCURING WITHIN INTERVAL
-.1 volts	6039	345
-.2 volts	5204	835
-.3 volts	4077	1127
-.4 volts	2885	1192
-.5 volts	1869	1016
-.6 volts	1077	792
-.7 volts	527	550
-.8 volts	241	286
-.9 volts	103	138
-1.0 volts	39	64
-1.1 volts	23	29
-1.2 volts	13	10
-1.3 volts	8	5
-1.4 volts		8

TABLE G-5

The values in the column of peaks between levels are the data points to be used in the construction of the distribution curve. It is a two lobed curve, symmetrical about the zero voltage point. In this form it is easy to determine if the beam deflected more in one direction than another. Of all the beams tested, none showed any significant asymmetry. To compare the experimental curve with a true Rayleigh distribution, the assumption had to be made then that the maximum point on the distribution coincided with the rms level and therefore also coincided with the peak of the true Rayleigh distribution. A Rayleigh distribution was plotted to satisfy this condition and comparisions

were made of the superimposed plots of the two curves. These plots are shown in Figure G-13. The conclusions which can be made from this are:

(1) Not enough data was available to get much of the distribution curve out at the 2 and 3σ points. Although the loops were as long as 20 seconds (tape loop machine capacity) the number of peaks at the 4 sigma level becomes very low. Therefore, the tails of the distributions are not well defined.

(2) It was found that the curves which were the most distorted were taken from tapes which also produced the most distorted spectral analysis. A hypothesis for this phenomenon is that in the time period of the tape loop, only several resonant build ups and decays occur and since some of these will be slightly off resonance, they will not reach the magnitude of an on-resonance response. The spectral analysis which shows several off-resonance responses usually has distortions in the peak response (one particular exception was the tape loop from the shaker table; this peak distribution was nearly an exact Rayleigh distribution but the spectral analysis was very distorted). In comparing the specimens which had greater than a Rayleigh distribution of peaks in the high stress region with specimens which sustained high damage levels, there was found to be no noticable correlation. This strengthens the belief that the tape loop time was too short and that if a longer sample time had been available the limiting distribution would have been a Rayleigh distribution.

(3) The following argument is presented to further support the existance of a nearly Rayleigh distribution in the 3σ and 4σ region since the peak measurements are too inconclusive in this respect.

a. The (C-D) hypothesis predicts a closer spacing than does the (P-M) hypothesis.

b. If the peak distribution were clipped in the high σ region, a less damaging situation would exist and the random-sine spacing would be closer than predicted using the Rayleigh distribution.

c. The spacing has been measured to be 2.6% greater than predicted using the (P-M) hypothesis and the Rayleigh distribution as assumptions. Since any assumptions other than these would result in less than the extreme spacing, it must be assumed that these conditions exist.

The final portion to be covered in this section is the analysis of the data taken during the fatigue property tests of the undamped specimens. This consisted of determining the S-N curve for random and sine and the (C-D) exponent "d".

The reduction of data to determine the S-N curves was straight forward. The test procedure is the same as for the run-out-to-failure portion of the multibeam tests. The test was interrupted when the Q dropped to 100 to make resonant frequency checks during the sine tests. The time to failure was obtained by interpolation between these check frequencies. A similar procedure was followed in the random testing when the narrow band output of the capacity probe transducer dropped out of the pass band of a narrow band filter set on the original resonance of the beam. Since it was difficult to run groups of beams at the same stress level, a least square curve fit was used with no

grouping of points. The cycles-to-failure and stress were converted to natural logarithms and the best straight line was fitted to this plot. The variance of the logarithm of stress was also computed. Points outside of a $\pm 3\ \sigma$ band about the curve were eliminated and a new line was fitted to remaining points. One or two such points were eliminated. Other points which were omitted were for samples in which some obvious procedural mistake was made (bad calibration, over stressing, amplifier drift, etc.).

The S-N curve equation is given for each set of beams, and in Fig. the points and curves are plotted for each set of beams.

Set 1. Sine: $N\sigma^{9.68} = 2.44 \times 10^{48}$ (24 points) Random: $N\sigma^{7.04} = 2.47 \times 10^{34}$ (18 points)

Set 2. Sine: $N\sigma^{6.39} = 4.97 \times 10^{34}$ (15 points) Random: $N\sigma^{6.55} = 8.75 \times 10^{32}$ (7 points)

1 SIGMA: $\pm 1.04\%$ 1 SIGMA: $\pm 1.15\%$

Set 3. Sine: $N\sigma^{7.94} = 5.03 \times 10^{41}$ (15 points) Random: $N\sigma^{7.66} = 7.8 \times 10^{37}$ (5 points)

1 SIGMA: $\pm 1.50\%$ 1 SIGMA: $\pm 3.55\%$

COMMENTS:

(1) The specimens in Set 1 were of the original configuration with no side notches and the region of high stress in the root region was not greased. It was attempted to run the test with groups of specimens at the same stress level. Post-test calibration checks were not made at this early stage and therefore the scatter is high on the sine testing. By the time the random tests were conducted, it was decided not to attempt to run blocks of specimens at the same stresses. The scatter on this test was better than for the sine test but the best feature of this test was that an attempt was made to run specimens at very high to very low stresses. Time to failure varied over a range of 1300 to 1 so that the slope was defined with a good degree of accuracy.

(2) The beams tested in the sine portion of Set 2 came from two separate sets of beams machined from different stock at different times. The equations for each set is:

$$N\sigma^{7.34} = 9.5 \times 10^{38} \text{ and } N\sigma^{5.85} = 1.89 \times 10^{32}$$

Although the slopes vary on these two sets, the region of definition is small enough that the line for each curve lies within the scatter band of the other curve. Several beams in the random portion were eliminated because of poor test procedure. The position of the sine and random curves in this test are higher than for the curves for beams in Set 1. This is because an approximate K_t was used instead of the actual K_f. Although an error is induced by not using K_f, it was felt that if that K_t was used consistantly throughout all the calculations no problems would result. The sine dwell test was conducted using beams from Set 2.

(3) The new amplifier was used for Set 3. In the random portion of this set three beams were excluded because of improper testing procedure.

(4) The measurement of the separation of the sine and random SN curve at $N = 10^6$ cycles was performed and shown here. Most of the correlation tests lasted about 10^6 cycles. The formula for the random curve (using C-D) should be:

$$N\sigma_r^d = \frac{C_0}{[2^{d/2}\Gamma(1+d/2)]}$$

where d is the (C-D) damage exponent and the slope of random curve. The ratio of the stresses are:

$$\frac{\sigma_s}{\sigma_r} = \left[\sigma^{d-b} 2^{d/2} \Gamma(1+d/2)\right]^{1/d}$$

Using the slope of the random curve for d; σ_s/σ_r being the ratio of the sine stress to the random stress at 10^6 cycles; and σ_s the sine stress at 10^6 cycles, it was found that very poor correlation existed.

Next it is assumed that the random and sine curves will be parallel using (P-M). The equation then becomes:

$$\frac{\sigma_s}{\sigma_r} = \left[2^{b/2} \Gamma(1+b/2)\right]^{1/b}$$

where b is the slope of the sine or random curve. A table is presented which has the ratios of the predicted spacing to the actual spacing for all sets of the beams using the b for the random equation and the b for the sine equation.

	Random b	Sine b
Set 1	1.043	1.186
Set 2	.808	.842
Set 3	.955	.980

TABLE G-6

The average of the two slopes in Set 3 produces a ratio of .972. This average slope of 7.8 was used in the computer program. It is considered that these results are nearly conclusive proof that for the material used in this project, the damage accumulation is linear. The average of all the above ratios is .969 while any comparison based on (C-D) damage accumulation is so unrealistic that it is not presented.

The computations used in getting the value of the (C-D)d term based on the following derivation:

$$N_1\sigma_1^d = n_1\sigma_1^d + n_2\sigma_2^d$$

where σ_1 and σ_2 are the stresses in a two level repeating test. N_1 lies on the S-N sine fatigue curve and exponent d is to be determined. This form of the equation can be expressed as:

$$(\sigma_2/\sigma_1)^d = \left(\frac{N_1 - n_1}{n_2}\right)$$

which is the form used to get the value of d. The data and results used in the computations are presented. ,The beams are from set 3.

Beam	σ_2/σ_1	fn (cps)	A_1 (g)	σ_1 (psi)	$N_1(\times 10^5 cy)$	$n_1(\times 10^5 cy)$	$n_2(\times 10^5 cy)$	$\frac{N_1 - n_1}{n_2}$	d
1	.66	313.5	600	3.68×10^4	3.2	.518	7.76	.3450	2.56
2	.615	314.0	647	3.97×10^4	1.8	.864	10.54	.0864	5.04
3	.615	312.3	650	4.03×10^4	1.5	1.203	20.6	.0144	8.72
4	.615	312.2	657	4.07×10^4	1.4	.515	6.78	.1305	4.19
5	.615	309.0	650	4.11×10^4	1.25	.529	7.83	.0918	4.91
6	.615	307.5	650	4.16×10^4	1.16	.675	9.10	.0533	6.04
7	.615	310.5	650	4.07×10^4	1.4	.513	7.53	.1179	4.41
								AVG:	5.13

TABLE G-7

The variance for this test was determined and it was found to be $\pm$1.76. Two extreme samples, numbers 1 and 3 were excluded as being too far out of line. The new d is then 4.92 and the variance is $\pm$.64. This number was used in the analysis.

A calculation of d was made for each set of beams and are presented. It was felt that more attention to detail was spent on the experiment mentioned above than for the two previous tests. For the second set of beams d = 5.68 but the variance was $\pm$1.85. For the first set of beams d = 6.87 with a variance of $\pm$1.34. By

excluding outlying failure points the value of d for the second set became 5.71 with a variance of $\pm$1.24 and for the first set d became 5.98 with a variance of $\pm$.59. The value of d/b which Corten and Dolan found as an average to be .85 for their experiments were in these tests:

Set 1: d/b = .618

Set 2: d/b = .896

Set 3: d/b = .632

The b value used was that for the sine S-N slope for that particular set of beams.

FIGURE G-13

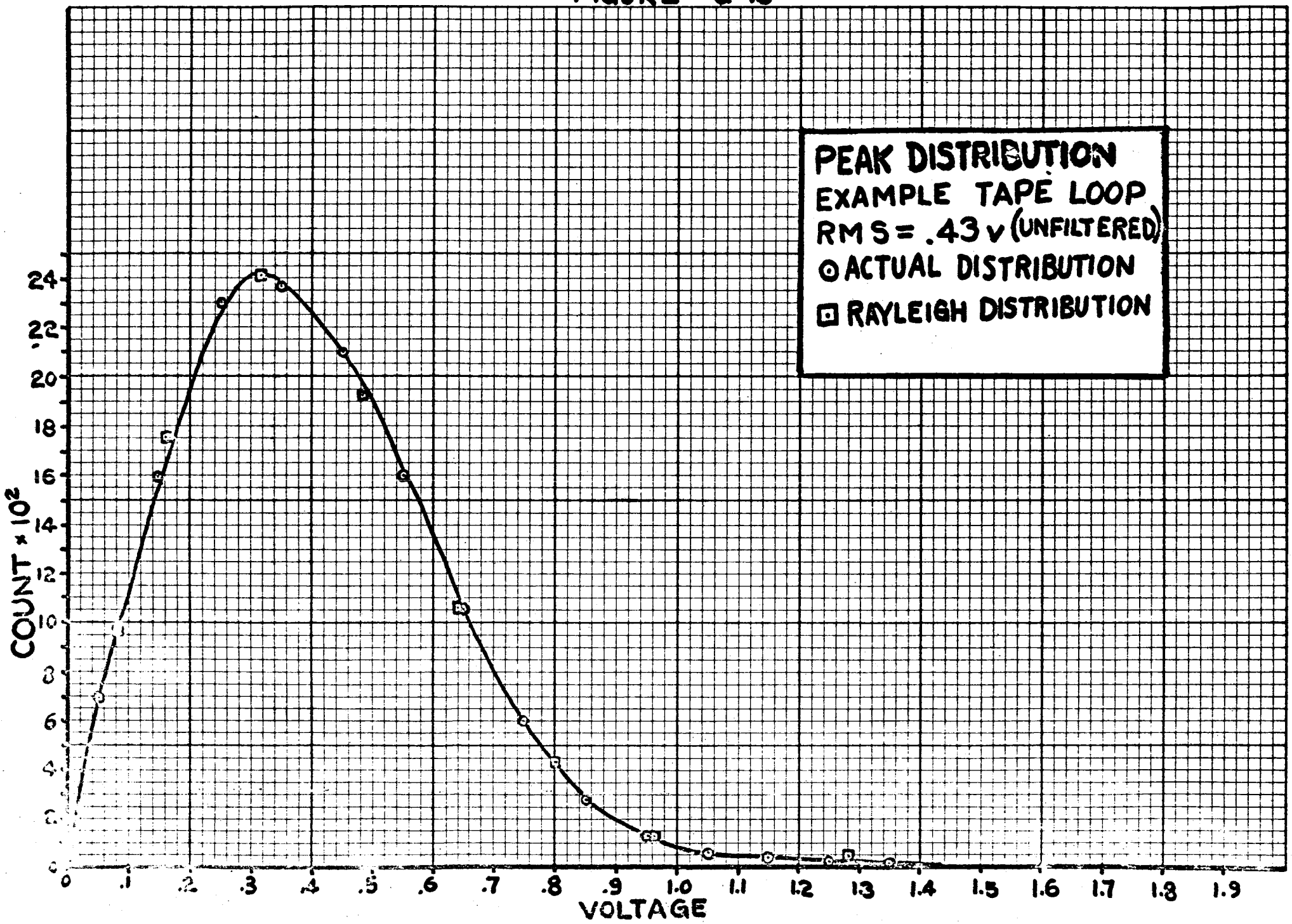

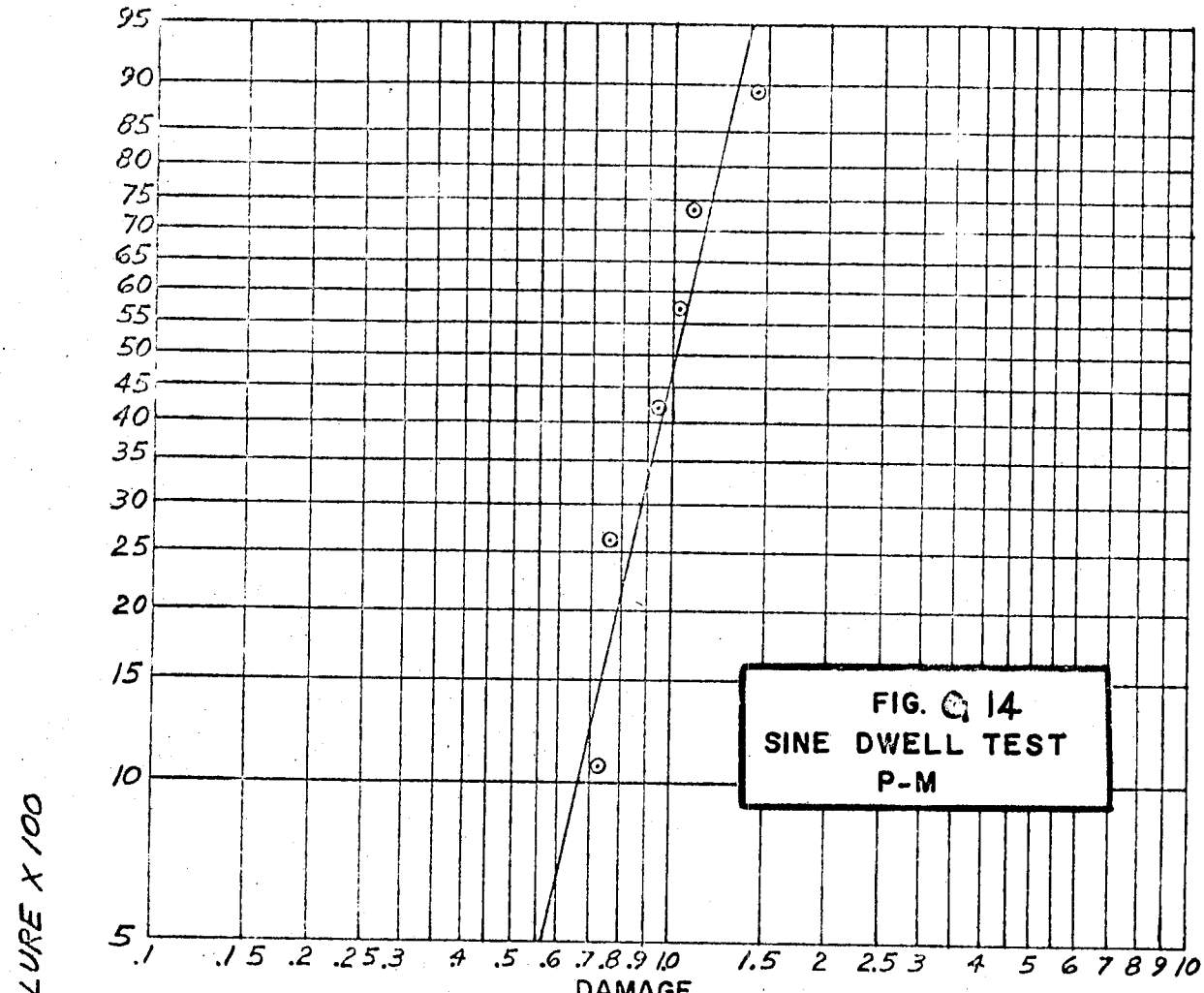

FIG. 14
SINE DWELL TEST
P-M

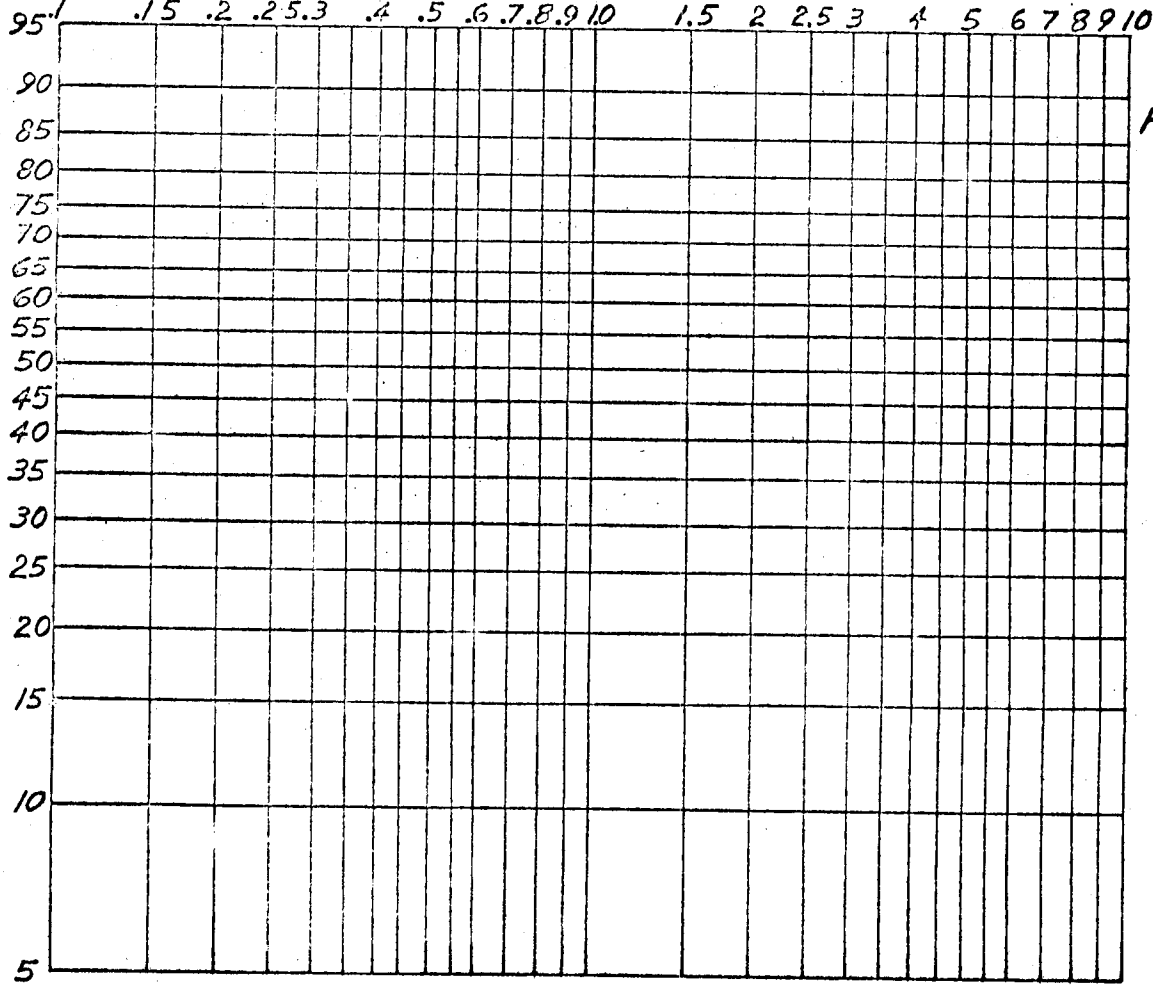

WEIBULL PROBABILITY PAPER

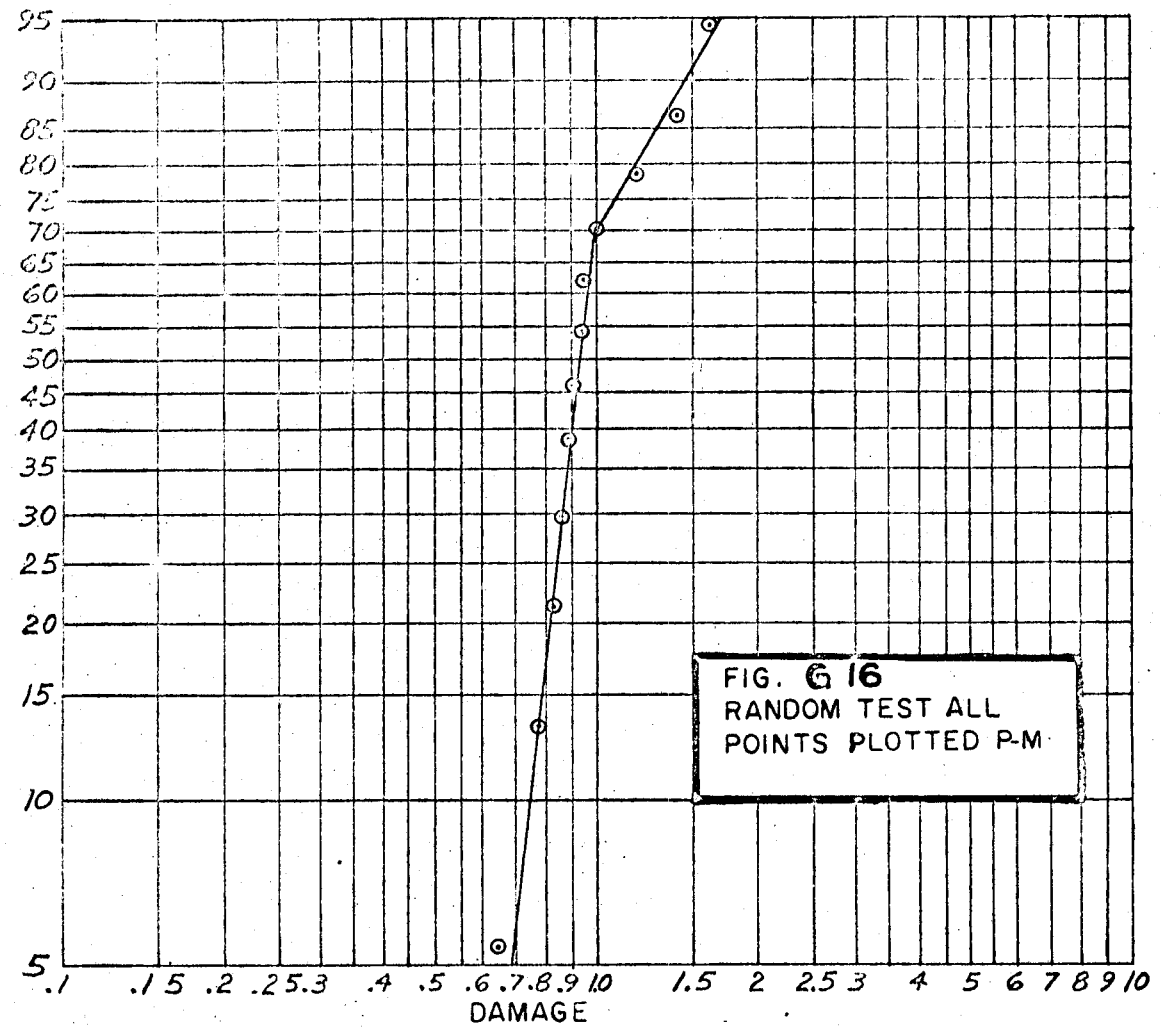

FIG. G 16
RANDOM TEST ALL
POINTS PLOTTED P-M

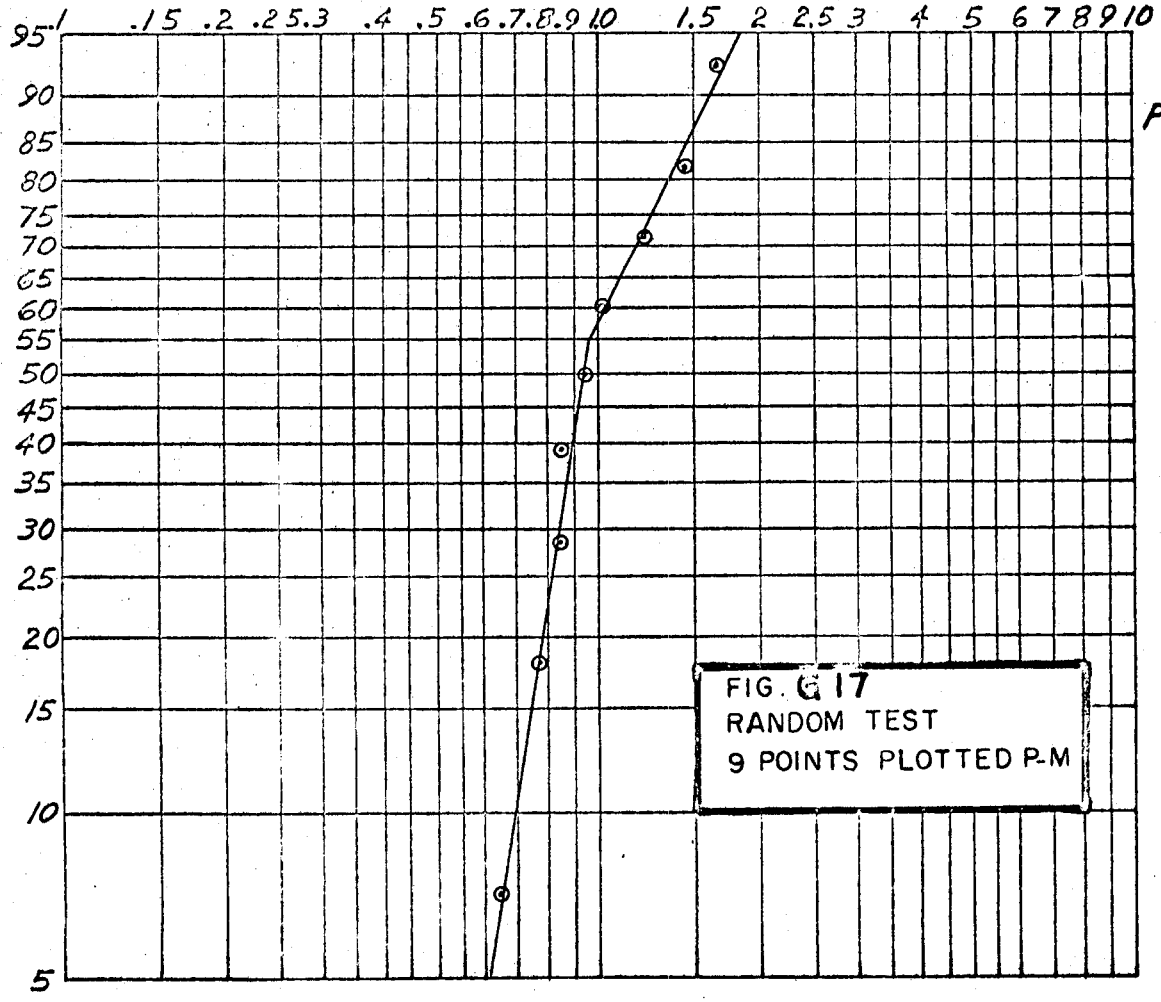

FIG. G 17
RANDOM TEST
9 POINTS PLOTTED P-M

WEIBULL PROBABILITY PAPER

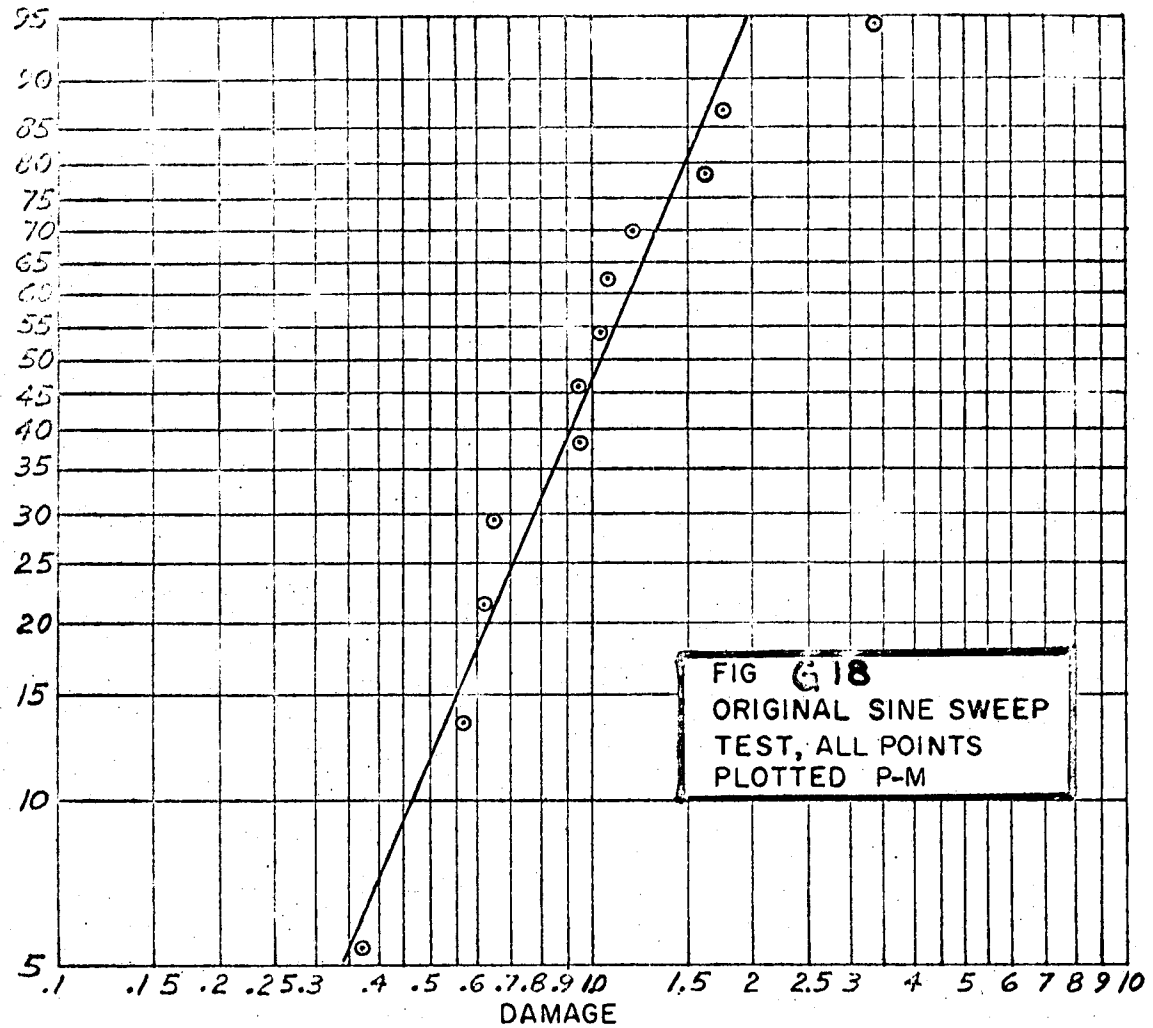

FIG G 18
ORIGINAL SINE SWEEP TEST, ALL POINTS PLOTTED P-M

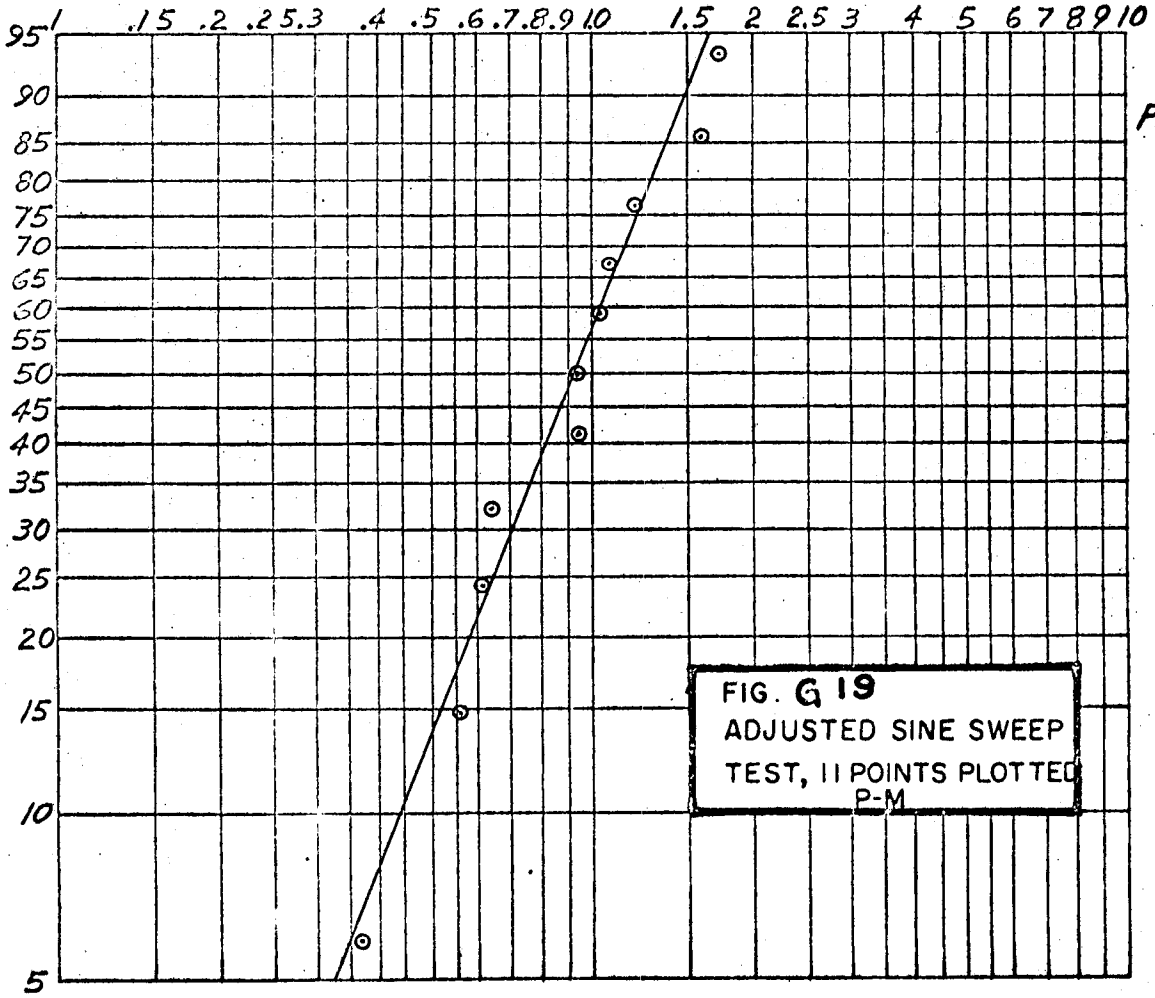

WEIBULL PROBABILITY PAPER

FIG. G 19
ADJUSTED SINE SWEEP TEST, 11 POINTS PLOTTED P-M

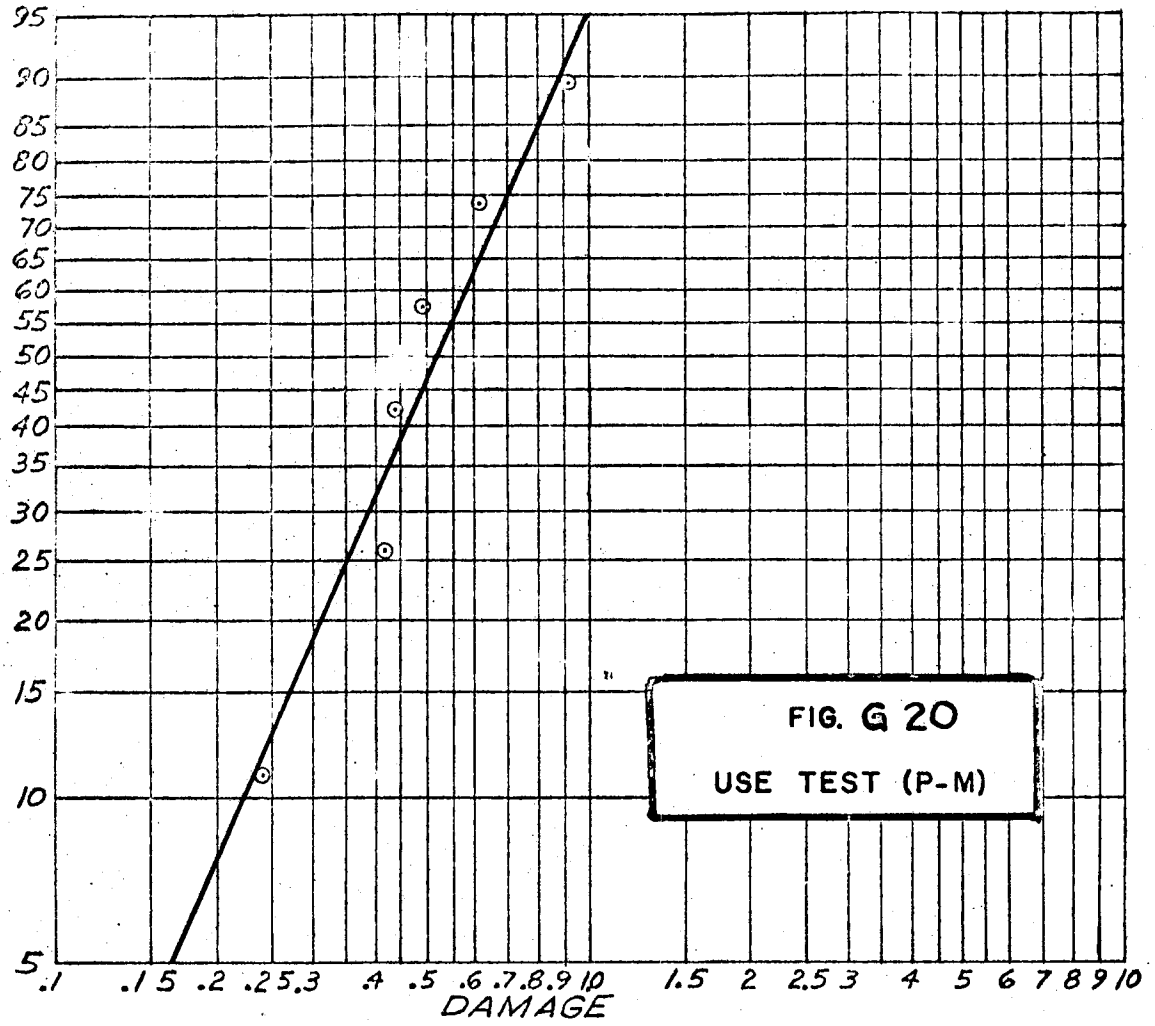

FIG. G 20
USE TEST (P-M)

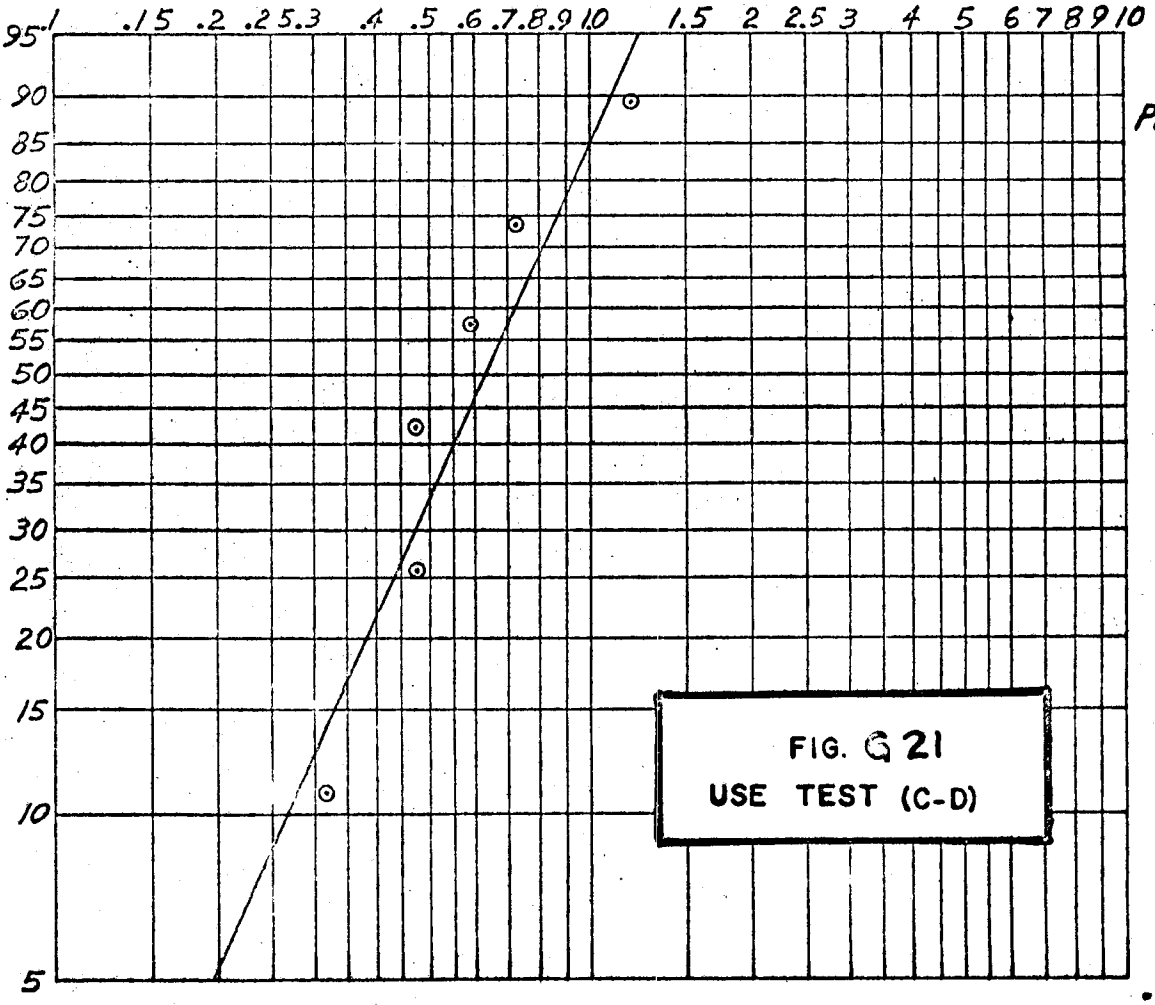

WEIBULL PROBABILITY PAPER

FIG. G 21
USE TEST (C-D)

FIGURE G-22

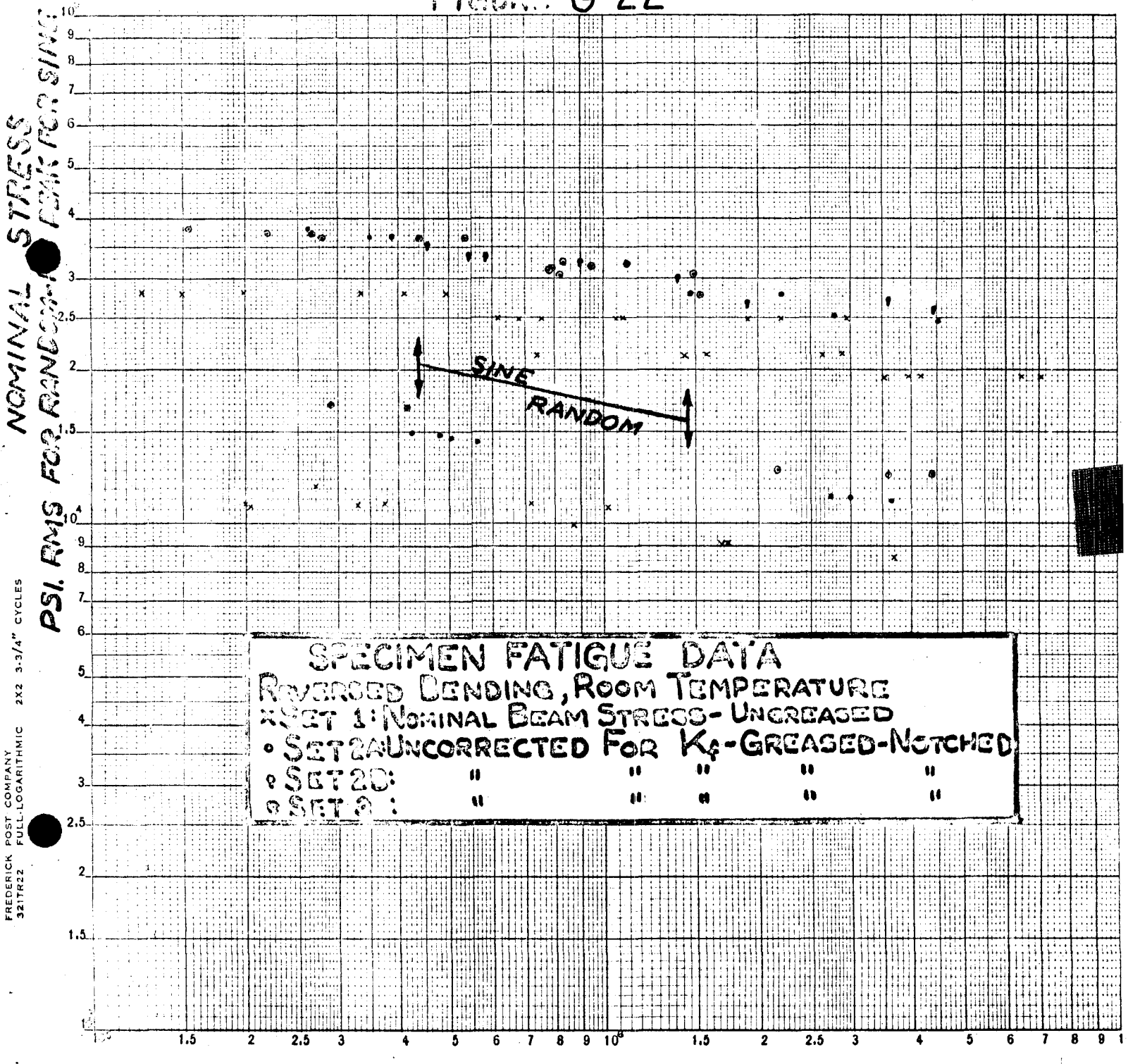
NOMINAL STRESS
PSI. RMS FOR RANDOM, PEAK FOR SINE
SINE
RANDOM
SPECIMEN FATIGUE DATA
REVERSED BENDING, ROOM TEMPERATURE
SET 1: NOMINAL BEAM STRESS - UNGREASED
SET 2A UNCORRECTED FOR Kf - GREASED - NOTCHED
SET 2B: " " " " "
SET 2: " " " " "
FREDERICK POST COMPANY
321TR22
FULL-LOGARITHMIC 2X2 3-3/4" CYCLES
CYCLES TO FAILURE

APPENDIX H

INSTRUMENTATION BLOCK DIAGRAMS

Figure H-1 is a functional block diagram of the instrumentation setup utilized for sinusoidal testing.

Figure H-2 is a functional block diagram of the instrumentation setup utilized for the random vibration testing.

SINE VIBRATION SET UP

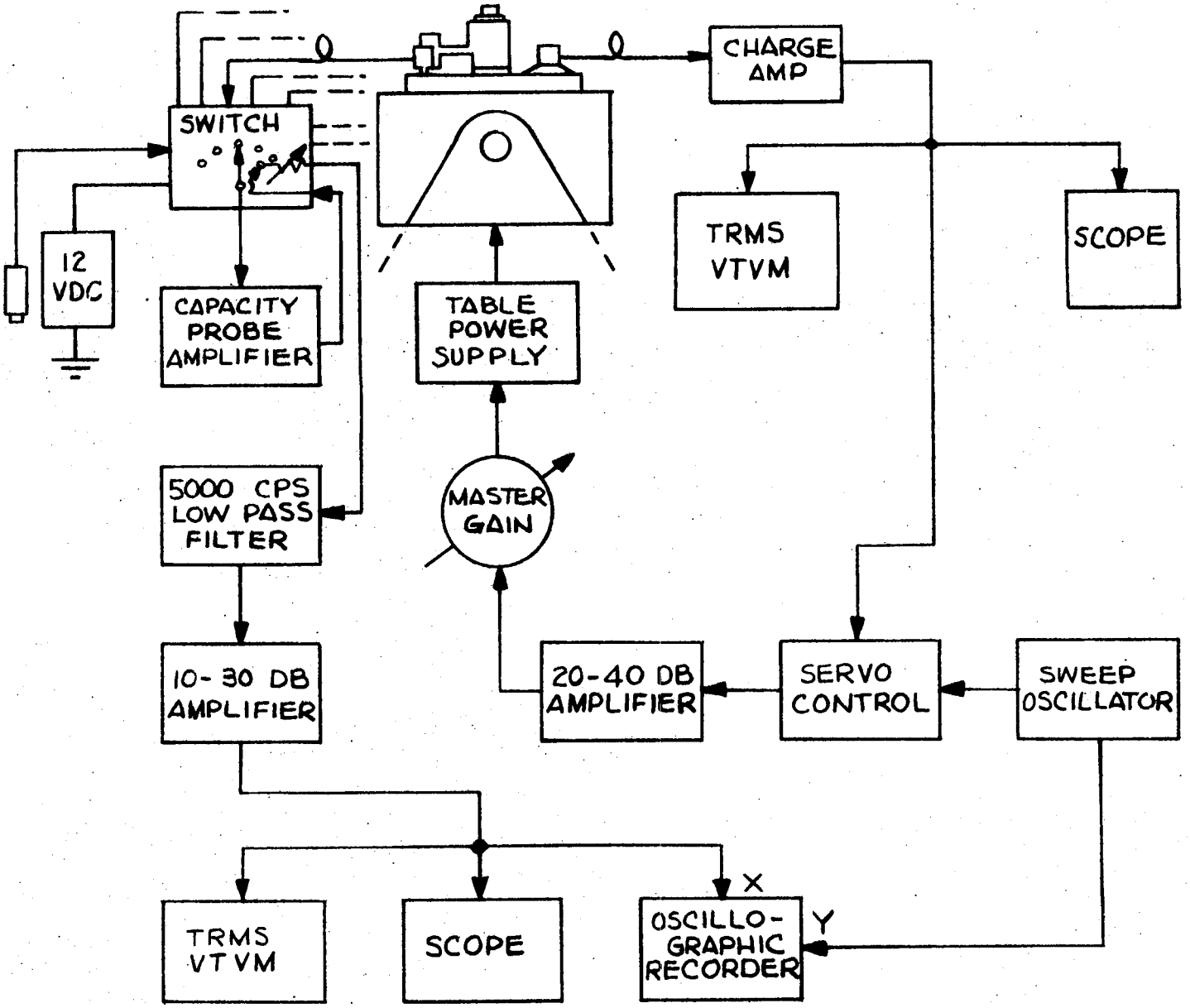

FUNCTIONAL BLOCK DIAGRAM

FIGURE H 1

RANDOM VIBRATION SET UP

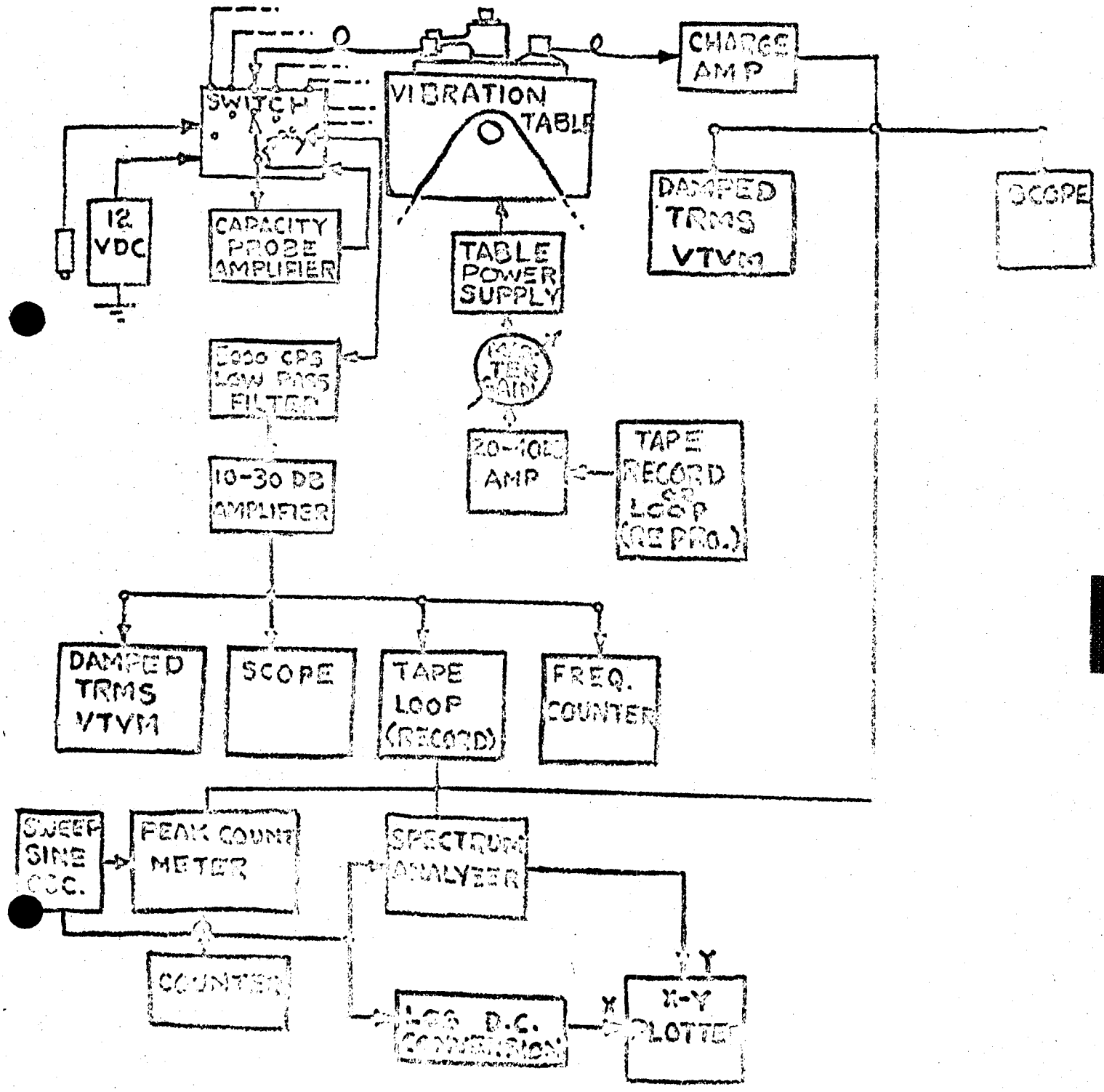

FUNCTIONAL BLOCK DIAGRAM

FIGURE H 2

APPENDIX J

EXAMPLE TEST DETERMINATION

An example is presented in this section to show how an equivalent vibration test would be generated. The field vibration for this example will be the same as that supplied by the contractor of this project. It consists of two random vibration portions (Figure J-1) and one sinusoidal sweep portion (Figure J-2). The specimen is considered to have a b of 7.8. The specimen resonances and Q's are:

1. f_n = 200 cps Q = 10
2. f_n = 400 cps Q = 30
3. f_n = 1200 cps Q = 12
4. f_n = 1700 cps Q = 10

It is desired to have the final equivalent test be a sine sweep test from 20 cps to 2000 cps lasting for one hour.

This data is put into the data deck by filling cards 1 thru 7A as shown in Appendix C. The plotted results of the computer output is shown in Figure J-3. It can be seen that from about 225 cps to 1500 cps the random vibration component of the field vibration is predominant and scaling to sine vibration is dependent upon the Q of the specimen. Above and below this frequency range, the dominant component is sine sweep vibration and no dependence upon Q is shown, since the scaling is done for similar types of vibration. The resonant points are plotted properly in the Q curves as shown in Figure J-4. Since it has been assumed thru out the development of the program that damage occurs only in the resonant region,

it now becomes possible to link up these four points with any line. The dotted line shown was chosen because it results in a more easily conducted test than some constantly varying level as would be possible with a sine sweep curve follower. This test is a compromise because it is one g too high at 400 cps and one g too low at 1200 cps. Since this is only about a 5% error, which is near the limit of most table servo systems, it is considered to be a reasonable test. If at this point it is seen that the level is too high, or the time too long, level scaling can be performed without rerunning the program.

FRED[illegible] POST COMPANY
321TR[illegible] FULL-LOGARITHMIC 2X3 3-1/3" CYCLES

FIGURE J 1

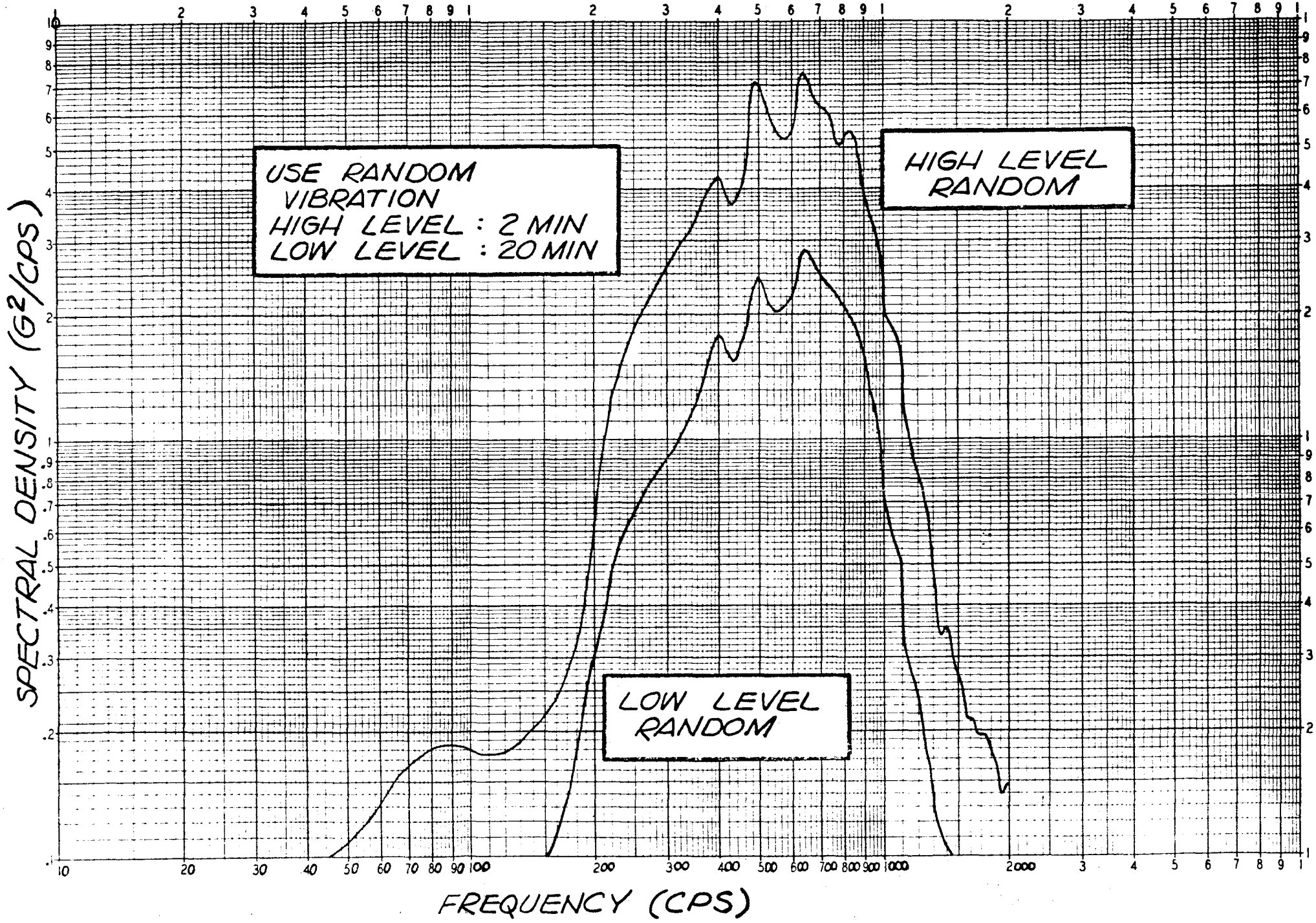

FRED[illegible]K POST COMPANY
3217 FULL-LOGARITHMIC 2X3 3-1/3" CYCLES

FIGURE J 2

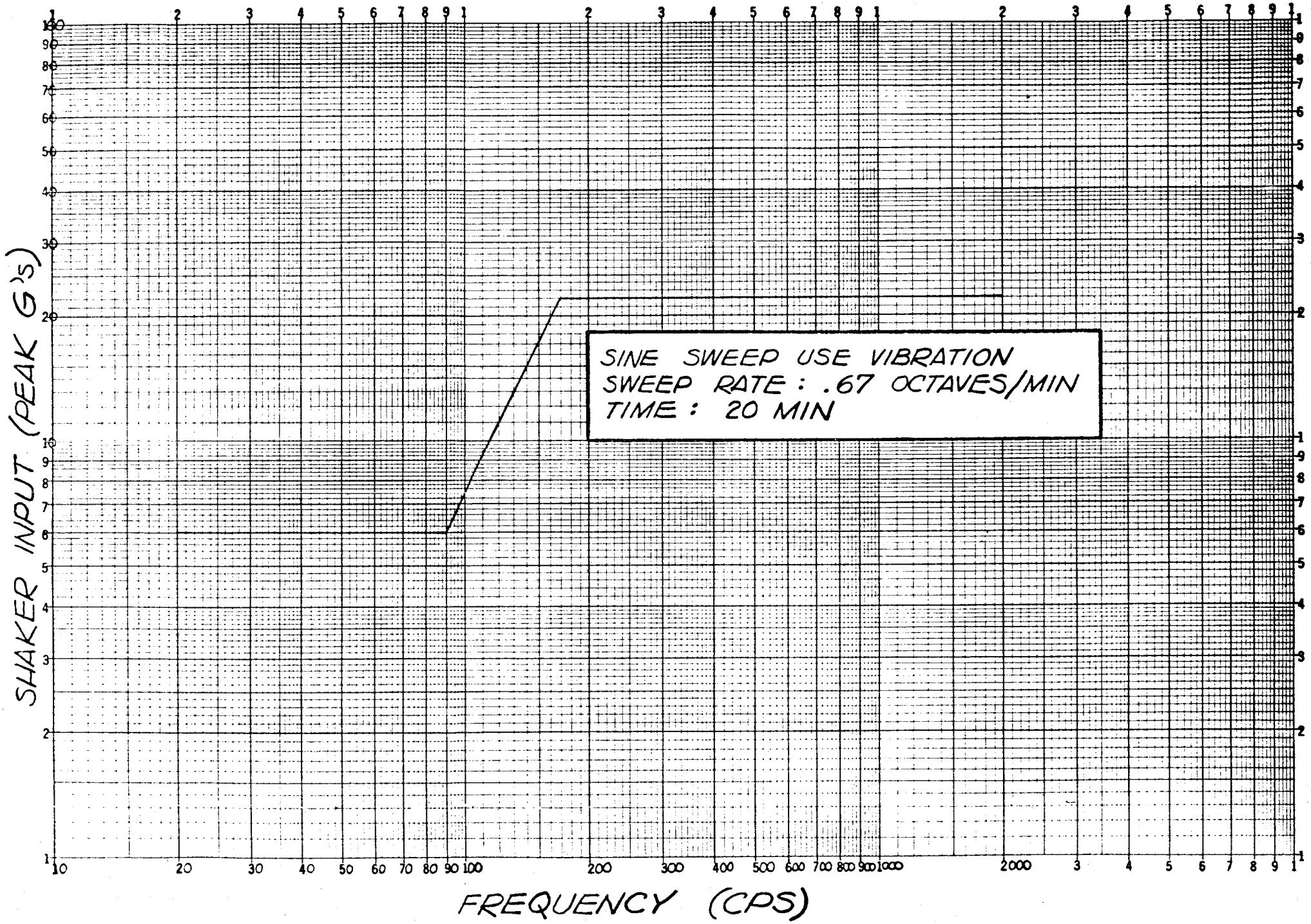

FRED[redacted] POST COMPANY
321T[redacted] FULL-LOGARITHMIC 2X3 3-1/3" CYCLES

FIGURE J-3

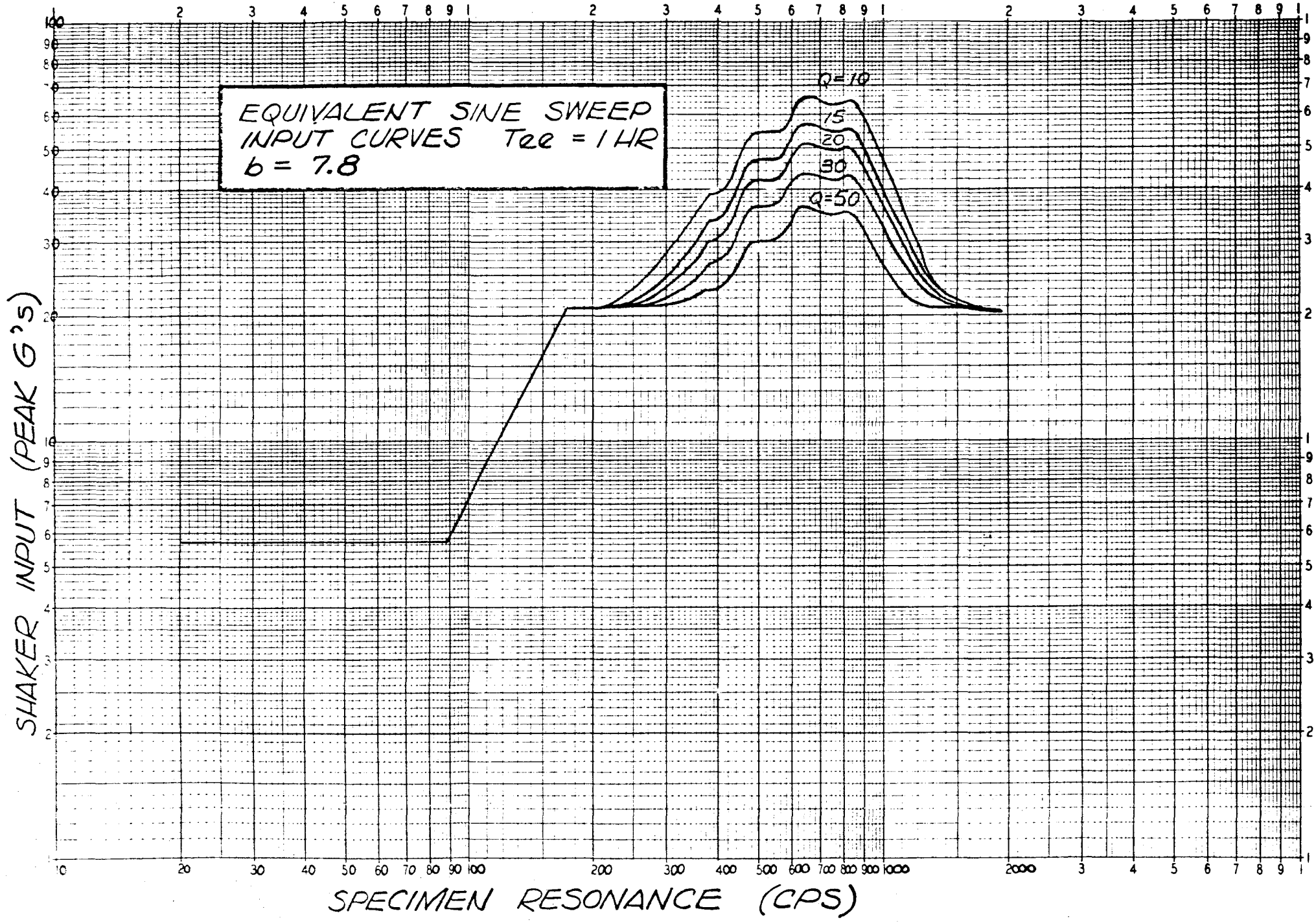

FREDERICK POST COMPANY
3217 FULL-LOGARITHMIC 2X3 3-1/3" CYCLES

FIGURE J-4